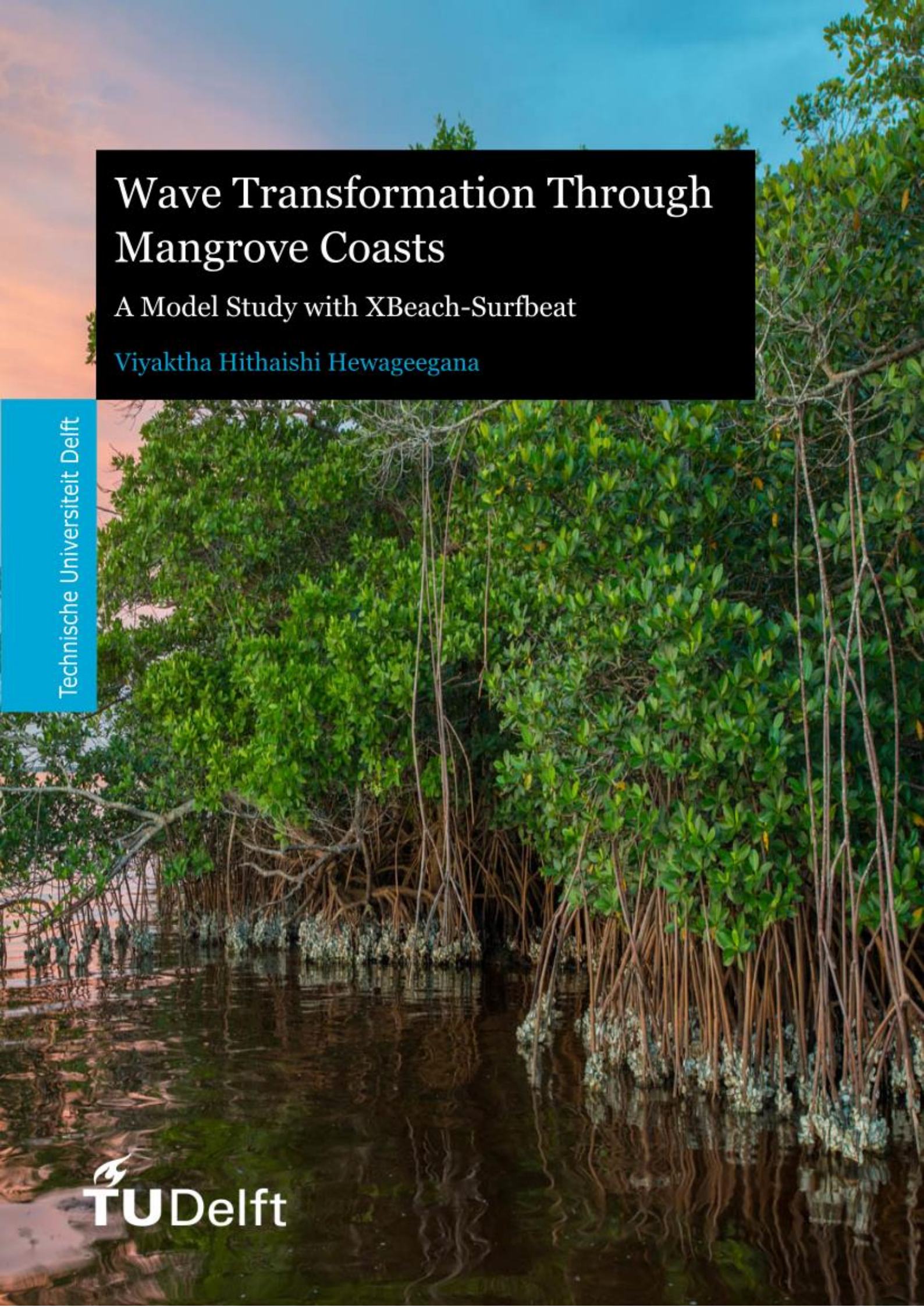

Wave Transformation Through Mangrove Coasts

A Model Study with XBeach-Surfbeat

Viyaktha Hithaishi Hewageegana

Technische Universiteit Delft

TU Delft

ERASMUS +: ERASMUS MUNDUS MOBILITY PROGRAMME

Master of Science in

COASTAL AND MARINE ENGINEERING AND MANAGEMENT

CoMEM

WAVE TRANSFORMATION THROUGH MANGROVE COASTS A MODEL STUDY WITH XBEACH-SURFBEAT

Delft University of Technology

10th July 2017

Viyaktha Hithaishi Hewageegana

The Erasmus+: Erasmus Mundus MSc in Coastal and Marine Engineering and Management is an integrated programme including mobility organized by five European partner institutions, coordinated by Norwegian University of Science and Technology (NTNU).

The joint study programme of 120 ECTS credits (two years full-time) has been obtained at two or three of the five CoMEM partner institutions:

- Norges Teknisk- Naturvitenskapelige Universitet (NTNU) Trondheim, Norway
- Technische Universiteit (TU) Delft, The Netherlands
- Universitat Politècnica de Catalunya (UPC). BarcelonaTech. Barcelona, Spain
- University of Southampton, Southampton, Great Britain
- City, University London, London, Great Britain

During the first three semesters of the programme, students study at two or three different universities depending on their track of study. In the fourth and final semester an MSc project and thesis has to be completed. The two-year CoMEM programme leads to a multiple set of officially recognized MSc diploma certificates. These will be issued by the universities that have been attended by the student. The transcripts issued with the MSc Diploma Certificate of each university include grades/marks and credits for each subject.

Information regarding the CoMEM programme can be obtained from the programme coordinator:

Øivind A. Arntsen, Dr.ing.
Associate professor in Marine Civil Engineering
Department of Civil and Transport Engineering
NTNU Norway
Telephone: +4773594625 Cell: +4792650455 Fax: + 4773597021
Email: oivind.arntsen@ntnu.no

CoMEM URL: https://www.ntnu.edu/studies/mscomem

CoMEM Master Thesis

This thesis was completed by:

Viyaktha Hithaishi Hewageegana

Under supervision of:

Prof.dr.ir. A.J.H.M. Reniers, TU Delft
Dr.ir. A.R. van Dongeren, Deltares
Dr. M.F.S.Tissier, TU Delft
Dr.ir. C. den Heijer, Deltares/TU Delft
Dr.ir. J.T. Dijkstra,Deltares
Ir. C.M.K. Nederhoff, Deltares
Ir. S.G. Pearson, Deltares/ TU Delft

As a requirement to attend the degree of
Erasmus+: Erasmus Mundus Master in Coastal and Marine Engineering and Management (CoMEM)

Taught at the following educational institutions:

Norges Teknisk- Naturvitenskapelige Universitet (NTNU)
Trondheim, Norway

Technische Universiteit (TU) Delft
Delft, The Netherlands

University of Southampton,
Southampton, Great Britain

At which the student has studied from August 2015 to July 2017.

Wave Transformation Through Mangrove Coasts

A Model Study with XBeach-Surfbeat

By

Viyaktha Hithaishi Hewageegana

In collaboration with

An electronic version of this thesis is available at
http://repository.tudelft.nl/

Correspondence with the author may be directed to:
the_vh@yahoo.com

"විද්‍යාව සර්ව ධනයයි"

"Wisdom is all Wealth"

Summary

Coastal defense mechanisms are an integral part in the safety of infrastructure and communities residing on coastlines around the globe. In long temporal and spatial scales, traditional “hard structures” for coastal defense can become infeasible. Incorporation of soft engineering methods for coastal defense can then be a viable solution. Vegetation belts along the coasts can be a prominent soft engineering application.

Many previous studies have been done to identify the protection offered by coastal vegetation. This thesis aims to identify mangrove vegetation interactions under hazardous wave conditions. Moreover, the study includes a comprehensive parameter space by accommodating the variation in wave climate, vegetation and bathymetry observed in the field.

The hydrodynamic-mangrove interactions are analyzed from the perspective of coastal hazard mitigation by vegetation. The study focuses on wave attenuation, setup variation and runup reduction by mangroves.

The investigations are carried out using a numerical modeling scheme, XBeach-Surfbeat.

Mangrove vegetation can substantially mitigate the effects of coastal hazards by waves (wave energy, wave induced flooding) faced in the hinterland. However, the level of mitigation depends on several factors. The most important factors are, vegetation density, mangrove forest width, wave height and water level.

Denser mangrove vegetation and wider forests increases the wave attenuation while deeper water depths in mangrove forests reduces the attenuation capacity.

The improved understanding of the hydrodynamic-vegetation interactions gained in this study can be used as a foundation for a Bayesian network. A better understanding of the effect of the different parameters on flood mitigation can then be attained.

Contents

List of Figures

List of Tables

Acknowledgment

This thesis concludes the Master of Science in Coastal & Marine Engineering and Management (CoMEM) program carried out at Delft university of Technology, Norwegian University of Science and Technology(NTNU) and University of Southampton.

I convey my deepest gratitude to my committee who helped in every possible way to make this thesis a success. I would like to thank Ap van Dongeren for selecting me for the studentship and for the invaluable guidance given throughout the thesis. Thank you, Prof. Ad Reniers, for chairing the committee and for the insightful feedback provided. Marion Tissier, for the critical point of view which helped to fine tune the thesis. Thank you, Jasper Dijkstra, for the guidance given for my thesis from a different perspective. A special thank you to Kees Nederhoff for helping me in everything from XBeach, thesis reviews to computer nodes. Your guidance and calm demeaner towards the issues helped me immensely. Thank you, Stuart Pearson, for the feedback and the encouragement given and finally thank you Kees den Heijer, for being part of my committee.

I would also like to thank Deltares for providing an excellent work environment. Thank you to my friends and colleagues at Deltares, Daniel, Carlos and specially Renan for helping me with your sound knowledge in everything and of course for the relaxing coffee break talks. Thank you my CoMEM colleagues for all the good times throughout the last two years.

I am forever grateful for the excellent opportunity I received to study in Europe and to learn from the best in the field of Coastal Engineering.

I whole heartedly acknowledge the EACEA/EU and CoMEM Board for the giving me this excellent opportunity to learn from the best in Europe. Thank you for selecting me and better yet my loving wife, Sanduni as well for the amazing program. I think we reaped the maximum benefit by improving our knowledge and ability to serve the world. Apart from the academics, we absorbed the rich culture and the immaculate work ethics which will help us excel as well-rounded professionals.

Thank you Sanduni, for being there for me and making the wonderful last two years even brighter.

Last but not the least, I convey my gratitude to my parents, my sister and my wife for the unconditional love and support at every step of the way. A special thanks to my sister for proof reading all kinds of documents throughout the years. I am forever grateful and in debt for the support of my loving family.

Hithaishi Hewageegana
Delft, July 2017

1 Introduction

1.1 Background

The coast has been at the center of human activities for millennia (Martínez et al., 2007). The vast economic and social benefits that are provided by the coastal area as well as the oceans have been a major reason for the coastal zones to become such an integral element of human civilization (Costanza ,1999). Due to the benefits offered, the coastal regions are inhabited by a large portion of the world's population. Small & Nicholls (2003) identified that within the 100km region from the coastline, the population density is almost three times the average population density of the planet.

However, with the increase of activity in the coastal zone, the losses due to coastal hazards have increased as well. In 2012, the US incurred a damage valued at $160 billion due to natural disasters out of which a substantial fraction have been due to coastal hazards (Sutton-Grier, Wowk, & Bamford, 2015).

Coastal defense mechanisms have been at the forefront in reducing coastal hazards. Over the last decade, there has been an increasing interest for the use of "soft" engineering applications for coastal defense rather than "hard" structural solution (Borsje et al., 2011). Soft protection methods vary in a wide range from the use of sand banks, dunes, ecological engineering and use of vegetation belts (e.g. Hanley et al., 2014; Lamberti & Zanuttigh, 2005; Sutton-Grier et al., 2015).

The advantages of soft engineering methods over the traditional hard structural applications become more apparent in large spatial and temporal scales. When the hinterland needs to be defended over long spatial scales, use of hard structures will become expensive and impractical. The traditional engineering applications are over-dimensioned and static. Due to climate change and increasing hazard levels, the capacity of the hard structures will eventually be overwhelmed (Borsje et al., 2011). The soft engineering applications are relatively inexpensive and the dynamic interactions of the system will allow the soft application to adopt to new conditions (e.g. accreting sand dunes and salt marshes). These qualities emphasize the benefits of using soft engineering applications especially at large spatial and temporal scales.

Coastal vegetation can be a prominent soft engineering application. The mitigation offered by vegetation to coastal hazards have been of interest as long back to the 1960s when the United States Army Corps of Engineers reports on the correlation between storm surge levels and saltmarsh widths in Louisiana between 1909 -1957 (Shepard et al., 2011). The benefits of vegetation in the coastal area became even more apparent after the major devastation from the Indian ocean tsunami (2004) (Tanaka et al., 2007; Das & Vincent, 2009). The result of these events is that the use of vegetation as a mitigation method for the coastal hazards has become an important area of research.

1.2 Problem description

The level of mitigation offered by vegetation varies in a wide range and will depend on a range of factors (Horstman et al. 2014 ; Mendez & Losada ,2004 ; Möller, 2006). These factors include vegetation properties (e.g. vegetation type, vegetation height, stem diameter, density drag coefficient and vegetation width), hydrodynamic properties (wave height, wave period, water depth, wave direction) and bed profile. Vegetation interaction with the hydrodynamics will govern the level of mitigation provided by vegetation.

Many studies have been conducted by previous researchers to assess the effect of vegetation on hydrodynamics. However, most of the field studies conducted focuses on low energy environments (Anderson et al., 2011). The previous studies also do not contain analysis of cases with a systematic variation in the hydrodynamic and vegetation parameters that are important to the level of mitigation offered by vegetation.

1.3 Objective

The objective of this thesis is to analyze the effects of coastal hazards on mangroves coasts. This is done by performing a numerical model study with XBeach-Surfbeat on mangrove vegetation with hazardous hydrodynamic environments. The study will focus on the factors that may affect the hydrodynamic interactions with mangrove vegetation.

1.4 Research question

The primary research question to achieve the objective of the study is:

What is the effect of mangrove vegetation on hydrodynamics and how do the different wave and vegetation factors affect these interactions?

The vegetation effects on hydrodynamic will be analyzed pertinent to the mitigation characteristics of vegetation on coastal hazards. Hence the analysis of the mangroves effect on hydrodynamic will be done under the following sub questions.

A. Variations in wave setup due to interactions with mangrove vegetation.
B. Attenuation of wave height/wave energy propagation (short wave & long wave) due to mangrove vegetation.
C. Effect on wave run up in the hinterland due to mangrove vegetation.

1.5 Research approach and report structure

An outline of the thesis is provided within this section.

After identifying the research objective and the research question to be answered, a thorough review of the research background on themes that are central to the current project was carried out. The research background section is provided in chapter 2.

In order to analyze the hydrodynamic interaction with the vegetation, sufficient data covering the entire parameter space should be generated. Application of a numerical model was chosen for the generation of output needed for the project. The selection of the numerical model, setting up and details of the modeling scheme implemented are provided in chapter 3.

The generated model data was then processed and analyzed focusing on the areas that were deemed important in regard to the interaction of vegetation and hydrodynamics. These sections include wave setup, wave height attenuation, wave energy propagation and runup. The analysis section is presented in chapter 4.

The discussion in chapter 5 provides the strengths and weaknesses of the project. The conclusions of the research are provided under two headings, conclusion towards research objective and conclusions towards research questions. Chapter 6 contains the conclusions of the research project.

Recommendations and next steps that can be implemented to improve the understanding and application of mangroves as a mitigation method are provided in chapter 7.

2 Research background

The research background chapter can be divided under two main headings. First, analysis of previous work carried out by researchers into areas that are pertinent to the current research. Second, introduction to process based numerical models to model vegetation-hydrodynamic interactions.

The analysis of previous work starts with a brief overview of the coastal vegetation around the globe. Then the importance of mangroves from a standpoint of protection offered is discussed. The rest of the section focuses on the hydrodynamic interaction with vegetation. This section is divided into three primary areas. Wave attenuation, wave setup variation and wave runup variation. Each of these sections provides details of the status quo in research.

The second half of the chapter explains the process based numerical models used to model vegetation effects on hydrodynamics, specifically XBeach. The governing equations for vegetation-hydrodynamic interactions and the empirical equations used during the analysis are presented.

2.1 Global coastal vegetation

Global coastal vegetation can be categorized under two main vegetation types: mangroves and salt marshes. The distribution of mangrove forests are mostly confined to tropical and subtropical regions with the largest percentage of these vegetation observed between 5°N and 5°S latitude (Giri et al., 2011). Saltmarsh vegetation also occurs on the intertidal region of a coast similar to mangroves. Unlike mangroves, saltmarsh vegetation can originate on any latitude in the world. However, in the tropical regions, mangroves dominate over saltmarsh (Songy, 2016). Figure 2.1 depicts global distribution of mangrove forests and saltmarsh.

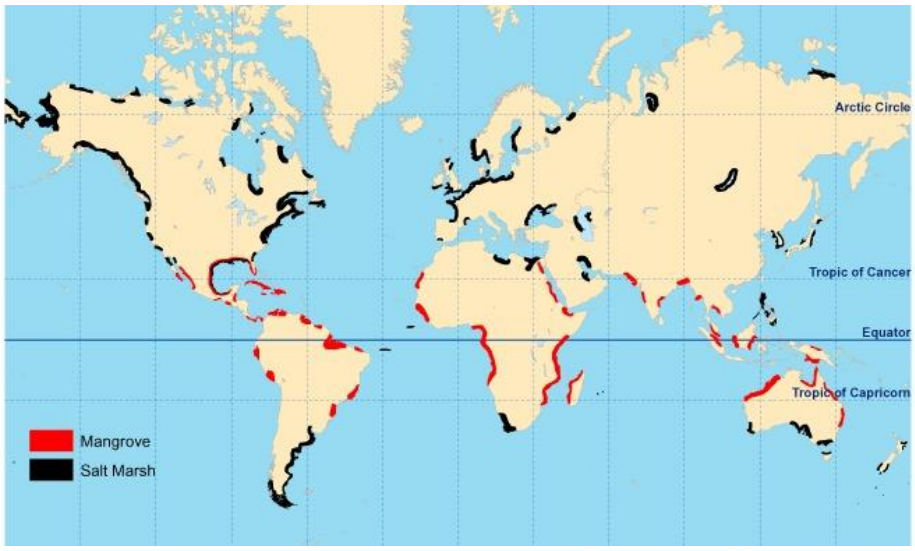

Figure 2.1: Global distribution of saltmarsh (black) and mangrove forests (red). (D'odorico et al., 2013)

Using satellite imagery and image classifications Giri et al. (2011) determined that the total mangrove cover in the year 2000 was 137,760 km^2, spread between 118 countries. However, 75% of the mangroves are found in just 15 countries (Figure 2.2).

Figure 2.2: Global mangrove forest distribution (Giri et al., 2011). The green color shows the mangrove areas

There are three dominant mangrove types: Red, Black and White mangroves. Red mangroves or *Rhizophora* can be identified by the prop roots that originate from the

stem. Black mangroves can be identified by their cone shaped roots (Figure 2.3). White mangroves are observed more landward compared to red and black mangroves.

Figure 2.3: Dense prop root structure of Red mangroves (left) and cone shaped pneumatophores roots of Black mangroves (right) (Janssen, 2016)

From analyzing a wide range of previous studies performed on mangroves, Janssen, (2016) provides values for V_{fac}(section 2.5) for the different mangrove vegetation. Table 2.1 provides the V_{fac} and height (h_v) for Red and Black mangroves. h_v is defined as the height from the ground level to the respective layer (Figure 2.4).

Table 2.1: Variation in vegetation factor (V_{fac}) and height(h) of medium dense Red and Black mangroves at three layers

Mangrove type	Roots		Stem		Canopy	
	$V_{fac}(m^{-1})$	$h_v\ (m)$	$V_{fac}(m^{-2})$	$h_v\ (m)$	$V_{fac}(m^{-2})$	$h_v(m)$
Red Mangroves	0.9	0.50	0.27	5	1.1	12
Black Mangroves	1.2	0.40	0.10	3	0.5	11

A zonation of mangroves in the intertidal region is common. In the Indo-Pacific region, black mangroves are mostly dominant on the lowest and the highest intertidal zones while the mid sections of the forests are dominated by red mangroves. Another common zonation configuration is that the red pioneers are located at the lower parts of the intertidal zone and black mangroves are found in the rest of the intertidal zone.

In the present study, red mangrove properties are taken to represent mangrove vegetation in the numerical model implementation.

2.2 Importance of coastal vegetation

Coastal wetlands have been recognized to have two main benefits. First, the stabilization effects of the vegetation improves sedimentation and reduce erosion on the coasts (Gedan et al., 2011). Second, the protection against storms (Sutton-Grier et al., 2015). The protection of coastal communities becomes even more important with the increase in population within the coastal zone (Small & Nicholls, 2003). In this thesis, the focus is towards the protection (reduction of wave setup, attenuation of wave energy and reduction in flooding) offered to the hinterland by coastal vegetation.

However, it should be noted that the reduction in erosion and improvement of sedimentation by vegetation is utmost importance to attenuation of storms by vegetation. These aspects become more important with sea level rise. The sedimentation induced by vegetation enables the vegetation to adapt to the new hydrodynamic conditions (dynamic system) whereas the hard structures (e.g. revetments) cannot adopt (static system) (Borsje et al. ,2011) .

Identifying the importance of vegetation, some countries implement specific vegetation policies. One of such policy is the preservation of areas for the protection of coastal hinterland, so-called greenbelt zones (Janssen, 2016). The policies behind such green belts differ according to zone and country. For example, from 1984-1990 Indonesia maintained an averaged greenbelt width of 200 m with a minimum of 100 m (Brown, 2007). In Sri Lanka, the forest conservation and the coast conservation departments rehabilitate coastal forests and shelterbelts within the prescribed setback lines (Samaranayake, 2006). In the Philippines and other South-East Asian countries consider a 50-100 m mangrove belt to be sufficient (Janssen, 2016).

However, concerns regarding the level of protection offered by the coastal vegetation have also been raised. These concerns mainly focus on the level of protection offered by vegetation in extreme events such as tsunamis (Gedan et al. ,2011; Feagin et al. ,2010). These studies also acknowledge that coastal vegetation provide a protective role but emphasize that it is not a “silver bullet “for all coastal protection problems.

2.3 Hydrodynamic and vegetation interactions

Numerous studies have been carried out with regard to hydrodynamic interactions with vegetation. These studies include field observations, physical model tests and numerical modeling. Most of these studies focus on one or more of the following themes.

a) Wave attenuation by vegetation
b) Setup variation due to vegetation
c) Runup variation due to vegetation

Bellow we consider all three.

2.3.1 Wave propagation and attenuation due to vegetation

As waves propagate through vegetation, they lose energy. The reduction of energy results in an attenuation of the wave heights (Anderson et al., 2011). The degree of attenuation depends on vegetation properties (geometry, buoyancy, density, stiffness, and spatial coverage) and hydrodynamic characteristics (incident wave height, period, and direction) (Mendez & Losada, 2004 ; Möller, 2006).

Several field studies have been conducted to identify the capability of mangrove vegetation to attenuate waves. However, most of the studies relating to wave attenuation have been done in low energy environments (Anderson et al., 2011). Janssen (2016) succinctly provides wave attenuation rates observed in the different

study sites of mangrove vegetation. The results are tabulated in Table 2.2 according to the wave attenuation rate calculation proposed by Mazda et al., (2006) (equation 2.1).

$$r = \frac{\Delta H}{H \Delta x} \tag{2.1}$$

Where ΔH is the wave height reduction observed after a distance of Δx propagation and H is the initial wave height.

Table 2.2: Wave attenuation rates observed at different mangrove field observations sites.

Source	Vegetation type	Wave height H(cm) Wave period T(s)	Wave attenuation (m^{-1})
Mazda et al. (1997)	Sparse Red mangroves (1/2 year old)	H= -, T=5-8	$r=1x10^{-4} – 1x10^{-3}$
	Dense Red mangroves (2-3 years old), up to 0.5m high	H= -, T=5-8	$r=8x10^{-4} – 1.5x10^{-3}$
	Dense Red mangroves (5-6 years old), up to 1m high	H= -, T=5-8	$r=1.5x10^{-3}– 2.2x10^{-3}$
Mazda et al. (2006)	Black mangroves	H=11-16 T=8-10	$r=2x10^{-3}– 6x10^{-3}$
	No vegetation	H=11-16 T=8-10	$r=1x10^{-3}– 2x10^{-3}$
Vo-Luong & Massel (2008)	Mixed Black and Red mangroves	H=35-40 T= -	Energy reduction factor =0.5-0.7 over 20m
Quartel et al. (2007)	Red mangroves	H=15-25 T=4-6	$r=4x10^{-3}– 1.2x10^{-2}$
	No vegetation	H=15-25 T=4-6	$r=5x10^{-3}– 2x10^{-3}$
Bao (2011)	Mixed vegetation Mixed vegetation	H=15-27, T=- H=55 T=-	$r=5.5x10^{-3}– 1x10^{-2}$ $r=1.7x10^{-2}$
Brinkman (2006)	Red mangroves	H=8-15 T=4	Energy transfer factor 0.15-0.75 over 40m
Zhang et al. (2014)	Red mangroves (fully grown)	H=100, T=-	$r=6x10^{-4}$

A large spread in the observed degree of attenuation is visible which is due to the variation in many different conditions. From the studies done by Quartel et al. (2007) and Mazda et al. (2006) it can be seen that the vegetation is capable of attenuating the waves at a much higher rate than of no vegetation conditions.

Previous studies have been also been conducted into identify the pattern of wave reduction in vegetation. Knutson et al.,(1982) found that there was an exponential reduction in the wave height and a rapid reduction occurring at the start of the vegetation. A reduction rate of 20% per m within the first 2.5m was observed in this study. Möller & Spencer, (2002) also made similar observation in early rapid dissipation of wave energy in vegetation.

Laboratory studies have also been performed to identify wave attenuation by vegetation (e.g. Fonseca & Cahalan (1992) ; Lovas & Torum (2001); Augustin et al. (2009)).

Tschirky et al. (2001) was able to identify several trends in wave attenuation.

i) Total attenuation increased with wider vegetation beds
ii) Higher density of vegetation resulted in greater reduction of waves
iii) Larger incident wave heights produced marginally high levels of attenuation
iv) lower water depths provided more attenuation
v) No clear pattern was visible with incident wave period and wave attenuation.

The wave attenuation can also be discussed according to the frequency of waves as well. There are significant differences to the propagation of high frequency sea waves and low frequency swell waves. In a study Jadhav et al. (2013) found that high frequency waves dissipated in the leading section of the vegetation however low frequency waves propagated to subsequent sections of the vegetation. Horstman et al. (2014) in a study on mangroves also made similar observations.

Apart from the above dependencies in wave attenuation, in study by Wu et al. (2016) found that the wave steepness also had an effect on the dissipation of energy. The study found the damping factor can increase two-fold when the wave steepness approximately doubles.

2.3.2 Setup variation due to vegetation

Wave induced setup is defined as the mean water level above the still water level (Nielsen, 1989). Setup is a key factor to consider in the vegetation environment. By applying linear wave theory in the shallow water limits Dean & Bender, (2006) showed that wave setup due to wave breaking is reduced by a factor of 2/3 in the presence in vegetation relative to a no vegetation case. Furthermore, the study also showed that for milder slopes the setup will be lower.

In a numerical model study on setup variation in vegetation was carried out by van Rooijen et al. (2016) using XBeach. An overall reduction of setup was observed. In the study, numerical model results obtained are validated using a laboratory study. The importance of the different force components acting on the water column is discussed. It was found that the wave induced vegetation force which occurs due to the orbital velocity component of the waves plays a crucial role in accurately predicting the setup level within the vegetation.

2.3.3 Runup variation due to vegetation

Wave runup height is defined as the vertical difference between the highest point of wave runup and the still water level (Schüttrumpf, Van der Meer, Kortenhaus, Bruce, & Franco, 2010). Tang et al. (2017) showed in a numerical model study the runup levels significantly reduced by due to the presence of vegetation. The study performed a series of test with varying vegetation diameters. The tests found the runup decreased with

increasing vegetation diameter and/or vegetation density. A maximum runup reduction of 87% compared to the bare slope was observed. Tang et al (2017) found that wave runup in the presence of vegetation is sensitive to the variation of the incident wave period. However, the study concluded that the attenuation of wave runup does not increase or decrease monotonically with incident wave period.

van Gent (2001) provided an empirical formula based on the surf similarity number to calculate the wave runup on a slope of a breakwater. The study found that the data were more in agreement with the formulae when the wave period was determined on the negative spectral moments ($T_{m-1,0}$) instead of $T_{m,01}$. The negative spectral moments give more weight to the lower frequency energy bands. van Gent (2001) reasons that runup will be governed by lower frequency wave motion than compared to the high frequency motion.

2.4 Process based numerical models for vegetation-hydrodynamic interactions

There are few numerical models which can model vegetation interaction with hydrodynamics. Those like Dynveg can model highly flexible vegetation interaction with hydrodynamics (Dijkstra & Uittenbogaard, 2010). SWAN-SL and SWAN-ML have also been used effectively to model vegetation (Wu et al., 2016).

For the numerical modeling section of the thesis, it was decided to use XBeach-surfbeat. The primary reason to use XBeach is because it is a time domain model which solves the non-linear shallow water (NLSW) equations. The importance of a time domain model is that it can simulate the low frequency waves which have been found to be important in wave propagation in vegetation (Phan, Vries, & Stive, 2011). Furthermore, XBeach has been successful in modeling vegetation interaction with hydrodynamics in previous studies (e.g. van Rooijen et al. (2015); van Rooijen et al. (2016); Songy (2016); Phan et al. (2011)).

A 1D (transect) model is incorporated in the XBeach for the present study. Use of a 1D domain will neglect effects of wave direction and non-uniform long-shore profile and vegetation. These factors will affect the wave heights and currents which will change the hydrodynamic interactions with vegetation. However, with the time constraints and parameter space to be covered a 1D model is the best option.

2.4.1 Introduction into XBeach and the governing equations

XBeach was initially developed as a phase averaged model that resolves the wave amplitude on the wave group scale (XBeach-surfbeat). The variation in the amplitude over space and time drives the low frequency (long wave) motions (van Rooijen et al., 2016). In the model, the low frequency motions are resolved using the non-linear shallow water equations (NLSWE). The short wave propagation is performed via a wave-action balance in which energy dissipation is possible due to wave breaking, bed friction and effects of vegetation.

A non-hydrostatic (phase resolving) mode was also developed for XBeach where continuity and conservation of momentum equations are used to resolve all wave motions (including the short waves) within the shallow water equations (Smit et al., 2014). The downside of XB-NH is it is much more computationally expensive compared to XB-Surfbeat.

Vegetation can be modeled both in the surfbeat and the non-hydrostatic mode. For the non-hydrostatic mode, vegetation is included within the shallow water equations as a force (F_v, equation 2.8). In the surfbeat version of XBeach, vegetation is included both in the wave-action balance (D_v, equation 2.5) and in the included within the NLSWE equations as a force (F_v, equation 2.8). A wave shape predictor is needed to accurately model the vegetation interactions in XBeach-surfbeat (van Rooijen et al. 2016). It was decided to use the surfbeat mode for the modeling due to the computational time saving.

In the following section, the governing equations in relation to vegetation effects on hydrodynamics in XBeach-surfbeat mode are discussed.

2.4.1.1 Short wave action balance

The wave forcing in the shallow water momentum equation (equation 2.8) is obtained from a time dependent version of the wave action balance equation (Roelvink et al., 2015). The propagation of short waves in the model domain will be calculated using this equation as a propagation of energy. For a 1D model the action balance equation can be presented as,

$$\frac{\partial A}{\partial t} + \frac{\partial C_{gx} A}{\partial x} = -\frac{D_w + D_v}{\sigma} \tag{2.2}$$

$$A = \frac{S_w(x,t)}{\sigma(x,t)} \tag{2.3}$$

Where S_w is the wave energy density, σ is the intrinsic wave frequency obtained as,

$$\sigma = \sqrt{gktanh(kh)} \tag{2.4}$$

h is the water depth, k is the wave number and C_{gx} is the group velocity obtained using liner dispersion relation. Two energy dissipation mechanisms for short waves are applied in the model. D_w, dissipation due to breaking and D_v, dissipation due to vegetation.

Within the vegetation, dissipation of energy due to vegetation becomes much more prominent over the dissipation due to wave breaking. A field study by Horstman et al. (2014) found the wave attenuation due to mangroves was predominantly due to the vegetation drag, and the dissipation of wave energy due to bottom friction and viscous dissipation was significantly lower than the effect of vegetation.

The dissipation due to vegetation (D_v) is calculated according to Dalrymple et al (1984) The derivation of the equation is given in (Appendix A)

$$D_v = (\frac{kg}{2\sigma})^3 \frac{\rho C_D b_v N_v sinh^3 kh_v + 3sinhkh_v}{6\sqrt{\pi}\, k cosh^3 kh} H_{rms}^3 \quad (2.5)$$

Where H_{rms} is the root mean square of short wave height, ρ is the water density, C_D is the drag coefficient, b_v is the vegetation stem width, N_v is the vegetation density. The vertical variation in the vegetation is also taken into account in the model using the method proposed by Suzuki et al. (2011)

$$D_v = \sum_{i=1}^{n_v} D_{v,i} \quad (2.6)$$

$D_{v,i}$ is the dissipation by vegetation by the i^{th} layer.

2.4.1.2 Shallow water equations

To solve the low frequency waves and the mean flows, the model uses the shallow water equations. The shallow water equations consist of two equations, the continuity equation (equation 2.7) and momentum conservation equation (equation 2.8). The equations are based on Lagrangian velocities (U^L) which is defined as the distance a water particle travels within a wave period (Roelvink et al., 2015). For a 1D model domain the equations can be presented as,

$$\frac{\partial \eta}{\partial t} + \frac{\partial U^L h}{\partial x} = 0 \quad (2.7)$$

$$\frac{\partial U^L}{\partial t} + U^L \frac{\partial U^L}{\partial x} = -g \frac{\partial \eta}{\partial x} + \frac{-\tau_{bx} + F_w + F_v}{\rho h} \quad (2.8)$$

Where η is the water surface elevation, U^L is the depth averaged Lagrangian velocity, τ_{bx} is the bed shear stress, F_w is the wave force due to the radiation stress variations and F_v is the wave averaged force due to vegetation.

The bottom friction (τ_{bx}) is calculated using the approach in Ruessink et al. (2001). Where the bed shear stress for a 1D model is calculated as,

$$\tau_{bx}^E = c_f \sqrt{(1.16 u_{orb})^2 + u_E^2} \quad (2.9)$$

Where u_{orb} is the orbital velocity of the waves and u_E is the depth averaged Eulerian velocity. The wave force F_w in the cross shore direction is calculated for a 1D model using the variation in radiation stress variation is cross-shore direction (Longuet-Higgins & Stewart, 1964).

$$F_w = -\frac{dS_{xx}}{dx} \quad (2.10)$$

Where S_{xx} is the radiation stress in cross shore direction, obtained from the wave action equation.

As the waves propagate through vegetation, a drag force is exerted by the waves on the vegetation. Due to the exerted force, an equal and opposite force acts on the water

column. The force induced by the vegetation is modeled using a Morison type formula. Dalrymple et al. (1984) presents the equation as,

$$F_v = \frac{1}{2}\rho C_D b_v N_v u|u| \tag{2.11}$$

The energy dissipation by vegetation D_v (equation 2.5) is based on the drag force (equation 2.11). The cumulative force due to vegetation over the submerged depth is,

$$F_v = \int_{-h}^{-h+h_{veg}} \frac{1}{2} C_D\, b_v N_v |u| u dz \tag{2.12}$$

h_{veg}, is the submerged depth of vegetation. The vegetation force exerted can be divided into two main components, the mean drag force ($F_{v,m}$) and wave-induced force due to emergent vegetation and/or nonlinear waves ($F_{v,w}$). Both components are based on (equation 2.12) with different velocity components.

The mean drag force induced by vegetation $(F_{v,m})$ is due to sea-swell phase averaged time scale (mean flow). The flows include undertow and unsteady infragravity (IG) currents (van Rooijen et al., 2016). $F_{v,m}$ is calculated using the Eulerian velocities (U^E).

The wave-induced force due to emergent vegetation and/or nonlinear waves ($F_{v,w}$) is due to the sea-swell wave orbital motion scale. Since, XBeach-surfbeat is phase averaged model, the incident wave phase data is lost. To circumvent the issue, an empirical wave shape model is implemented (van Rooijen et al., 2016). Using the wave shape model, net $F_{v,w}$is calculated over a wave period.

2.5 Modeling of vegetation in XBeach

XBeach can be set up to model the effect of vegetation. XBeach allows the vegetation to have horizontal and vertical variations in vegetation parameters. The vertical variation in vegetation is especially important in mangroves where a significant vertical variation in trees is observed (Janssen, 2016).

Due to the differences in vegetation characteristics in mangroves over the vertical, a layering of mangroves in the vertical was proposed by Suzuki et al. ,(2012). The vertical layers are divided as the roots, stem and the canopy where there is significant variation in characteristics. A vegetation factor (V_{fac}) can be defined as in equation 2.1,

$$V_{fac,i} = b_{v,i} N_i \tag{2.1}$$

Where $b_{v,i}$ is the diameter of the vegetation and N_i is the number of trees/stems in a square meter (m^{-2}) on the i^{th} layer. The V_{fac} values changes with the layer and with the type of mangrove.

XBeach essentially treats the vegetation as rigid cylinders. The physical parameters (height of the vegetation (h_v), stem diameter (b_v), number of tree stems in a square meter (N_v) and the drag coefficient (C_D)) of these cylinders can be changed accordingly

to represent vegetation (section 3.2.2). Figure 2.4 provides a schematic drawing of how the vegetation is represented in XBeach.

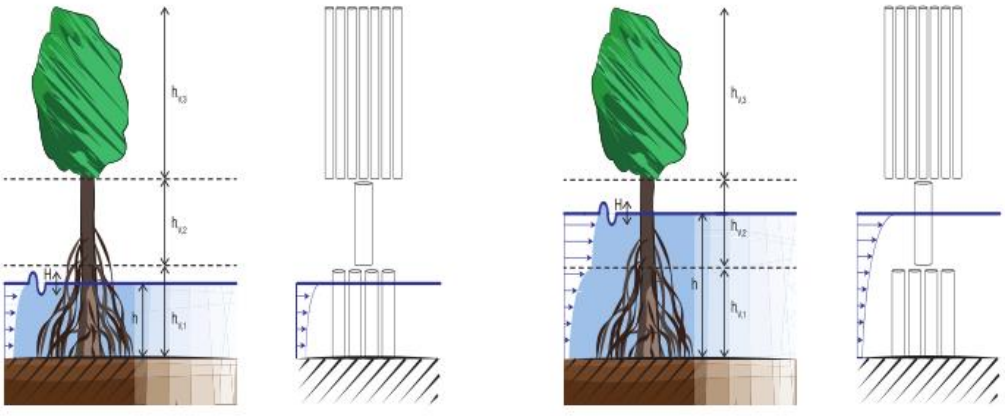

Figure 2.4: Representation of vegetation in XBeach (including vertical layering) for two different submergence levels (Janssen, 2016).

2.6 Empirical formulas

2.6.1 Runup calculation hinterland of the vegetation

In XBeach-surfbeat mode, the model calculated runup levels only considers the long waves and will not include the contribution to runup due to the short waves. Neglecting the contribution from the short waves will lead to an under prediction of the runup levels.

Hence the runup is calculated using an empirical formula proposed by van Gent (2001). This specific method is used because; the runup formulation is based on wave parameters at the toe of the structure. Whereas other runup formulations use wave parameters in the offshore. Due to the vegetation, there are significant differences in the wave climate in the offshore and end of the vegetation.

Oosterlo,(2015) was able to successfully model the empirical results for runup obtained by van Gent, (2001) using XBeach.

Due to the stochastic nature of the incoming waves, each wave will have a different runup level (Schüttrumpf et al., 2010). Similar to many runup formulae, the van Gent (2001) method calculates the runup as the wave runup level exceeded by 2% of incident waves ($z_{2\%}$) relative to still water level. The runup formulation proposed can be presented as,

$$\frac{z_{2\%}}{\gamma H_s} = C_0 \xi \qquad for\ \xi \leq p \qquad (2.13)$$

$$\frac{z_{2\%}}{\gamma H_s} = C_1 - \frac{C_2}{\xi} \qquad for\ \xi \geq p \qquad (2.14)$$

$$\xi = \frac{tan\varphi}{\sqrt{\frac{H_s}{L_0}}} \tag{2.15}$$

$$C_2 = \frac{0.25C_1^2}{C_0} \tag{2.16}$$

Where p is defined as, $p = \frac{0.5c_1}{c_0}$ and $c_0 = 1.35\ and\ c_1 = 4.7$,$H_s$ is the significant wave height at the toe of the structure, γ the reduction factors for roughness and wave angle. ξ is surf similarity parameter and φ is the slope of the structure. For the calculation of the surf similarity number(ξ), the wave length is calculated as,

$$L_0 = \frac{gT_{m-1,0}^2}{2\pi} \tag{2.17}$$

The wave period used in the calculation is $T_{m-1,0}$(section 2.3.3). The calculation procedure used to obtain the runup for the models are given in section 3.4.

3 Model setup

The model setup chapter presents the selection of parameters to implement in the numerical model. The parameter selection comprises mainly of hydrodynamic and the vegetation parameters. After the selection of parameters, setting up of the model domain; selection of profile; grid resolution and modeling time sections are discussed. The computational setup section provides process used in XBeach to generate the outputs. Finally, procedure of calculation of wave spectra and total wave for the runup calculation is provided.

3.1 Model selection

The data for analysis can be collected either by field observations, physical model tests or numerical model implementation. Field observations into the area of hydrodynamic-vegetation (mangrove) interactions have been carried out by previous researchers in different environments and under different conditions (Table 2.2). However, it was noted that, most of the studies carried out are done in low energy environments and interactions during extreme events are less common. As this research is concerned with extreme events and due to reduced control over the parameter variations, use of previous field observations will not be suitable.

Physical modeling to identify wave interaction with vegetation has also been performed successfully by previous researches (e.g. Wu & Cox (2015); Augustin et al., (2009); Möller et al. (2014) ; Lovas & Torum, (2001)). Since the research project aims to cover a large parameter space (section 3.2) physical model testing will be infeasible. This leads numerical modeling to be the most viable option.

Numerical modeling of hydrodynamic and vegetation interaction has been performed successfully in the past with good accuracy (e.g. van Rooijen et al. (2016) ; Augustin et al., (2009); Phan et al., (2011) ; Songy (2016)).

Due to the aforementioned reasons and previous success in research carried out using XBeach to model vegetation effects (section 2.4), it was decided to use XBeach-surfbeat for the numerical modeling.

3.2 Parameter selection

The ultimate goal of the modeling work in XBeach is to generate a synthetic data set of hydrodynamic forcing, vegetation and bed characteristics, and wave and water level that will represent reality. The parameters to be incorporated in the models will thus have to be chosen to represent the actual ground scenarios. The input needed for the models can be broadly categorized under three main sections: hydrodynamic, vegetation and bed geometric parameters.

3.2.1 Hydrodynamic forcing parameters

The wave climate is a significant driver for the hydrodynamic process within the environment. The interaction between waves and vegetation will depend on hydrodynamic parameters such as wave height, wave period and wave direction (Mendez & Losada, 2004).

The hydrodynamic forcing parameters of interest are wave height, wave period, highest astronomical tide and storm surge level.

Offshore wave data derived from the ERA-Interim (ERA-I) database, linked to the Dynamic Interactive Vulnerability Assessment (DIVA) points around the globe were used as wave climate source. The wave data was filtered by location to provide the wave data for global mangrove areas. Since the focus of this thesis is on effect of vegetation on

coastal hazards during the extreme events, the 100-year return period events were chosen to represent the wave climates of the models.

Figure 3.1 provides the global distribution of mangroves according to USGS (Giri et al., 2011). The point locations on the map portray the locations where the data for the hydrodynamic inputs were extracted. The extraction points are selected to represent the global variation.

The found wave climate parameters are varied throughout the models to derive different sets of input conditions. To make sure implausible combinations of offshore wave heights and wave periods are not considered in the models, wave steepness derived from the data was used as an input parameter instead of using wave period as a direct input. By using wave steepness, the wave period will be calculated according to the wave height. The resulting wave periods will then simulate short wind waves up to long swell wave conditions appropriately. A JONSWAP spectrum with the significant wave height and the corresponding peak period obtained from wave steepness was applied at the boundary. The other parameter values needed for the implementation of the JONSWAP spectrum were kept at the default values apart from the directional spreading coefficient (s) which was set 10,000 (Appendix B), which correspond to no directional spreading.

The wave climate parameter ranges for mangrove areas from the data are tabulated in Table 3.1.

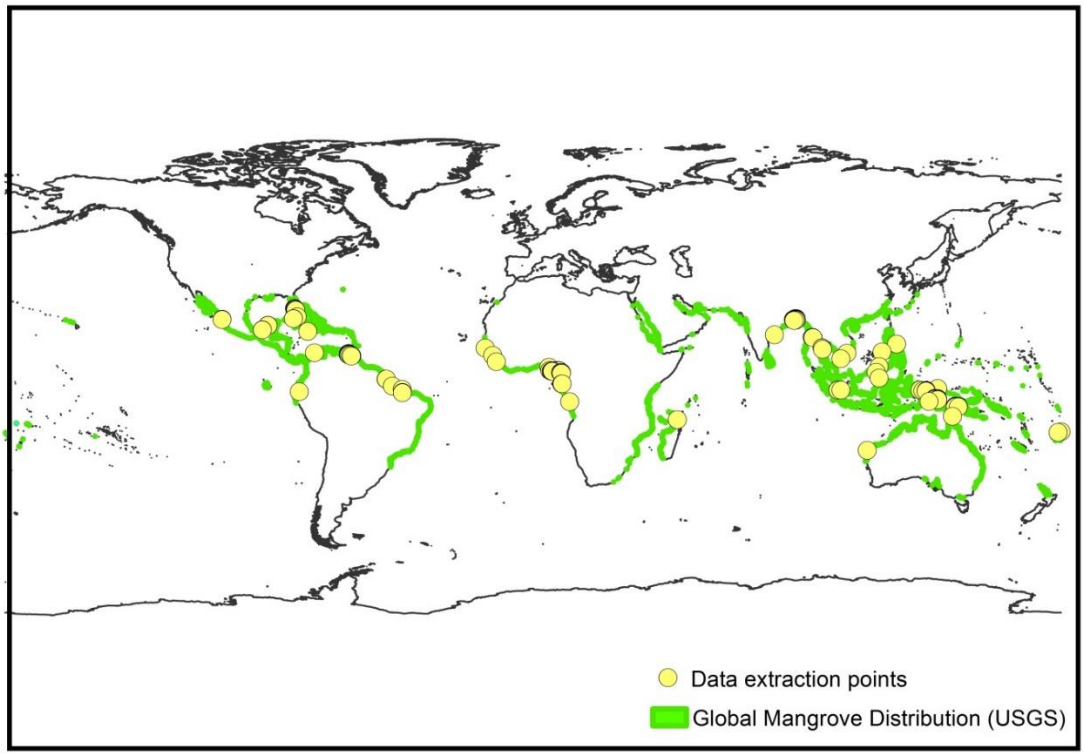

Figure 3.1: Global distribution of mangroves vegetation (USGS) (Giri et al., 2011) overlaid with the locations where the hydrodynamic data were extracted for the input parameters.

Table 3.1: 100-year return period offshore wave parameter range for global mangrove forest distribution

Wave parameter		Range
Significant wave height	[m]	1 - 7
Wave Steepness	[-]	0.02 - 0.05
Storm surge	[m]	1 - 4.5
Highest astronomical tide	[m]	0.5-3.5

3.2.2 Vegetation and bed geometric parameters

The vegetation input parameters required by XBeach are given in section 2.5. These parameters vary along the vertical significantly for plants like mangroves. The vertical variation in vegetation is very important and needs to be accounted for.

The vertical variation in vegetation density was taken into consideration by dividing the mangrove vegetation into three main segments over the vertical. The three segments are root system, stem and canopy.

Janssen,(2016) summarized the characteristic parameters of mangroves under plant type and vegetation density (Table 3.2). In this thesis, a constant nominal drag coefficient of 0.6 was applied over the entire height of the tree.

Table 3.2: Vertical variation of red mangrove parameters for different densities (Janssen, 2016)

Density	Roots			Stem			Canopy	
	N_v [roots/m^2]	b_v [cm]	h_v [m]	N_v [stems/m^2]	b_v [cm]	h_v [m]	V_{fac} [m^{-1}]	h_v [m]
Sparse	15	1	0.3	0.3	20	2	0.1	10
Medium	45	2	0.5	0.6	45	5	1.1	12
Dense	70	3	1.0	0.9	75	8	4.5	12

In order to reduce the number of input parameters for XBeach, vegetation factor (V_{fac}) was then varied for the different model runs.

Mangrove vegetation is mostly found in areas where the ground slope is very mild. For an example in the Mekong delta the sea bed slope is in the order of 1/500 (Albers, San, & Schmitt, 2013). Within the numerical model implementations, the profiles slope ranging between 1/300 and 1/1000 were considered.

Mangrove forests are found in the intertidal zone of the coastlines.(Giri et al. (2011); Suzuki et al. (2011)). The width of the intertidal zone will be a function of the profile slope and the highest astronomical tide (HAT). Hence the resultant mangrove vegetation widths were calculated for each model according to the profile slope and HAT. The resulting mangrove forest widths were in the range of 150m-3500m.

3.3 Computational setup for the model

Computational setup needs to be configured for the numerical model to be implemented in XBeach. The computational setup of the model is threefold,

1. Configuration of grid geometry and boundary conditions
2. Selection of grid resolution
3. Choosing a model runtime and spin-up duration.

Appendix B provides the procedure, tests and the analysis conducted to configure the said components of the computational setup.

From the results obtained in Appendix B, a grid geometry of profile containing a profile break located at 12.5m depth and a truncated slope of 1/300 is used in the analysis. The grid will be a non-equidistant grid with a minimum grid resolution of 1m. A schematic diagram of the configured computational grid setup and inputs are provided in Figure 3.2.

Four observation points are located within the model domain for the extraction of high frequency point output. The first observation point (*Obs 1*) is located offshore at a depth of 17.5m and will represent the offshore wave climate offshore of the vegetation. The second observation point (*Obs 2*) is located just in front of the mangrove vegetation. The point also coincides with the MSL as well. Observation point 3 (*Obs 3*) and Observation point (*Obs 4*) are located at the middle and the end of the vegetation respectively. A run-up gauge is also used to find the run-up over the slope behind the vegetation.

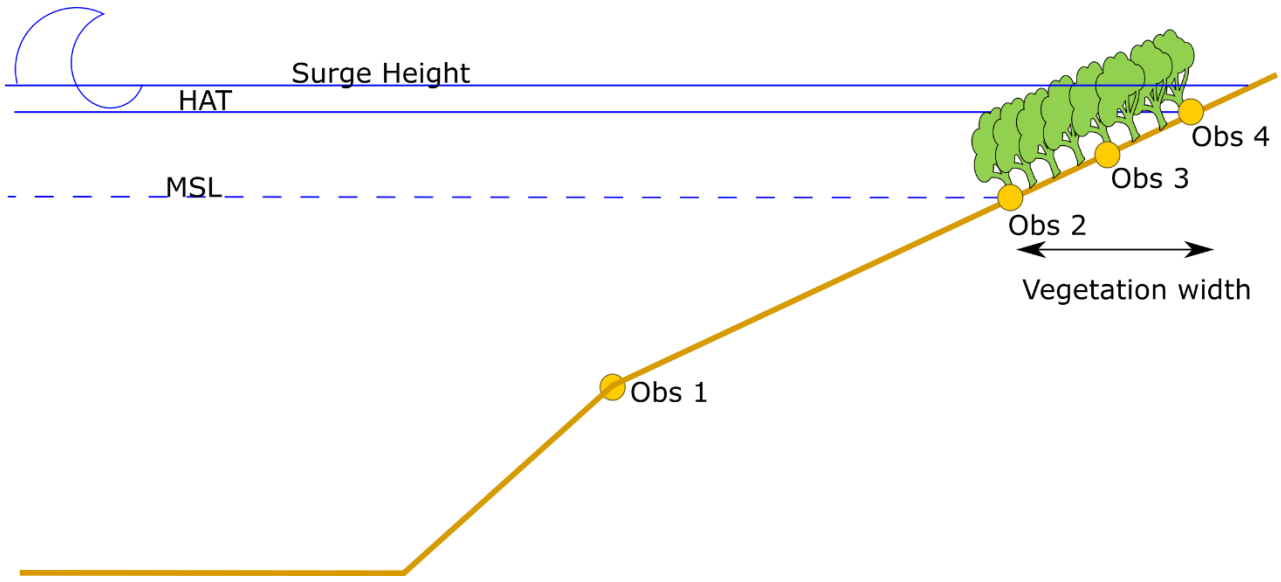

Figure 3.2: Schematic setup of the numerical model setup applied in XBeach

3.3.1 Generation of Input combinations

The hydrodynamic input parameters (section 3.2.1) were divided into bins. For example, the offshore significant wave height (Hs) varies between 1m-7m (section 3.2.1) and was divided into 4 equal bins of 144 unique uniformly distributed values within each bin. The other parameters were also divided into such bins. The values on each bin were then matched with the other parameter values to create a unique set of 576 input permutations.

Figure 3.3 provides the hydrodynamic input values for each of the model runs. The values in the model runs are paired from each input parameter to create the input conditions for the model.

This hydrodynamic set of model runs was then imposed on different vegetation densities (dense vegetation, medium dense and sparse vegetation) and on a base case of without vegetation. Each counterpart model run has the same input signal (no wave randomness). Thus, any model output variation is the result of the differences from the vegetation.

The runup for the models was calculated using an empirical formula (section 2.6.1). For the calculation, a 1/10 slope was considered just behind the vegetation for all models. The slope was considered smooth. This slope section was not included in the XBeach model.

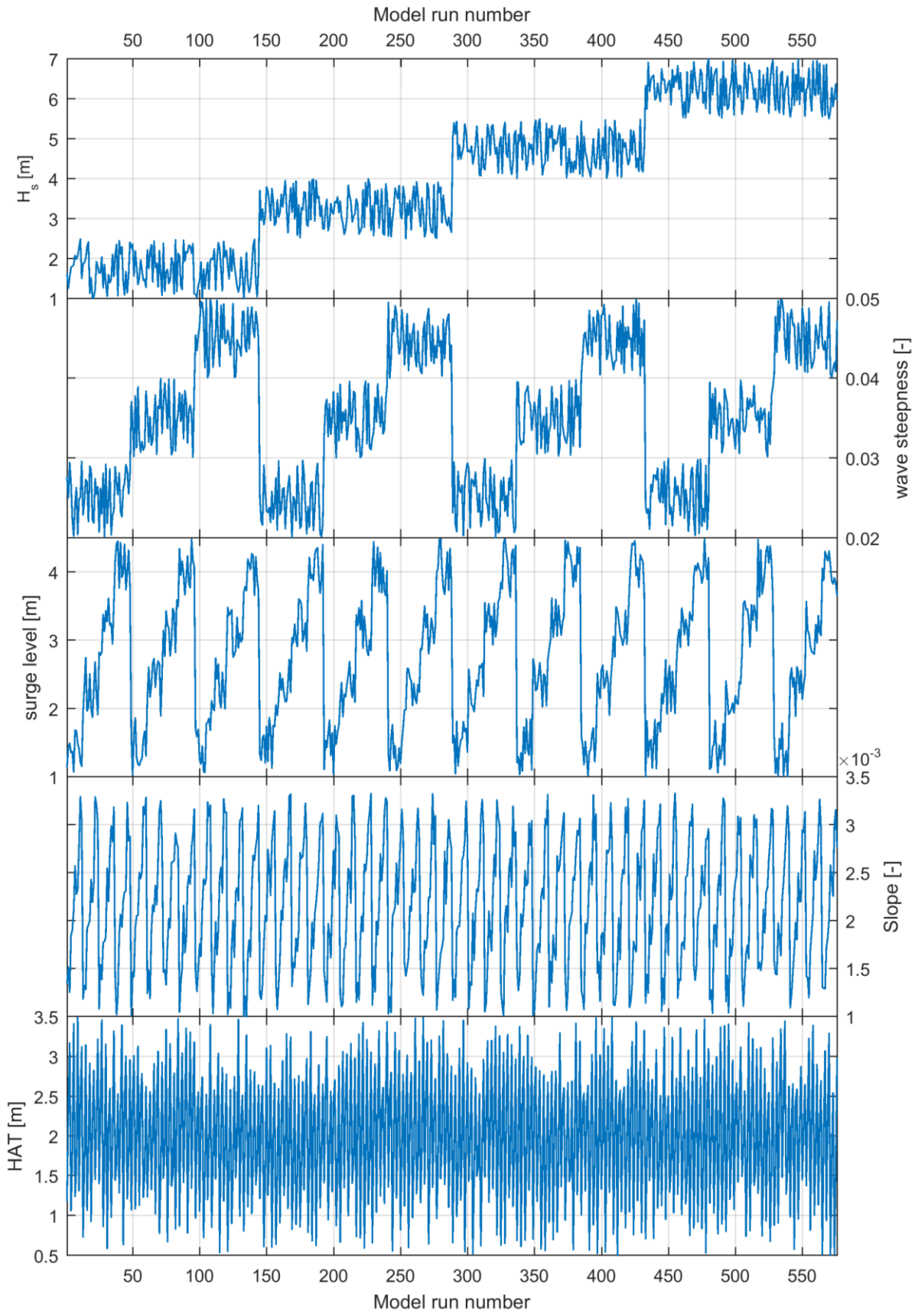

Figure 3.3: Hydrodynamic input parameters for each of the model runs. In order get the input of a specific model run, the corresponding parameter values for each model run number should be paired together.

3.4 Calculation of wave spectrum and outputs for the empirical runup formula

Total wave height and the wave period at the toe of the structure are required as input conditions for the runup formula presented. These input conditions can be derived from wave spectra.

XBeach surfbeat calculates the long wave surface elevation and the short wave height separately. Hence, the high frequency (short wave) spectrum and the low frequency (long wave) spectrum are calculated separately. The total spectrum is then obtained by addition of the spectral density values in the two spectra in the corresponding frequencies.

3.4.1 Calculation of the high frequency (short wave) spectrum.

XBeach provides the short wave height as a point output. The time series of the short wave height at the observation points were used to calculate root-mean-square wave height (H_{rms}). The calculated H_{rms} was then converted to significant short wave height (H_{sw}) using,

$$H_{sw} = \sqrt{2}H_{rms} \tag{3.1}$$

XBeach surfbeat does not calculate a change in the wave period for the short wave height. Hence, the input peak wave period (T_p) combined with the calculated $H_{m0}$is used to calculate a JONSWAP spectrum while keeping the other parameters same as the input.

3.4.2 Calculation of the low frequency (long wave) spectrum

Long wave surface elevation time series at the observation points were used to calculate the long wave spectrum. First the water surface elevation signal was de-trended. The frequency resolution at which the spectral density is calculated was kept at 0.001Hz. The wave signal was then split into smaller overlapping sections using the Welch method with a maximum overlap of 50%. The Welch method reduces the noise in the spectrum in exchange for reducing the frequency resolution. The split segments were then windowed using a Hann window.

3.4.3 Calculation of the wave period and total wave height from the spectra

The total wave height of the model at a point will be due to both the long wave and the short wave height. The significant short wave height at a point can be by the equation 3.1. The long wave height at an observation point can be obtained by the variance in the long wave time series as follows,

$$H_{lw} = 4\sqrt{var(\eta(t))} \tag{3.2}$$

Where H_{lw} is the long wave height and $\eta(t)$ is the wave elevation time series.

The total wave height H_{tot} can be obtained by calculating the wave energy at each band and equating the energy values to the total energy at a point. The resulting equation for H_{tot} can be provided as,

$$H_{tot} = \sqrt{H_{sw}^2 + H_{lw}^2} \tag{3.3}$$

The wave period was obtained from the calculated total wave spectrum by using the spectral moments. The spectral moment m_k is defined as,

$$m_k = \int_{f=0}^{\infty} f^k s(f) df \tag{3.4}$$

Where $s(f)$ is the spectral density at frequency$f$. The wave period $T_{m-1,0}$ can be calculated as,

$$T_{m-1,0} = \frac{m_{-1}}{m_0} \tag{3.5}$$

Figure 3.4 provides the total spectrum derived from the high frequency, low frequency wave spectra and the corresponding wave period ($T_{m-1,0}$) at observation point 2 for an example model run.

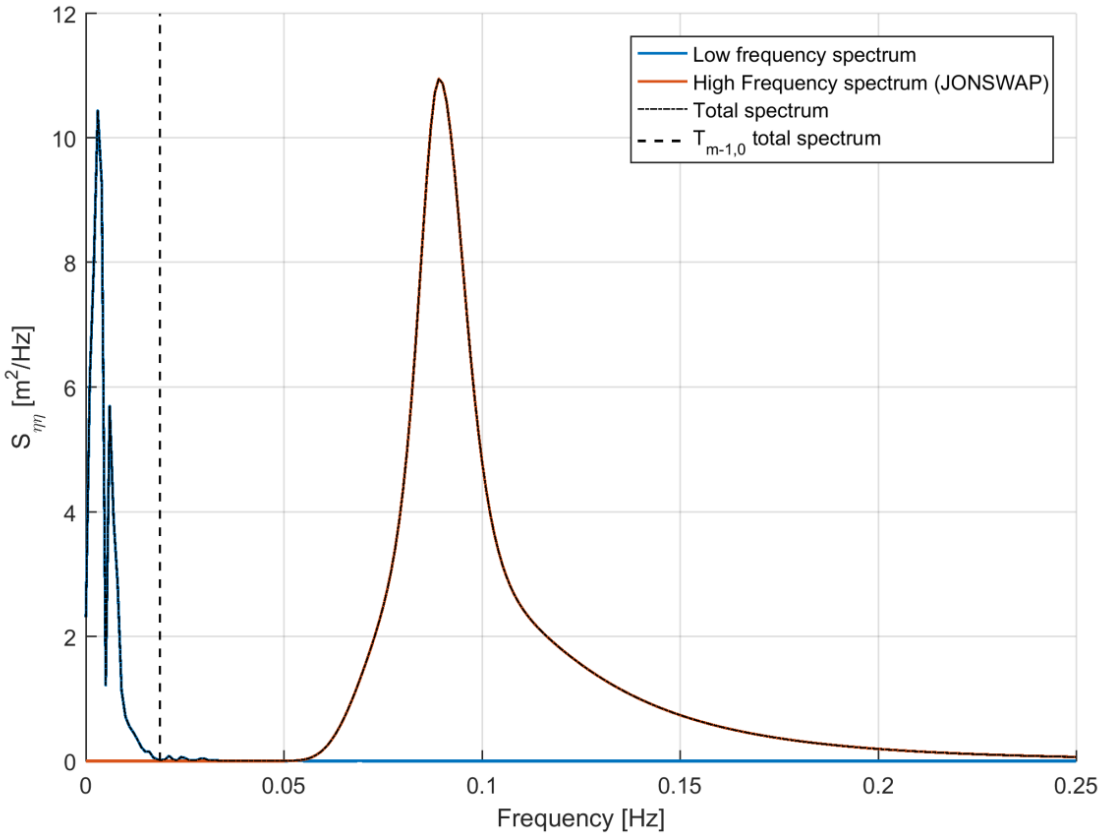

Figure 3.4: Total wave spectrum and the wave period found via the combination of the high frequency and low frequency wave spectra

3.4.4 Splitting the incoming and reflected wave signal

The spectra calculation at the toe of the structure as given above was performed considering both the incoming and reflected wave signal, as most of the reflection was observed before the vegetation. However, in order to calculate the attenuation of the long waves due to vegetation, the incoming component should be split from the reflection component.

The splitting of the signals is performed using the GLM velocity and the water level signal at the observation points. The method is based on Guza, et al, (1984):

$$\eta_{in} = \frac{\eta c_{out} + Q}{c_{in} + c_{out}} \tag{3.6}$$

$$\eta_{out} = \frac{\eta c_{out} - Q}{c_{in} + c_{out}} \tag{3.7}$$

Where η_{in} and η_{out} are the incoming and the reflected wave signals respectively. $Q = uh$ where u is the velocity and h is the water depth.

The long wave height and wave period at the start of the vegetation are calculated in a similar manner as given in section 3.4.3.

4 Analysis

The Analysis chapter presents the investigation of the outputs derived from the XBeach models. The areas of interest were wave setup, wave transformation, energy propagation /dissipation and runup.

The wave setup section starts by looking into the governing equations and to find the dominant processes that affect setup.

Wave height variation within vegetation section is discussed under three main sections. The high frequency, short wave transformation (H_{sw}), the low frequency long wave transformation (H_{lw}) and the total wave transformation (H_{tot}). The H_{sw} and H_{lw} sections start with analyzing the governing equations which affect the wave transformation. Relationships are then made between the different parameters that affect the propagation/dissipation.

The wave energy section primarily focuses on the energy variation of waves in frequency as waves pass through the vegetation.

Finally, wave runup is analyzed at the end of the vegetation using an empirical formula.

4.1 Wave Setup due to vegetation

4.1.1 Analysis of forces affecting the wave setup

Setup is the increase of the mean water level due to the hydrodynamic action on the profile. In the model setup tested an initial storm surge level is prescribed (section 3.2.1). Hence the setup($\Delta\eta$) referred here is the increase in the mean water level above the initial surge level (still water level (SWL)) ($\Delta\eta = \bar{\eta} - SWL$).

The water level variations in the model domain are governed by the nonlinear shallow water equations(NLSWE) (Roelvink et al., 2015) (equation 2.7 & 2.8)

The model results are analyzed only after the model has reached a stationary condition. Hence, it can be assumed that there is no variation of parameters in time. The time varying parameters in equation 2.7 and 2.8 can then be neglected.

The setup due to vegetation will be dependent on the forces acting on the water column. The forces in the water column are balanced by the pressure gradient due to the increased water level. The equation 2.8 can then be rewritten as,

$$g\frac{\partial \eta}{\partial x} = \frac{-\tau_{bx} + F_w + F_v}{\rho h} \tag{4.1}$$

Initial results showed that the bed shear stress is significantly lower within the vegetation where the wave forces (F_w) and the vegetation induced drag force (F_v) dominate. The observation is confirmed by Horstman et al. (2014) where in a field study on mangroves found similar results. Hence, the effect of bed shear in the variation in setup can be neglected.

The short wave energy of the waves starts to dissipate as it encounters the vegetation (equation 2.5). The attenuation of energy results in the reduction of radiation stress. The radiation stress gradient generated results in an onshore directed force (F_w) (equation 2.10). The magnitude of the force will depend on the short wave dissipation rate. Dense vegetation will induce a higher wave force due to the increased dissipation compared to sparser vegetation. The positive F_w force will result in a positive water level gradient (equation 4.1) which will result in a setup.

The vegetation induced force on the water column is composed of a combination of different processes. The force exerted on the water column by vegetation (F_v) during wave propagation, irrespective of the process is given in (equation 2.12). The velocity used in the equation will vary according to the different processes. The components of the vegetation force can be discussed as follows,

The vegetation force can be divided into two main components, the mean drag force ($F_{v,m}$) and wave-induced force due to emergent vegetation ($F_{v,w}$).

The mean drag force ($F_{v,m}$) on the vegetation is from the mean currents due to undertow and infragravity (IG) currents. The IG current induced force can be considered within the mean drag force as the IG wave orbital excursions are much

larger than the spacing between the vegetation (van Rooijen et al., 2016). The total vegetation induced force (F_v) can thus be provided as,

$$F_v = F_{v,m} + F_{v,w} \tag{4.2}$$

In the numerical model scheme, the undertow-induced force is calculated using the Eulerian velocities (U^E). The IG currents induced force is calculated using the Lagrangian velocities (U^L).

The wave-induced force ($F_{v,w}$) is due to the orbital velocity of the waves. Under linear waves, the orbital velocities averaged over a wave period will be zero. Thus, the wave induced force will become zero. However, in the instances of emergent vegetation or nonlinear (skewed) waves the time averaged force will not be zero (van Rooijen et al., 2016). In shallow waters, the waves will be skewed. Furthermore, due to the mangrove tree heights, the vegetation will be emergent as well. Hence the wave induced orbital motion scale forces become important.

For the calculation of the wave-induced force ($F_{v,w}$) an empirical wave shape model is used as XBeach-Surfbeat is a phase averaged model.

The behavior of the wave setup is directly affected by the force calculation on the water column. Neglecting the bed shear stress, the forces acting on the water column will be balanced by the pressure gradient (wave setup).

Wave setup will vary significantly if certain parts of the vegetation force are neglected. To understand the importance of the different components of the vegetation force to wave setup, set of model runs were conducted for a fixed input condition by turning on/off the different vegetation force components. No other parameters were changed between the models. From the output data, the various vegetation forcing can be derived. Since the wave force (F_w) is dependent on the short wave energy dissipation (radiation stress gradient), F_w will be not affected by the changes in the vegetation force exerted on the water column. The Figure 4.1 shows the variation in the setup with different components of the vegetation force.

The undertow currents will be offshore directed which will induce an offshore directed force on the vegetation. Hence an equal and opposite force ($F_{v,undertow}$) will act on the water column in the onshore direction (red line). The positive $F_{v,undertow}$ will result in a positive water level gradient, setup (van Rooijen et al., 2016).

The wave-induced force ($F_{v,w}$) acts in the offshore direction (purple line) of the wave propagation (offshore direction). The negative force will result in a set down (van Rooijen et al., 2016). The direction of the infragravity current related force ($F_{v,IG}$) in the given model (blue line) acts on the onshore direction.

The difference in setup due to the components of F_v can be observed in Figure 4.1. The black line provides the setup variation considering all the forces.

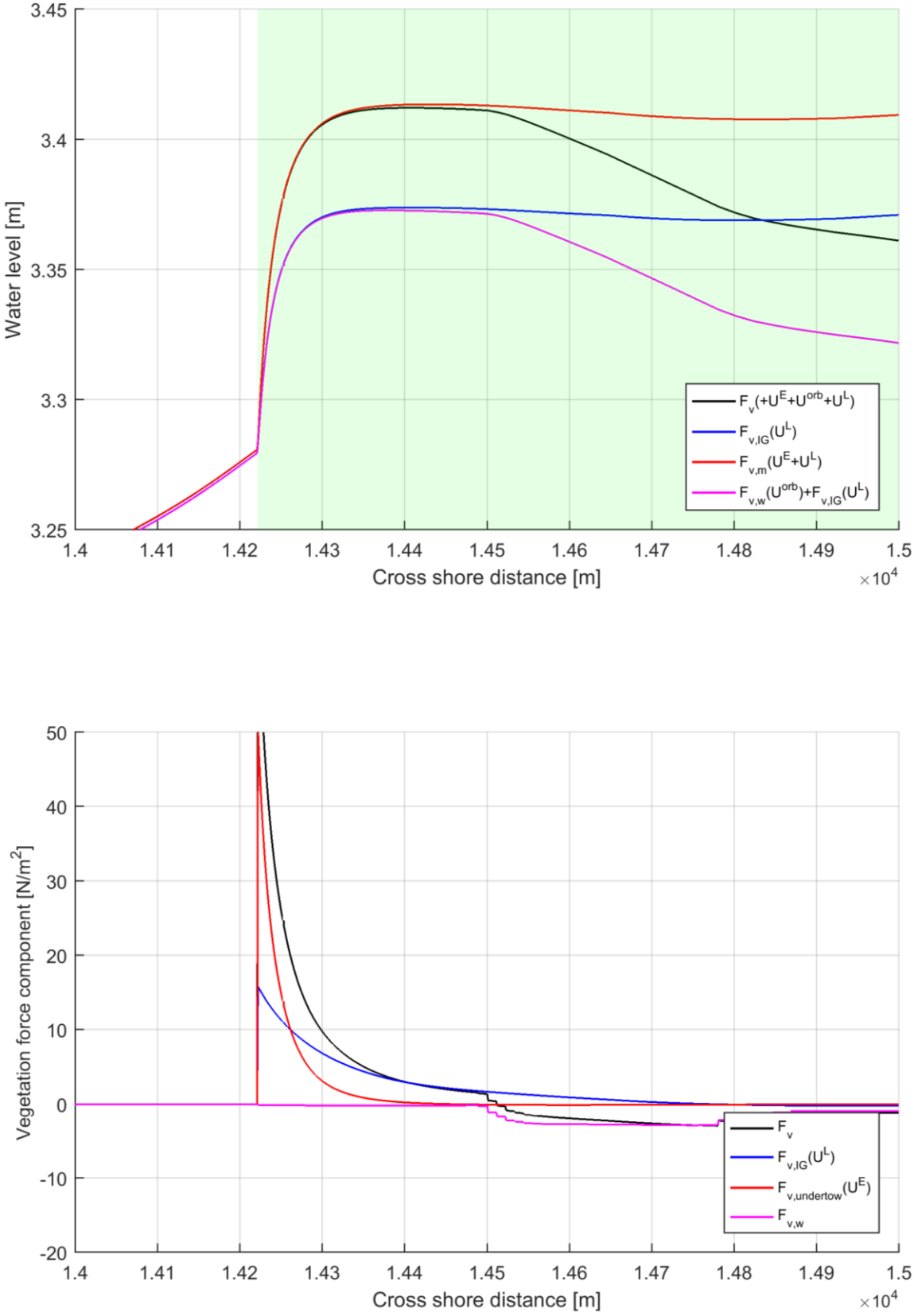

Figure 4.1: Variation in water level across the vegetation width (top plot) according to the different vegetation force components acting on the water column (bottom plot) (for one example model run)

Figure 4.2 provides the setup variation within the vegetation for an example model run considering all vegetation forces. It can be noted that initially, there is an increase in setup. The increase can be associated to the onshore directed wave force and the vegetation force component. A decrease of setup can also be noted. The set down corresponds to the negative vegetation force due to the offshore directed $F_{v,w}$ component.

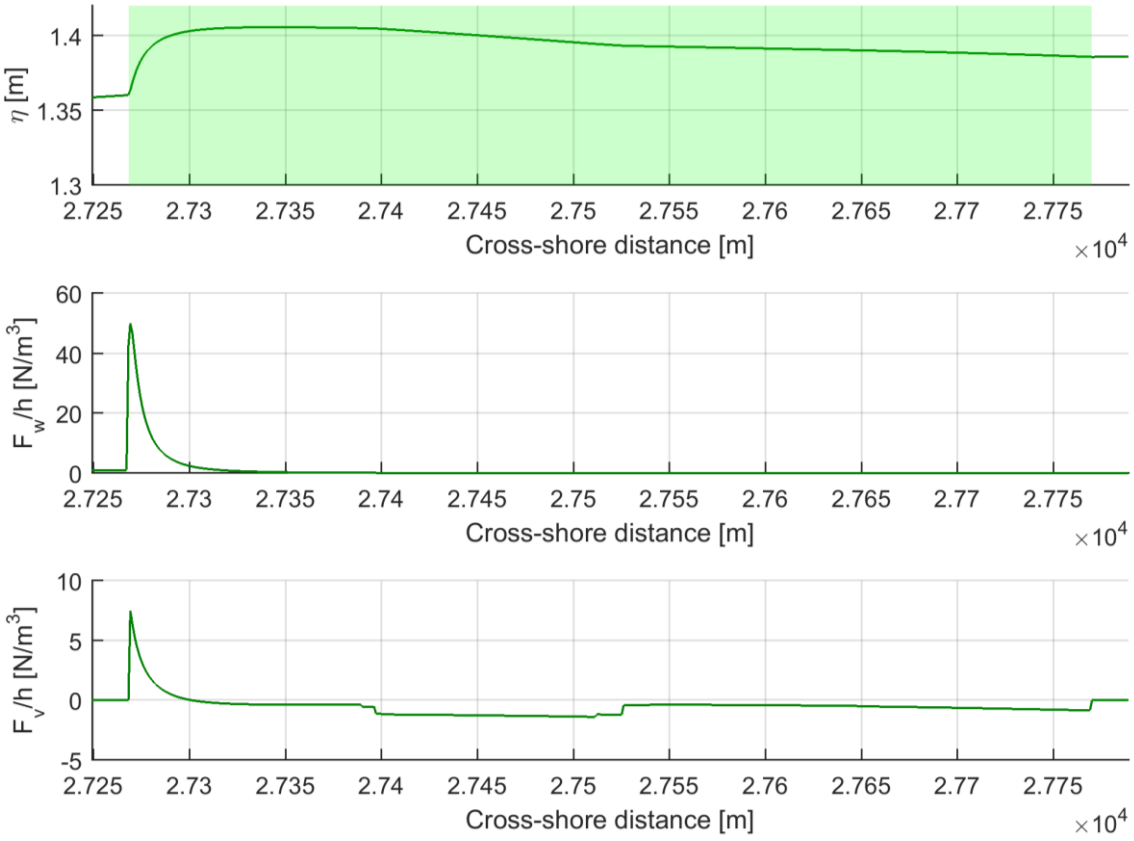

Figure 4.2: Setup variation within vegetation (top plot) and the corresponding forces acting on the water column. Depth averaged wave force due to radiation stress (middle plot) and vegetation force (bottom plot) (for one example model run).

The total force applied on the water column will be the addition of the wave force and the vegetation force. Equation 4.1 was derived from simplifying the momentum equation. The equation can be further reduced (within vegetation) by neglecting the bed shear stress. The equation is then reduced to,

$$g\frac{\partial \eta}{\partial x} = \frac{F_w + F_v}{\rho h} \tag{4.3}$$

If the above made assumptions are correct, the equation (4.3) should be able to correctly model the water level variation within the vegetation. The hypothesis can be checked for its validity by calculating the water level at the end of the vegetation due to the cumulative action of the forces and comparing the predicted value with the water level modeled by XBeach.

The calculation was done as follows. Water level variation within a grid cell (from equation 4.3);

$$\Delta\eta_i = \frac{(F_{wi} + F_{vi})}{\rho g h_i} \Delta x_i \tag{4.4}$$

Where Δx_i is the grid resolution h_i water depth and F_{wi} wave force and F_{vi} vegetation force at a given grid cell (i).

Total variation in the water level within in vegetation;

$$\Delta\eta_{predict} = \sum_{i=1}^{n} \Delta\eta_i \tag{4.5}$$

n is the number of grid cells within the vegetation. The XBeach modeled water level variation can be taken as

$$\Delta\eta_{XB} = Zs_{start\ of\ vegetation} - Zs_{end\ of\ vegetation} \tag{4.6}$$

Figure 4.3 provides the graph between $\Delta\eta_{predict}$ and $\Delta\eta_{XB}$. A satisfactory fit of the hypothesis can be observed for dense and medium dense vegetation cases (RMSE of 8.4 mm, 9.2 mm and 16.8mm for dense, medium and sparse vegetation respectively).

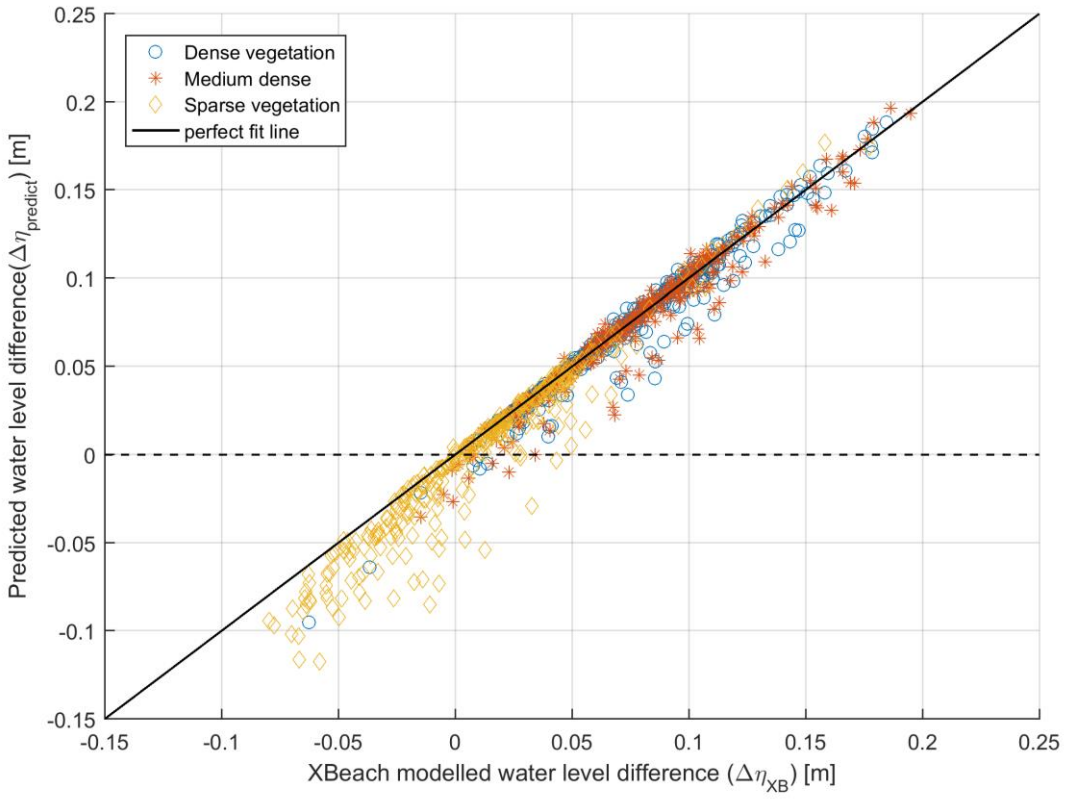

Figure 4.3: XBeach modeled water level difference vs. the Predicted water level difference across the vegetation (results for three mangrove densities and all model runs). The points above the dashed line corresponds to a setup and points below to a set down compared to the water level at the start of the vegetation.

It can be observed that the XBeach modeled water level and the predicted water level using the hypothesis agree satisfactorily. Hence, it can be concluded the wave setup within vegetation can be explained by F_w and F_v.

A deviation from the hypothesis is observed for models where a set down is experienced. The deviation is such that the predicted (calculated) water level is over predicting the reduction. One reason for the deviation was found to be as very shallow water depths at the calculation point. Since the forces are depth averaged, at very shallow water depths, the forces calculated will increase considerably, over predicting the reduction. Since sparse vegetation shows more reduction in the water level as the wave propagates (Figure 4.5), results for sparse vegetation are more susceptible for the deviation.

4.1.2 Effect of vegetation on setup

From the findings of the previous section, it can be concluded that the water surface elevation variation within the vegetation will be governed predominantly by the wave force and the vegetation force. Since the different force components are dominant at different locations the water level variation will change across the vegetation. The forces are also highly influenced by the vegetation density.

Figure 4.4 provides an example model results of setup variation across the vegetation for different vegetation densities. The figure also provides the wave force (F_w) and the vegetation force (F_v) acting on the water column. Significant differences in water level for the different vegetation densities can be observed.

The denser vegetation has a larger positive force due to the higher short wave dissipation (equation 1.5). The wave force reduces with the decreasing vegetation density. The resultant increase in setup within the less dense vegetation can also be noticed to be smaller than the denser vegetation.

Figure 4.4 also provides the water level variation for the non-vegetated case. In the non-vegetated case, the setup depends on the dissipation of energy due to wave breaking and the bed shear stress. Due to wave breaking induced radiation stress gradient, a setup in the non-vegetated case can be observed.

It can also be observed that the location of the maximum setup varies for the different vegetation (Figure 4.2). As the denser vegetation dissipates the wave energy at a higher rate, the short wave energy will reduce quickly. The resulting wave force only acts along a small distance. As the vegetation becomes less dense, the dissipation rate per unit length will be less. The reduced dissipation rate of energy will result in short waves propagating further into the vegetation. Thus, the wave force will prevail for a longer distance in sparser vegetation compared to dense vegetation. The difference in the wave force action length consequently affects the setup. Higher density vegetation has the maximum setup forming more at the front of the vegetation compared to less dense vegetation.

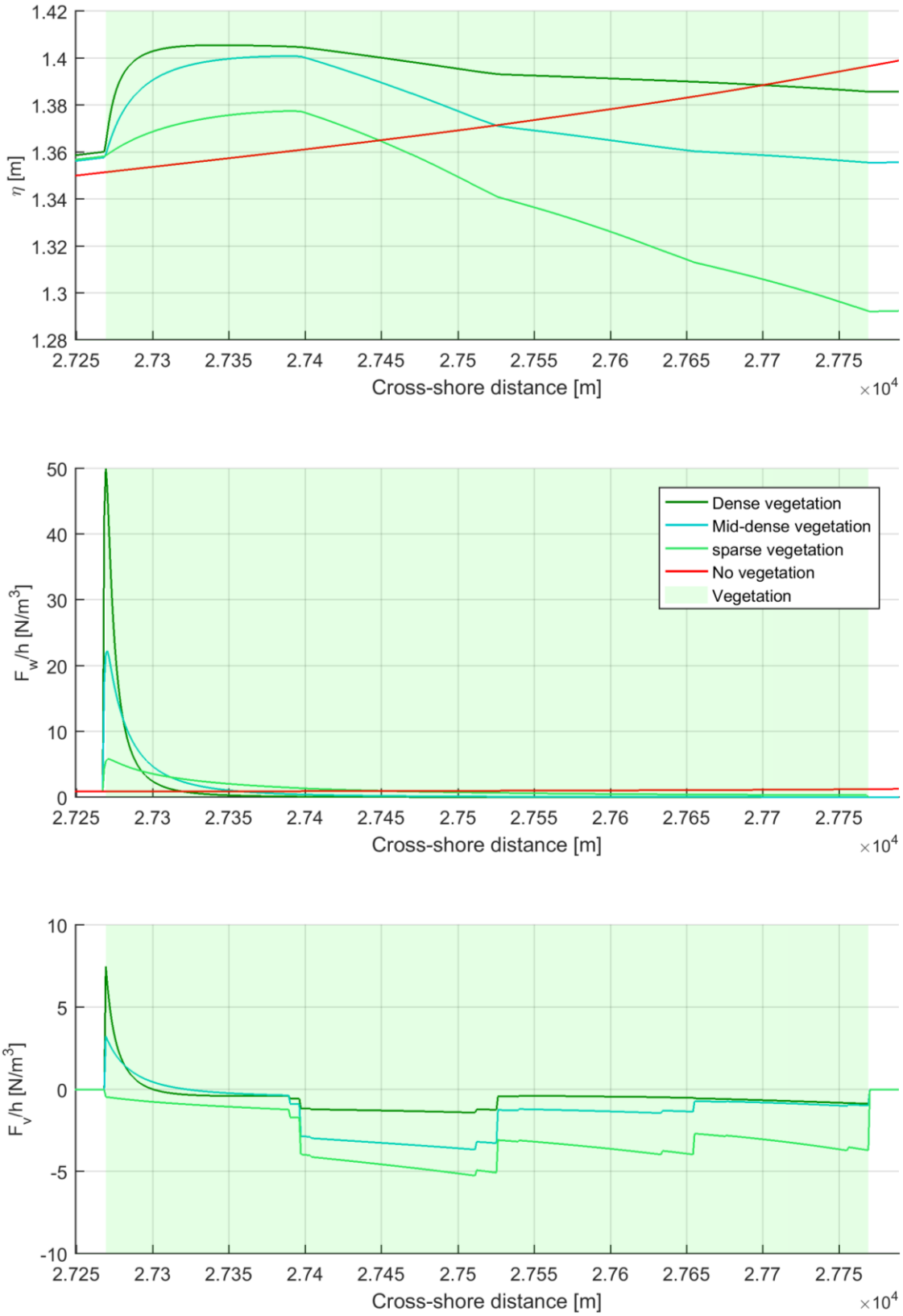

Figure 4.4: Variation of wave setup across the vegetation (top plot) and the corresponding wave force (F_w) (middle plot), vegetation force (F_v) (bottom plot) acting on the vegetation for the different vegetation densities. The green shade shows the width of the vegetation (for one example model run).

The short wave energy dissipation becomes small (smaller F_w) as the wave propagates through the vegetation. Hence, the wave-induced vegetation force ($F_{v,w}$) becomes dominant reducing the water elevation. Contrast to the wave force, sparse vegetation shows a higher $F_{v,w}$, resulting in a larger reduction in water level.

In cases where the increased setup due to rapid short wave energy dissipation by vegetation will not reduce, a higher water level than the non-vegetated case can occur at the end of the vegetation. This increased water level at the end of the vegetation is an undesirable outcome when using vegetation to reduce coastal hazards. Figure 4.5 provides the setup values for all model runs at the end of vegetation relative to corresponding non-vegetated cases. 50% of the models in dense vegetation case results in a lower setup compared to the non-vegetation case. For the medium and sparse vegetation, the percentage stands at 59% and 83% respectively.

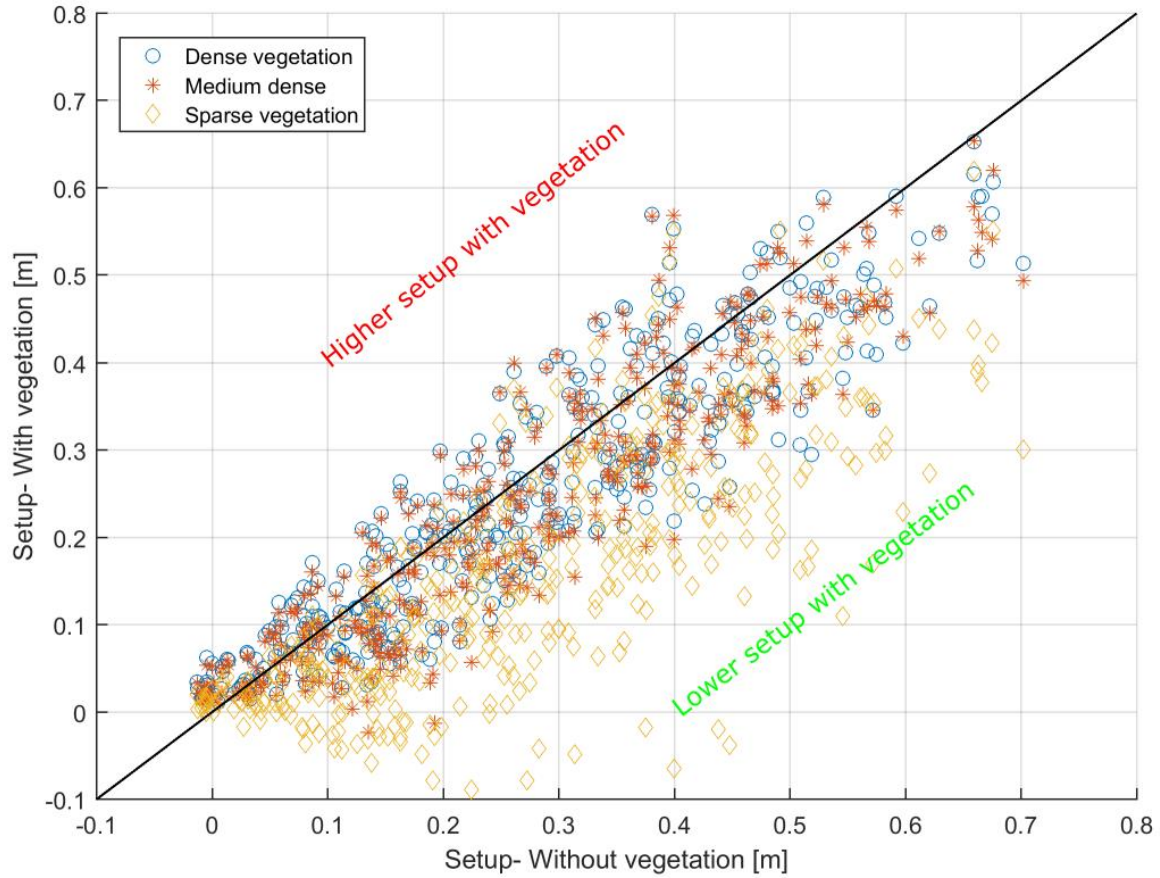

Figure 4.5: Comparison of the setup at the end of vegetation of each model compared with the corresponding non-vegetated case (all model cases). The data points above the black line refers to cases with higher setup than the non-vegetated model and points below the line shows the models where the setup is lower than the non-vegetated case.

It is observed that for sparse vegetation a reduced setup is achieved for most of the models. Denser vegetation fails to reduce the setup compared to the sparse vegetation.

The setup is reduced due to $F_{v,w}$. From Figure 4.4 it can be observed that the in less dense vegetation a larger $F_{v,w}$ force is induced on the water column compared to dense vegetation thus reducing the setup.

$F_{v,w}$ occurs due to the orbital velocity induced drag on the vegetation. The wave orbital velocity will be a function of the short wave height, wave period and the water depth (van Rooijen et al., 2016). Figure 4.6 presents the total force and short wave height variation across an example model run for all three vegetation densities. It can be observed the total force changes direction (becomes negative) for less dense vegetation at a higher short wave height compared to dense vegetation.

The onshore directed force (positive component) comprises of the wave force F_w and $F_{v,m}$. F_w depends on the radiation stress gradient due to vegetation (equation 1.5). For the same hydrodynamic input conditions, denser vegetation will induce a larger F_w force. $F_{v,m}$ depends on the undertow current magnitude (U^E). Similar to the wave force denser vegetation will provide a higher $F_{v,m}$(equation 1.11) for the same undertow current.

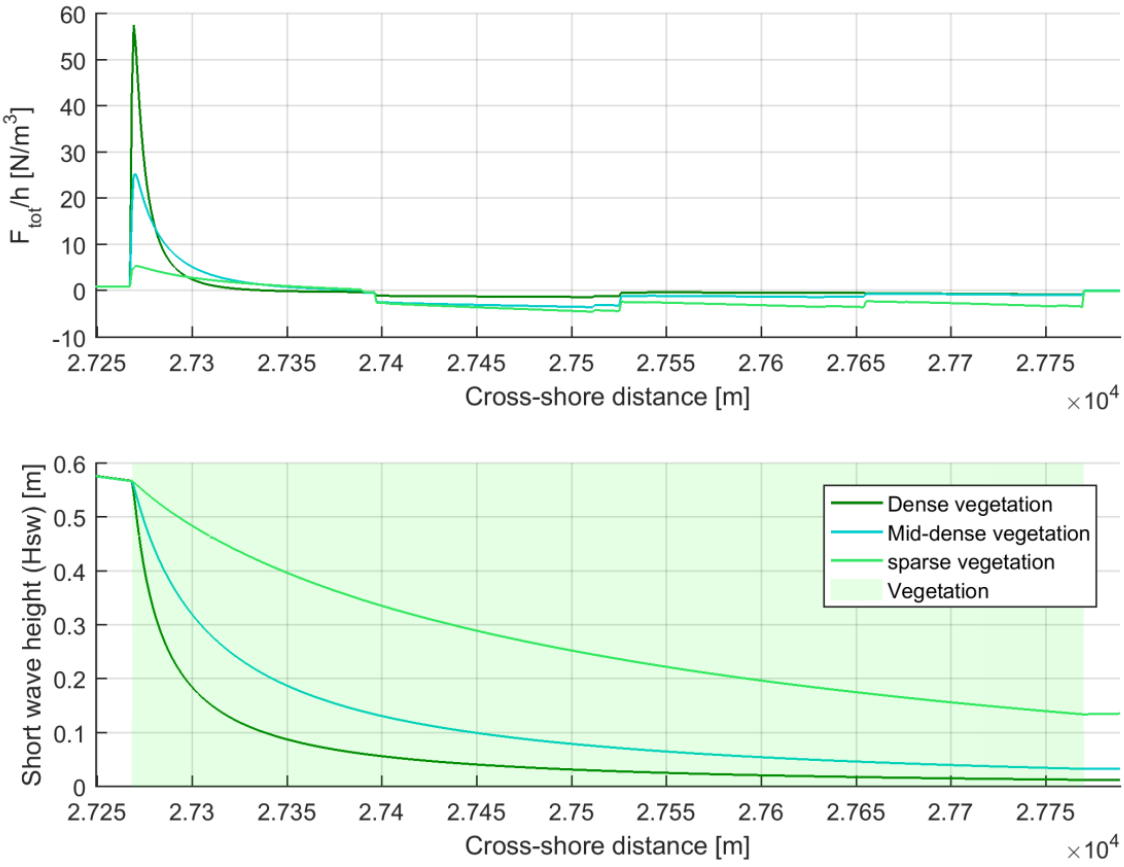

Figure 4.6: Variation of depth averaged F_{tot} (top plot) and short wave height (bottom plot) across the vegetation for three densities of mangrove vegetation (for one example model run).

Since dense vegetation induce higher positive forces, $F_{v,w}$ cannot become dominant in the total forcing as the comparative magnitude of $F_{v,w}$is much smaller than the other forces (Figure 4.1). Thus, in denser vegetation, for the $F_{v,w}$become dominant the short wave height has to reduce a lot. $F_{v,w}$ is also a function of the short wave height. Even

when $F_{v,w}$ start to dominate the total force, as the wave height is small $F_{v,w}$ will be low in magnitude.

In lesser dense vegetation, as the $F_w$and $F_{v,m}$ induced by the vegetation will be comparatively small, $F_{v,w}$ will start to dominate at larger wave heights (Figure 4.6). Since $F_{v,w}$ is dominating at higher wave heights, $F_{v,w}$ will be large. Larger $F_{v,w}$ will then lead to a lowered vegetation setup.

From all the model runs, the short wave height at the point where the total wave force changes direction was obtained. The mean wave height at direction change for all models for dense vegetation stood at 0.17m while the wave height for medium dense and sparse vegetation was at 0.25m and 0.61m respectively.

From the results obtained, the setup due to the vegetation reduces with reducing vegetation density. However, as the vegetation density reduces even further, the setup should trend back to the non-vegetated model results.

Figure 4.7 provides the setup variation across the vegetation for increasing sparseness in vegetation. N_v of the vegetation is changed in the models (Table 4.1) while keeping all the other parameters constant. The density of vegetation used in the models runs are provided in Table 4.1.

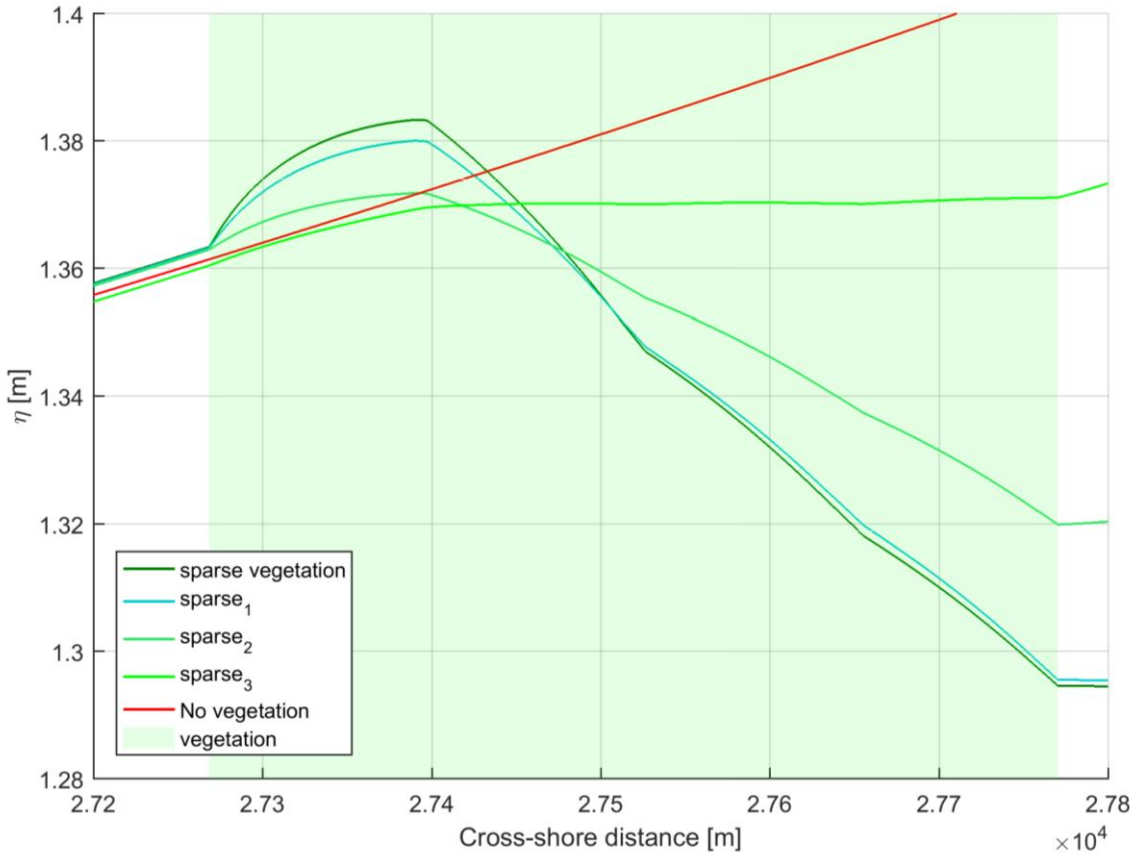

Figure 4.7: Wave setup variation across vegetation width for increasing sparseness in density of vegetation. The green shade represents the vegetation forest width.

Table 4.1: vegetation density in increasing sparse vegetation

Vegetation	N_v
sparse vegetation (original)	13
sparse$_1$	10
sparse$_2$	5
sparse$_3$	1

It can be observed that, as the vegetation density reduces even further, the setup trends back to the non-vegetated model result. Hence it can be concluded that the wave setup reduction in sparse vegetation reaches a maximum at a certain density and the will limit back to the non-vegetated setup with increasing sparseness.

The initial surge level within the vegetation will have an effect on the propagation of the short wave within vegetation (section 4.2.1). Higher water depth will have a lower dissipation compared to lower water depths. Hence at deeper water depths, for the total force to change direction ($F_{v,w}$ become dominant) the waves will have to propagate further into the vegetation.

4.2 Wave transformation through vegetation

Transformation of waves through vegetation can be discussed under three main headings; the transformation of short waves, transformation of long waves and the total wave height transformation. There are fundamental differences in theory for the growth, transformation and dissipation of the short and long waves.

4.2.1 Transformation of short waves

From equation 1.10 It can be noted that the other than the vegetation parameters, the vegetation dissipation is also a function of wave height, wave period and the water depth. The variation in D_v with wave height and water depth is presented in Figure 4.8. As expected the energy dissipation increase with short wave height($D_v \propto H^3$) . Water depth also plays a significant role in energy dissipation. For a given short wave height, a shallower water depth induces a higher dissipation of energy by vegetation and vice versa for deeper water depths.

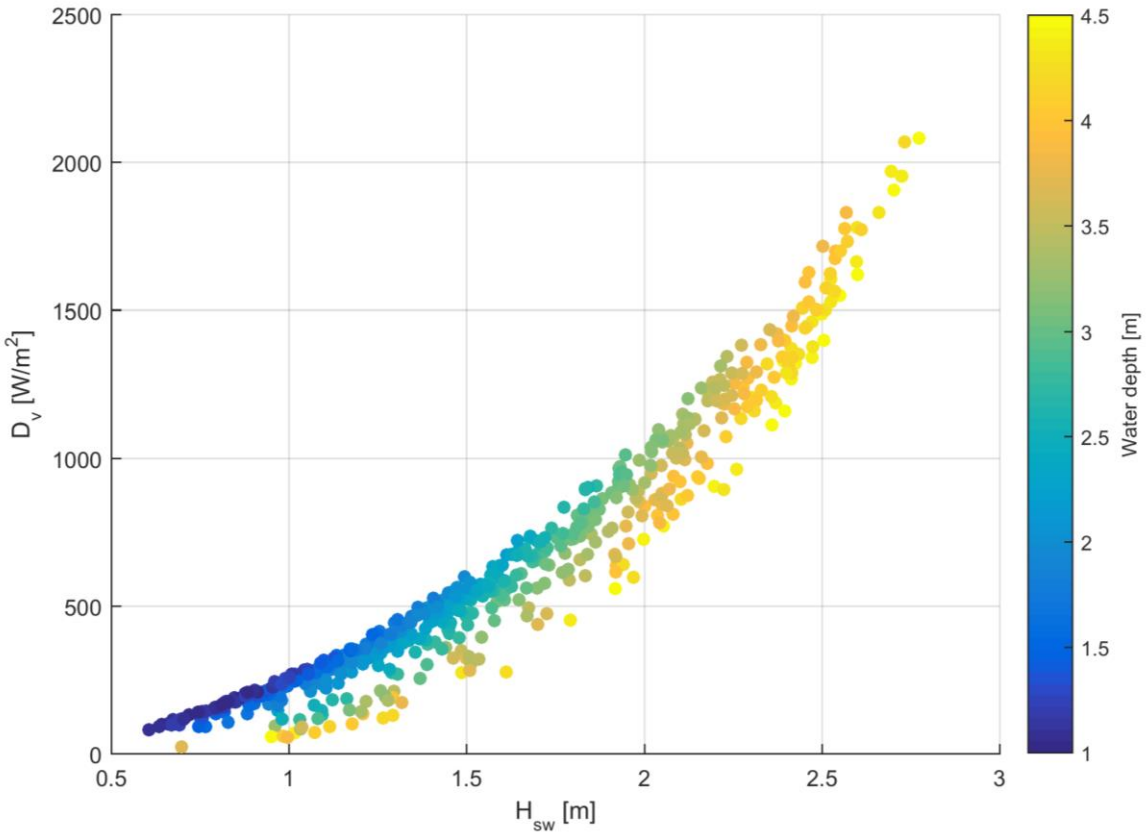

Figure 4.8: Variation in dissipation of energy due to vegetation for dense vegetation case with short wave height and the depth of water (dissipation values measured at observation point 2 for all models).

A relationship with wave period and the energy dissipation was also observed where longer wave periods induced higher energy dissipation.

The dissipation of energy within the vegetation will govern the wave height through the vegetation. Figure 4.9 provides short wave height (H_{sw}) variation across the vegetation for one of the model runs. As expected, the dense vegetation shows the largest attenuation in wave height and sparse vegetation shows the lowest. The non-vegetated model shows an almost linear reduction in wave height which can be associated with wave breaking. An interesting observation is that most of the wave attenuation occurs within few meters of the vegetation. This observation is also backed by field studies done by Knutson et al. (1982) and Möller & Spencer (2002).

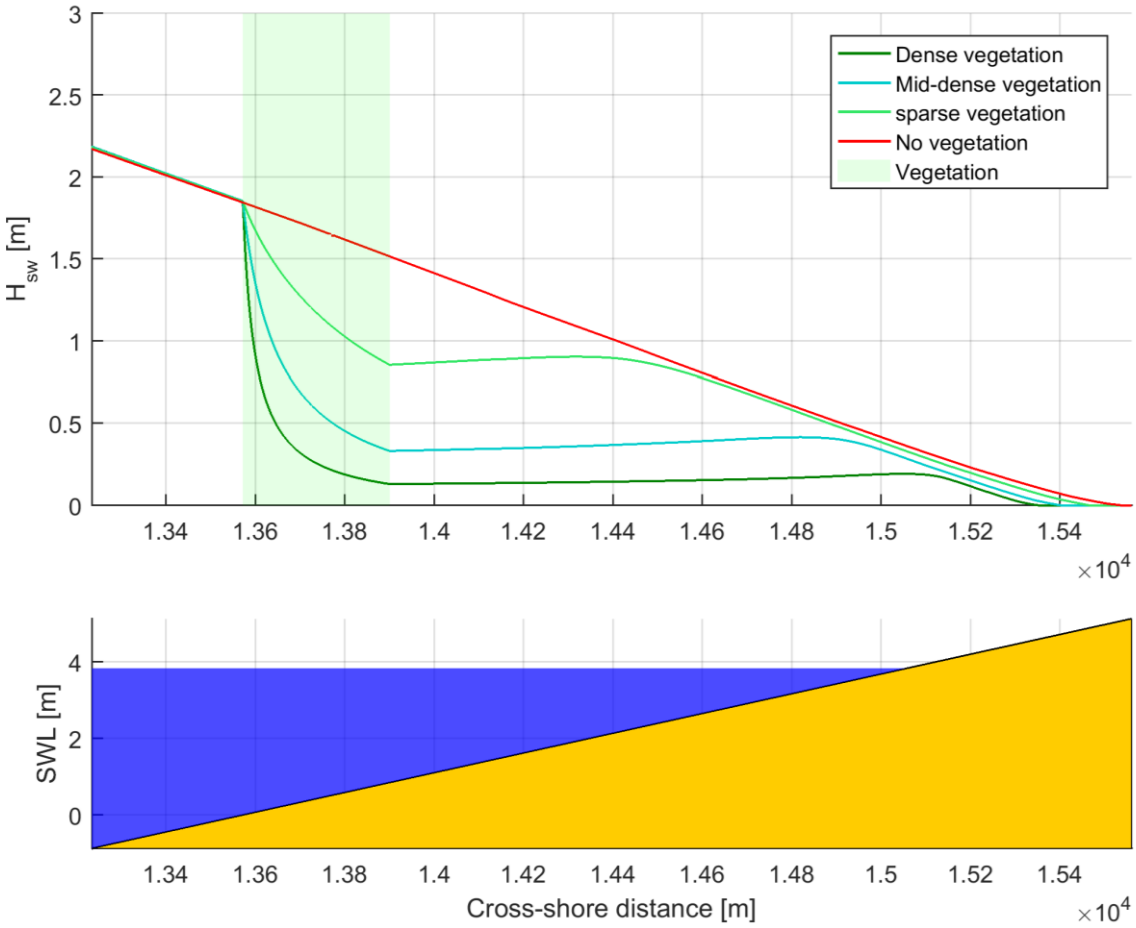

Figure 4.9 : Short wave height variation across the vegetation width for different vegetation densities (for one example model run). The bottom plot shows the SWL and the bed profile.

The rate of short wave attenuation across the vegetation can be calculated as the reduction in short wave height (ΔH_{sw}) as a ratio of the vegetation width required for the reduction (x) (equation 2.1). Figure 4.10 provides rate of short wave attenuation achieved by the models according to the wave height and the water depth. The attenuation rate is calculated by the wave height attenuation observed within the first 100 m of the vegetation. The short wave height at the start of the vegetation is taken as a proxy to the wave height variation across the vegetation. It should be noted that the wave attenuation rates will change significantly (the pattern will not change) with the chosen distance for the calculation due to the nonlinear wave attenuation pattern within the vegetation (Figure 4.9).

The attenuation rate increase with the wave height due to the increase in energy dissipation by vegetation at larger wave heights (equation 1.5). The water depth also has a clear effect where deeper water depths show a reduced attenuation while shallower depth shows a larger attenuation rate. The observation is consistent with the results in the energy dissipation (Figure 4.8). Similar pattern of wave attenuation can be observed for medium dense and sparse vegetation with lower attenuation rates compared to denser vegetation (Figure 4.11).

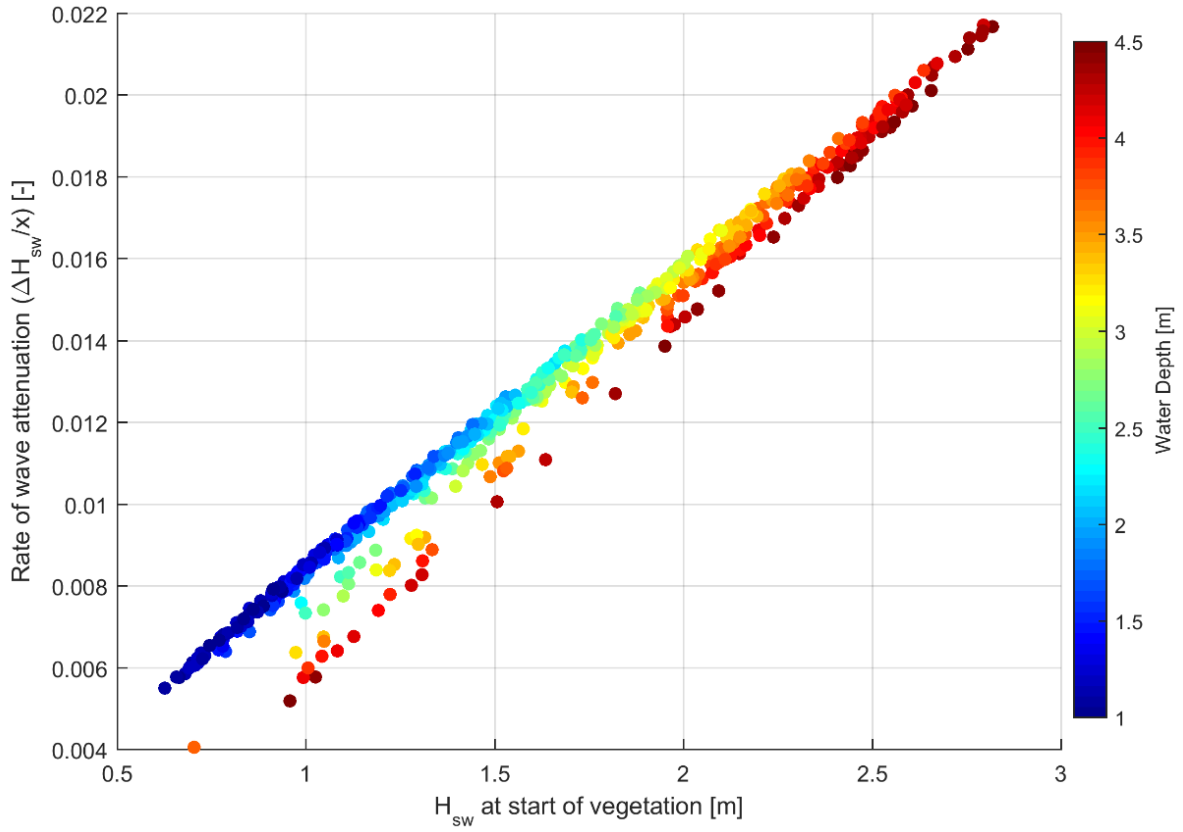

Figure 4.10: Rate of short wave attenuation across the dense vegetation as a function of the wave height and water depth for all model runs.

Table 2.2 provided wave attenuation rates observed in field studies for mangroves. Since exact mangrove densities and wave conditions are not known in these field studies, direct comparison of values cannot be made. However, it can be noticed that the attenuation rates found in the numerical model is larger than values observed in the field. For example, in the study by Mazda et al., (1997) a attenuation rate varying from $1.5x10^{-3}$ m^{-1} - $2.2x10^{-3}$ m^{-1} was observed for dense vegetation over 100m. In the numerical model, the range stands at $4.0x10^{-3}$ m^{-1} - $2.2x10^{-2}$ m^{-1}. In the same field study, sparse vegetation also provided lower dissipation rates than the numerical model.

However, the dense mangrove vegetation in the field study is much shorter with a height of only of 1m whereas the numerical model study the vegetation was taller (Table 3.2) which leads to a higher attenuation. Furthermore, the observations in the field studies provided in Table 2.2 are made at low wave heights (order of centimeters). The wave heights applied in the numerical model is higher than the field observations which will also lead to a larger attenuation rate compared to the field studies.

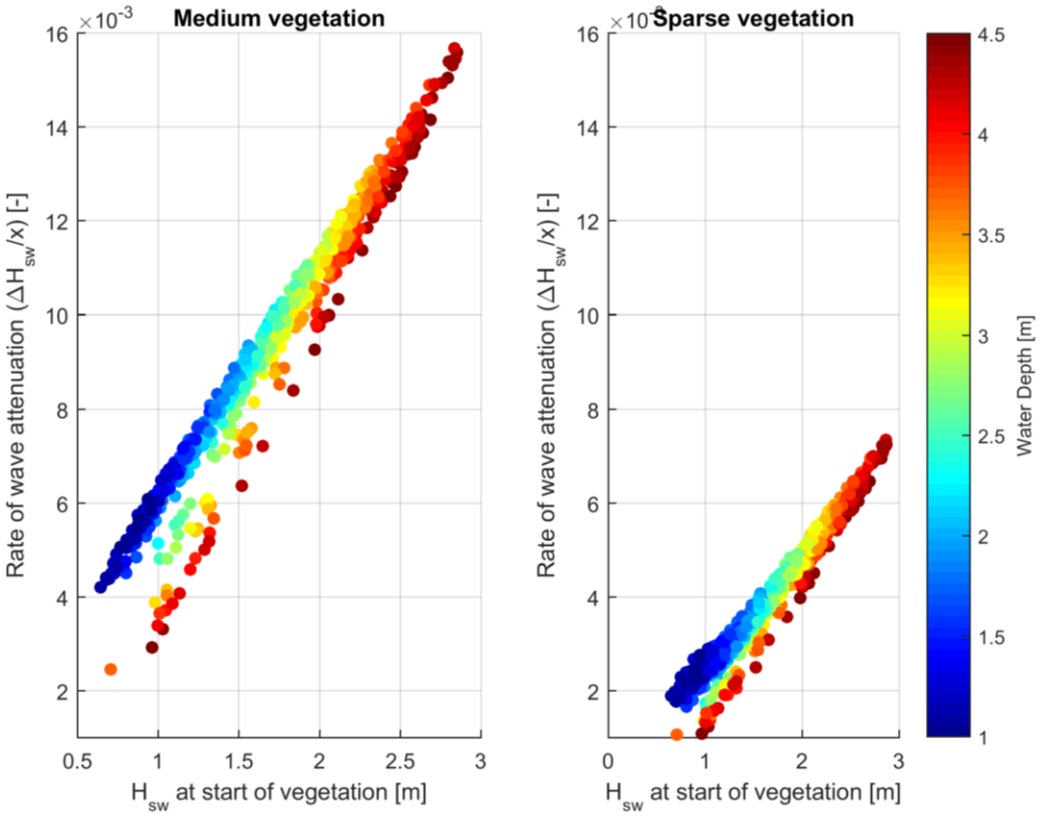

Figure 4.11 Rate of short wave attenuation across the medium and sparse dense vegetation as a function of the wave height and water depth for all model runs.

Figure 4.12 provides the vegetation width needed for attenuation of short wave energy by 90% for the dense vegetation case. Contrary to the observations made earlier, majority of the model outputs show an increase in propagation distance with increasing wave height.

Results in Figure 4.12 show that cases which have a deeper water depth propagates further into the vegetation for a given wave height. It can be assumed that the shorter wave propagation distances observed in the lower wave heights occurs due the shallow water depths which increases attenuation (Figure 4.10).

To check the assumption, a new set of model runs were performed with the same incident wave heights and wave periods as the current model runs. The slope and the storm surge level were made constant for all the input conditions. A slope of 1/500 and a surge level of 3.5m were used. By making the slope and the surge level constant, the water level variation across the model was made the same for all runs. The dissipation distance required in the short wave energy for the new set of model runs were also analyzed. The resulting distances are given in Figure 4.13. A significant difference in the propagation/attenuation of the short waves can be observed between the two sets of results. Figure 4.13 shows a drastic reduction in distance of propagation as the wave height increases. The results also suggest influence of the wave period in the dissipation distance is small.

From the difference between the results of the two sets of model runs it can be concluded that the reason for the reduced wave propagation distance in the lower short

wave heights is due to the shallow water depths. Attenuation of short wave energy is pronounced at low water depths which would hamper the propagation of the wave within the vegetation.

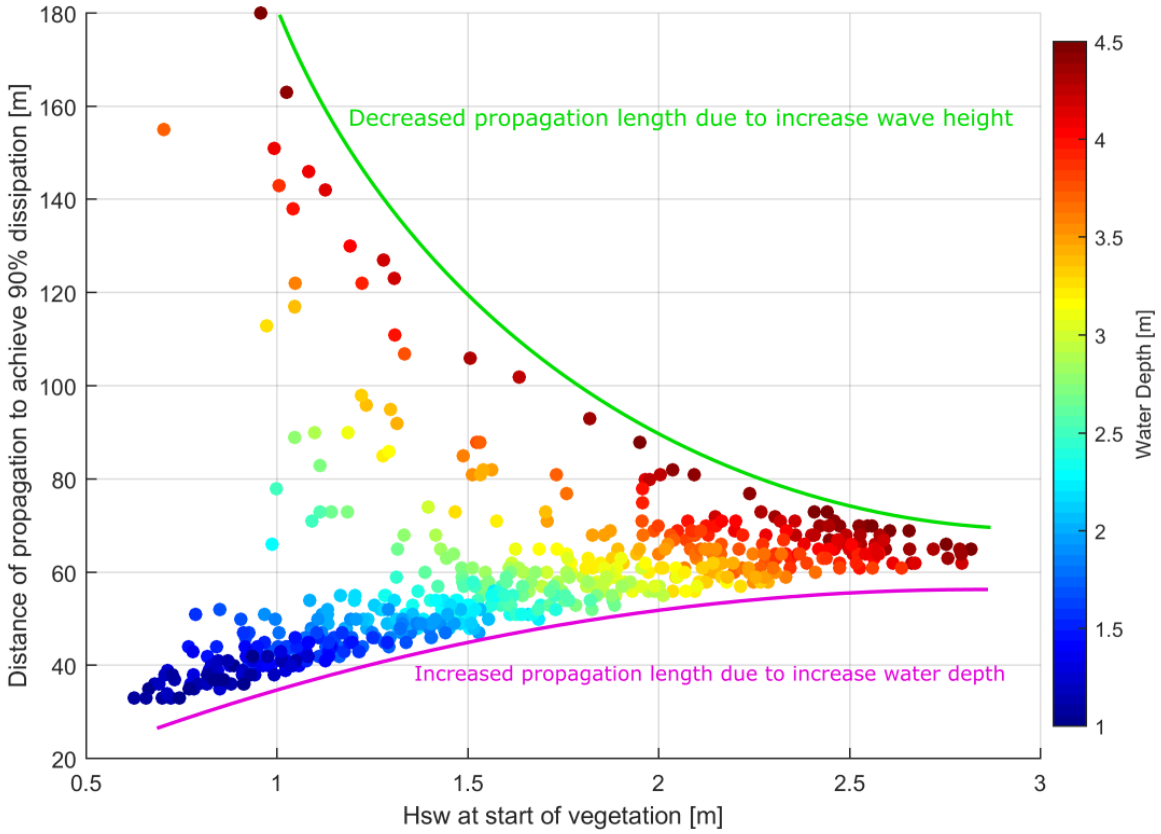

Figure 4.12: Vegetation width needed for attenuation of short wave energy by 90% (for all dense vegetation model cases). The point colors represent the water depth.

Finally, it can be concluded that the water depth within the vegetation is a crucial factor in wave transformation through vegetation. A reduction in energy attenuation by vegetation (increase in propagation distance) was also observed with increasing water depths in studies performed by Horstman et al. (2014) and Tschirky et al. (2001).Through field and laboratory observations, the studies found a reduction in wave attenuation with increasing water depths.

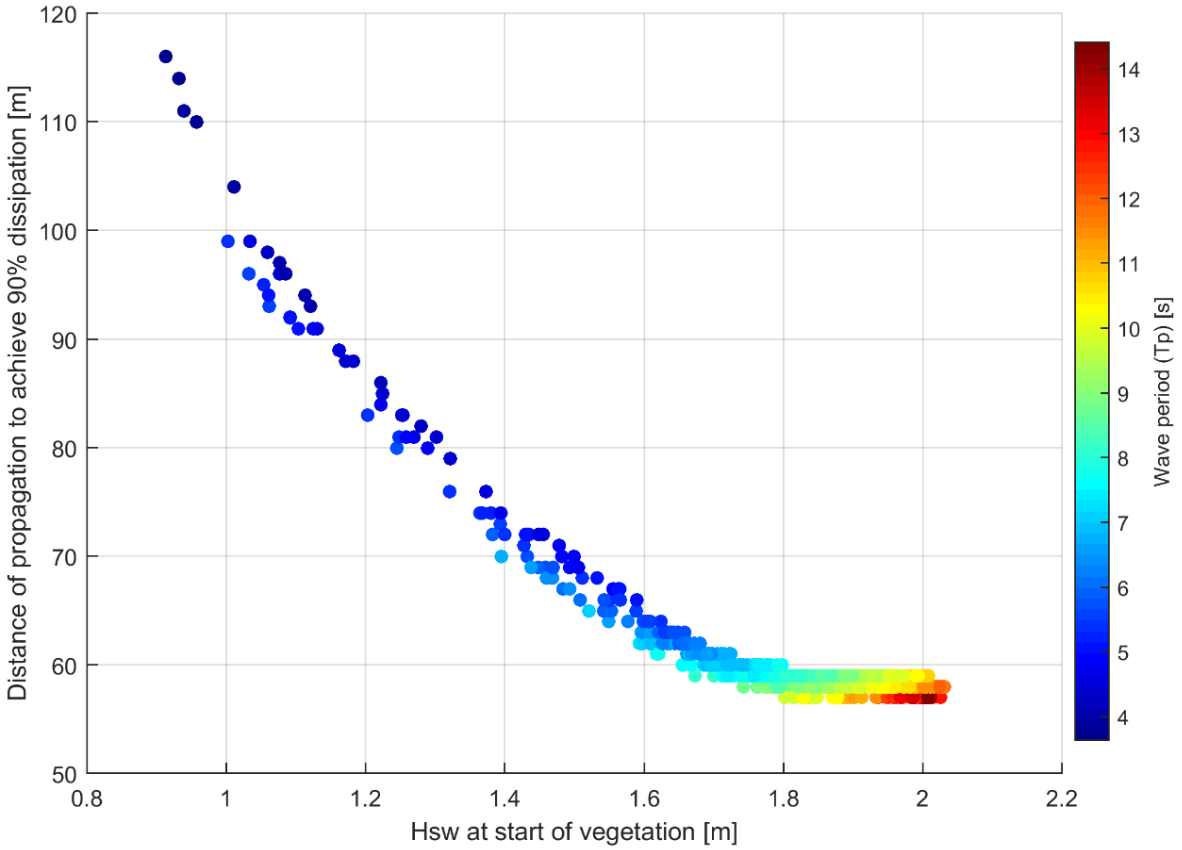

Figure 4.13: Vegetation width needed for dissipation short wave energy by 90%. Results for the models with same profile slope and surge level. Data point color provides the wave period.

4.2.2 Transformation of long waves

Transformation of long waves are important in the vegetation context as they become prominent over the short wave after certain distance of propagation within the vegetation (Horstman et al., 2014) . The increase in long wave energy over the short wave energy can also be observed in section 4.4.

The long wave surface elevation due to forced long waves in a uniform depth is provided by Longuet-Higgins & Stewart (1964) which has been approximated by Battjes et al. (2004) as ,

$$\eta_{lw} \cong -\frac{S_{xx}}{\rho\sigma^2 h^2} \tag{4.7}$$

Where, S_{xx} is radiation stress and σ the wave frequency and h the water depth. It should be noted that the equation 4.7 is only valid for a uniform depth sea bed.

For larger forcing (higher short waves) at a certain depth the forced long waves will be higher. The wave frequency also affects the amplitude of the wave with larger wave periods resulting in higher wave heights.

The growth/shoaling of the long wave amplitude across a sloping bottom is a function of h^{-a} where a depends on the normalized bed slope (van Dongeren et al., 2007). The normalized bed slope is defined as,

$$\beta = \frac{h_x}{\omega}\sqrt{\frac{g}{h}} \tag{4.8}$$

Where, $h_x$is the bed slope, ω is the radial frequency of the long waves and h is the characteristic depth. van Dongeren et al. (2007) uses the wave breaking depth as the characteristic depth. Values of $\beta < 0.3$ corresponds to a strong growth of the long waves. Since the bed slopes used in this study are very mild (1/300 -1/1000) all models in this thesis fall into this category.

van Dongeren et al., (2007) found that a reduced with increasing β. Hence, growth of the shoaling long waves will increase with increasing β (steeper slopes and longer wave periods).

4.2.3 Attenuation of long waves due to vegetation

Figure 4.14 provides an example model run of long wave transformation across a vegetation patch. Even though the incoming wave signal is equal in all four cases presented (3 vegetation densities and non-vegetated case), an increase of wave heights before the vegetation can be observed for the vegetated models.

The increase can be associated with the reflection generated due to the vegetation. Variation in long wave height offshore of the vegetation relative to a no vegetation case was also observed in a study by Tang et al. (2017). The study claimed the variation occurred due to the phase differences in incoming and reflected waves due to the vegetation.

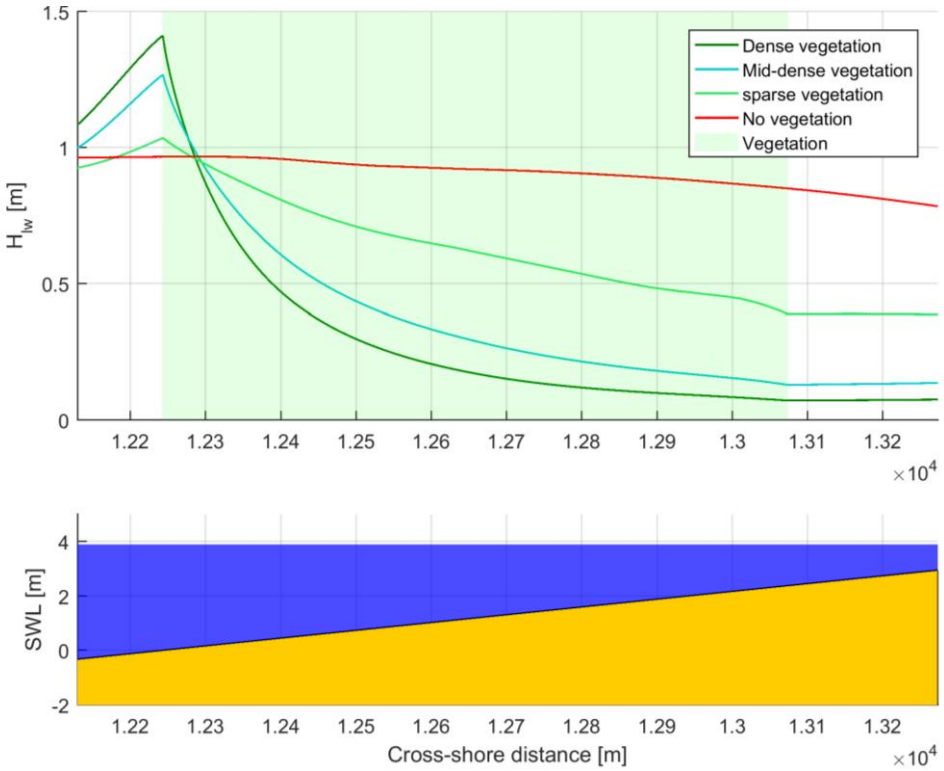

Figure 4.14: Long wave height (total) variation across a vegetation patch for different vegetation densities and no-vegetation case. The bottom plot provides the bed profile at the location (for one example model run).

The model output long wave signal is split at the start of the vegetation in order to identify the long wave height of the incoming wave as given in section 3.4.4. Figure 4.15 provides the split reflected and the incoming wave signals for the total output wave signal given in Figure 4.14. The attenuation of the incoming wave signal height as the wave passes through the vegetation can be observed.

The reflected wave height increases in the offshore direction due to the accumulation of reflection signals. A quick increase in reflected wave height can be observed near the start of the vegetation. The increase is higher for dense vegetation and reduces with vegetation density.

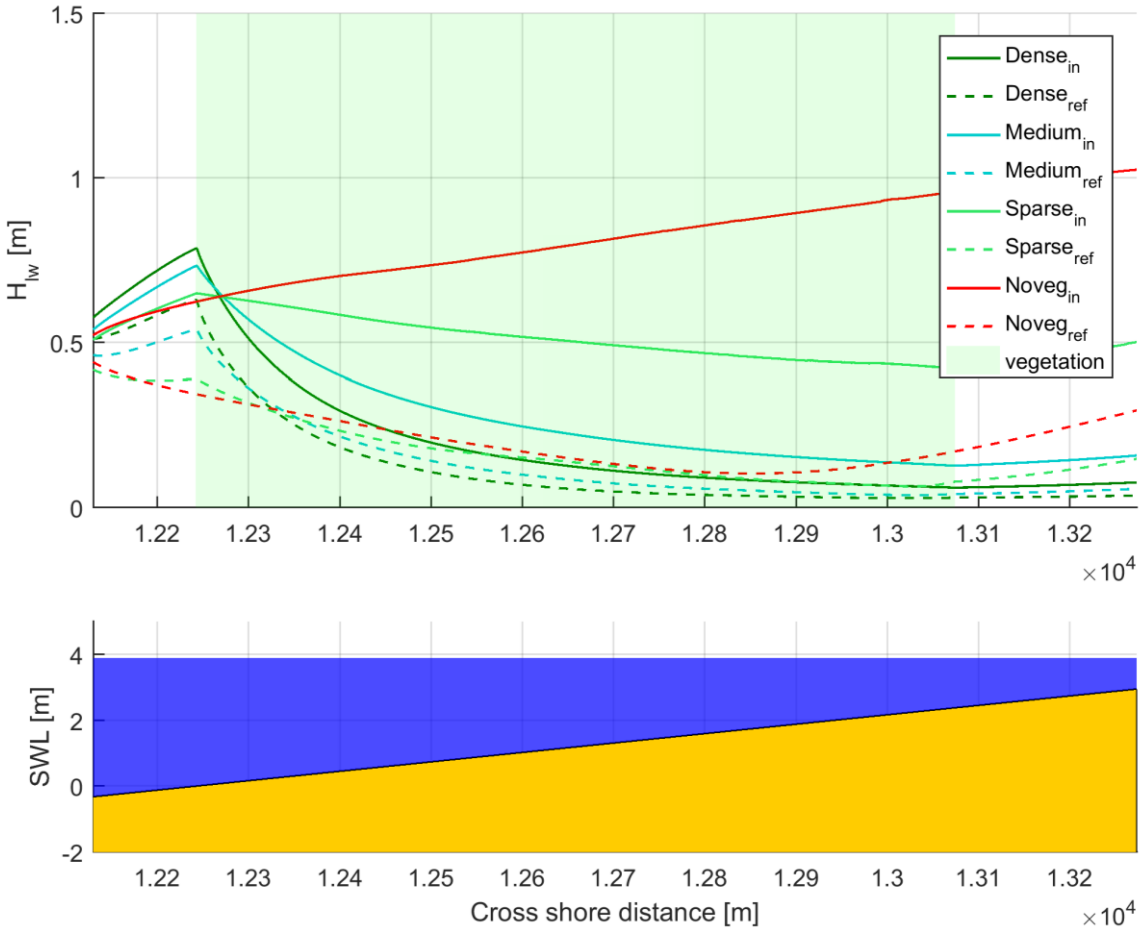

Figure 4.15: Incoming and reflected long wave height variation across the vegetation for different vegetation densities and no-vegetation case. The solid lines show the incoming wave height and the dashed line shows the corresponding reflected wave height.

Similar to the attenuation of the short waves within the vegetation, an attenuation of the long waves is also observed.

For denser vegetation, a greater attenuation of the wave height is observed compared to lesser dense vegetation. The observation is similar to the short wave attenuation.

The attenuation of long wave height can be associated with the energy dissipation due to bottom friction, wave breaking and dissipation due to vegetation (van Dongeren et al. 2007). Dissipation due to wave breaking is much more significant than dissipation due

to bottom friction. A comparison between the attenuation due to vegetation (focus of the study) and other attenuation mechanisms can be performed by analyzing the attenuation in the incoming long wave for the non-vegetated case and the vegetated case.

Since all counterpart models have the same input conditions any increased attenuation observed in the vegetation models over the non-vegetated models should be due to dissipation induced by vegetation.

In order to quantify the effect of the vegetation induced attenuation of long waves, the reduction in incoming long wave height the models were compared. It was found that vegetated models were incurring a higher wave attenuation compared to the unvegetated models.

The short wave height variation across the vegetation can be described using the short wave action balance provided in equation 2.2. The variation of the long waves across the vegetation is governed by the nonlinear shallow water equations (equation 2.7 & 2.8). However, the long wave height is not intrinsically presented within the NLSW equations. Hence to explain and understand the long wave height variation across the vegetation, the following method is used.

The effect of the vegetation within the numerical model is applied in a similar manner to a frictional element (use of Morison type equation to model vegetation induced force equation 1.11). Hence it can be assumed that the energy dissipation due to vegetation will act in a comparable way to friction. The energy dissipation of long waves due to bottom friction is presented by Henderson, (2002) as follows,

$$\frac{d\left(\sqrt{gh}\frac{1}{8}\rho g H_{rms,lo}^2\right)}{dx} = f_{cw}\rho\left(\frac{g}{h}\right)^{\frac{3}{2}}\frac{H_{rms}}{\sqrt{8}}\frac{H_{rms,lo}^2}{8} \tag{4.9}$$

Where, $H_{rms,lo}$ long wave height, H_{rms} short wave height and f_{cw} is the friction coefficient.

To adjust the equation in order to model the energy attenuation by vegetation, a factor (v) instead of the friction coefficient is substituted. Factor v will take into account the vegetation density, varying the energy attenuation according to the vegetation. Due to the very mild slopes the variation in h will be small. Hence assuming the wave celerity $(\sqrt{gh})$ to be a constant the equation 4.9 can be rewritten as,

$$\Delta E = d\left(\frac{1}{8}\rho g H_{rms,lo}^2\right) = \frac{v\rho g}{h^2}.\frac{H_{rms}}{\sqrt{8}}\frac{H_{rms,lo}^2}{8}.dx \tag{4.10}$$

Where ΔE is the energy attenuation due to vegetation. The left-hand side (LHS) of equation 4.10 presents the XBeach modeled energy attenuation. The LHS can be found by the output long wave height energy variation within the vegetation. The right-hand side (RHS) of equation 4.10 presents the predicted energy attenuation, which can be calculated from the parameters in the equation.

The constant factor v can be found by plotting a best fit line between the XBeach modeled and the predicted reduction values. Half of the total number of model runs was randomly selected to calculate the factor v. The found values for v varied from 0.362, 0.136 and 0.032 respectively for dense, medium and sparse vegetation.

In order to validate the found formula between the predicted energy attenuation and XBeach modeled energy attenuation, the remaining half of model run results were used. Figure 4.16 provides predicted and the XBeach modeled energy attenuation for the different model runs at different vegetation densities. Dense vegetation shows a good correlation ($R^2 = 0.86$) between the modeled and the predicted values. A reduction of correlation can be observed as the vegetation density reduces (medium dense vegetation, $R^2 = 0.83$ and sparse vegetation $R^2 = 0.76$). The increased energy reduction by mechanisms other than vegetation as the vegetation density reduces was discussed previously. The reduction in correlation to the proposed equation can be associated with the other dissipation mechanism gaining prominence in sparse vegetation. In general, it can be concluded that equation 4.10 will be suitable to understand and explain the long wave attenuation within the vegetation.

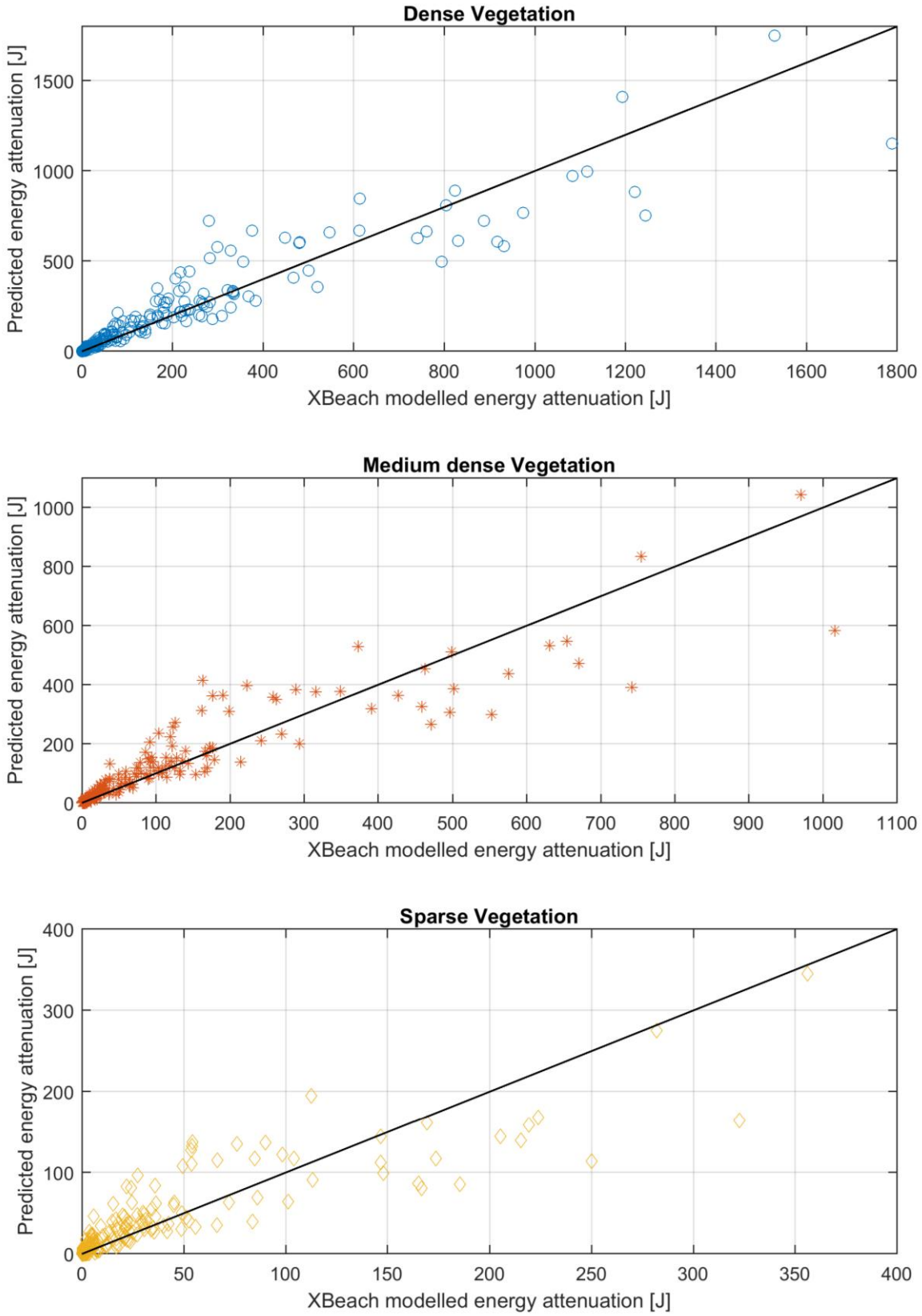

Figure 4.16: Predicted energy dissipation vs. the XBeach modeled energy attenuation of long waves due to vegetation. Plots for the three vegetation densities. The black lines in plots represent predicted attenuation= XBeach modeled attenuation.

4.2.4 Transformation of long waves across the vegetation

Figure 4.17 provides the long wave transformation across the vegetation for all model runs. The long wave height represented is normalized by the wave height at the start of the vegetation.

Higher propagation distance (less attenuation) of long wave height across the vegetation is observed compared to short waves in the presence of vegetation.

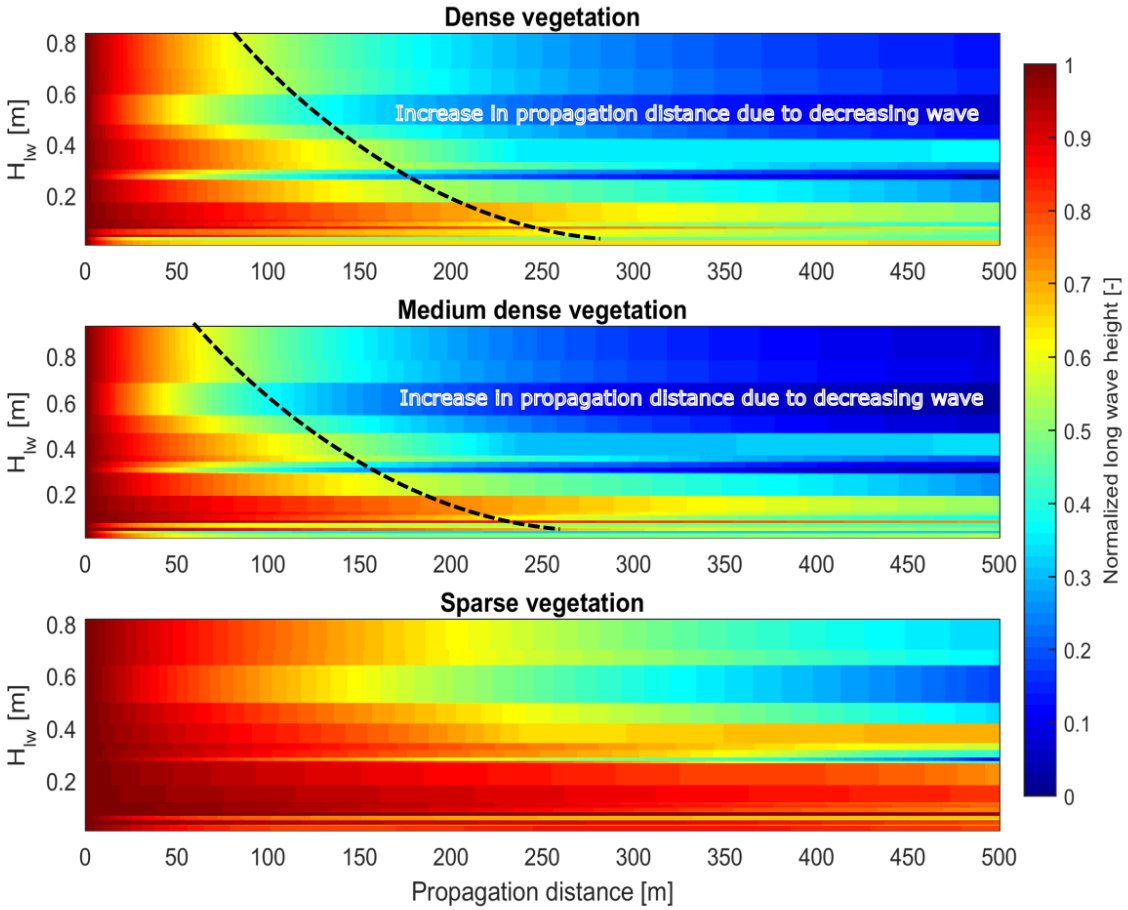

Figure 4.17: Long wave height variation across the vegetation for three densities of vegetation. The wave heights are normalized by the H_{lw}at the start of the vegetation. The color represents the normalized wave height (for all model runs).

Even though the general patterns of increased propagation distance with lower wave heights are observed, variations to the pattern can also be observed. The variation to the pattern suggests other factors such as the water depth also affect the propagation of the waves across the vegetation.

Similar to the short wave analysis, a rate of attenuation for the long wave heights can be calculated by taking the ratio between attenuated wave height (ΔH_{lw}) for a vegetation width of $x = 100\,m$ (equation 2.1). Figure 4.18 provides the rate of long wave attenuation observed for H_{lw}.

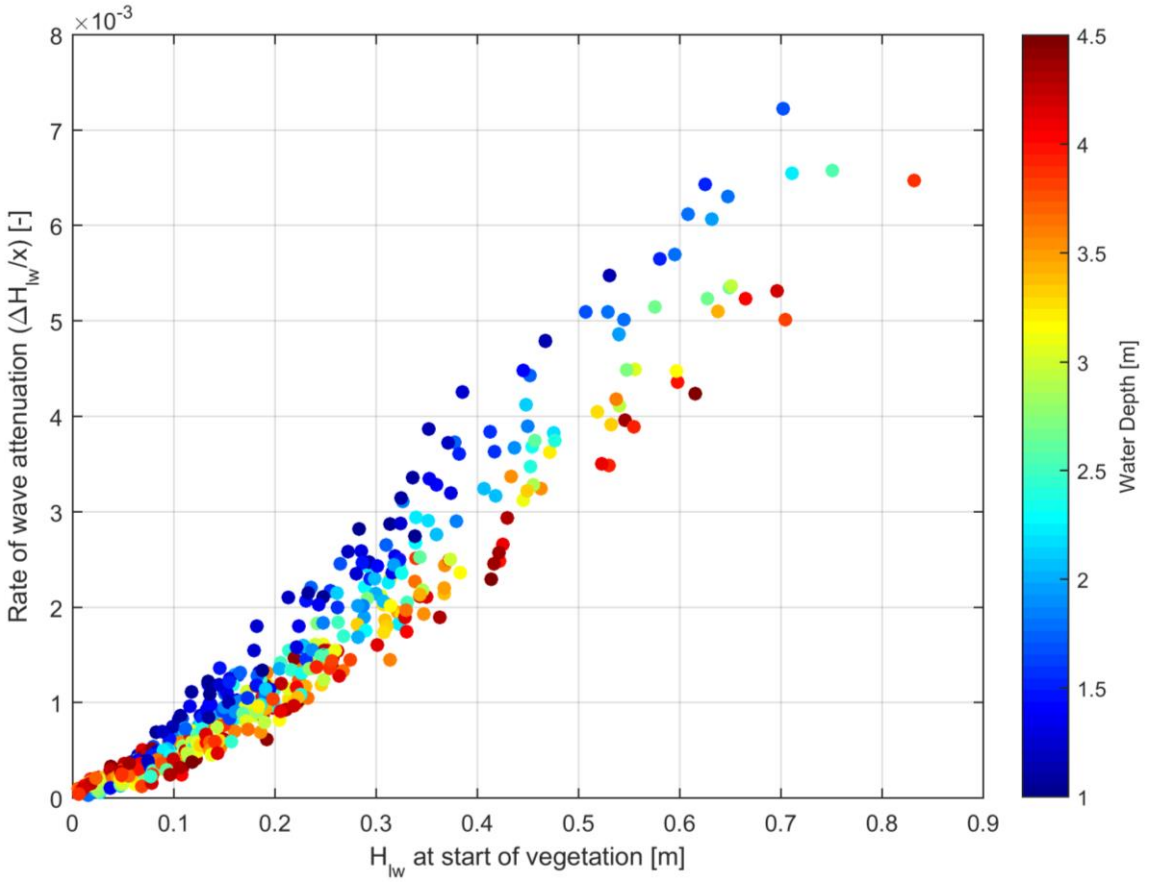

Figure 4.18: Long wave attenuation rate in dense vegetation (all model runs) as a function of the long wave height and the water depth.

Similar to short wave attenuation, an increased attenuation rate is observed for larger H_{lw}. The effect of the water depth on the wave height attenuation is similar to that of short waves.

The energy reduction rates in long waves are predicted by equation (equation 4.10). The formula suggests, the energy attenuation rate should increase with the long wave height, short wave height and should decrease with water depth. The dependence of short wave propagation with water depth was such that, deeper water depths will have a lower attenuation (Figure 4.10 and Figure 4.12).

Figure 4.19 provides the vegetation width required for the dense vegetation case to attenuate 50% of the long wave energy. The propagation distance reduces with increasing long wave height. For a given wave height considerable deviation in propagation distance is observed. The variation in distance of propagation is due to the water depth and the short wave height.

From Figure 4.19, it can be observed that the scatter in points can be explained by the water depth. At a given H_{lw} value, shallower water depth results in lower propagation distance within the vegetation (higher reduction rate).

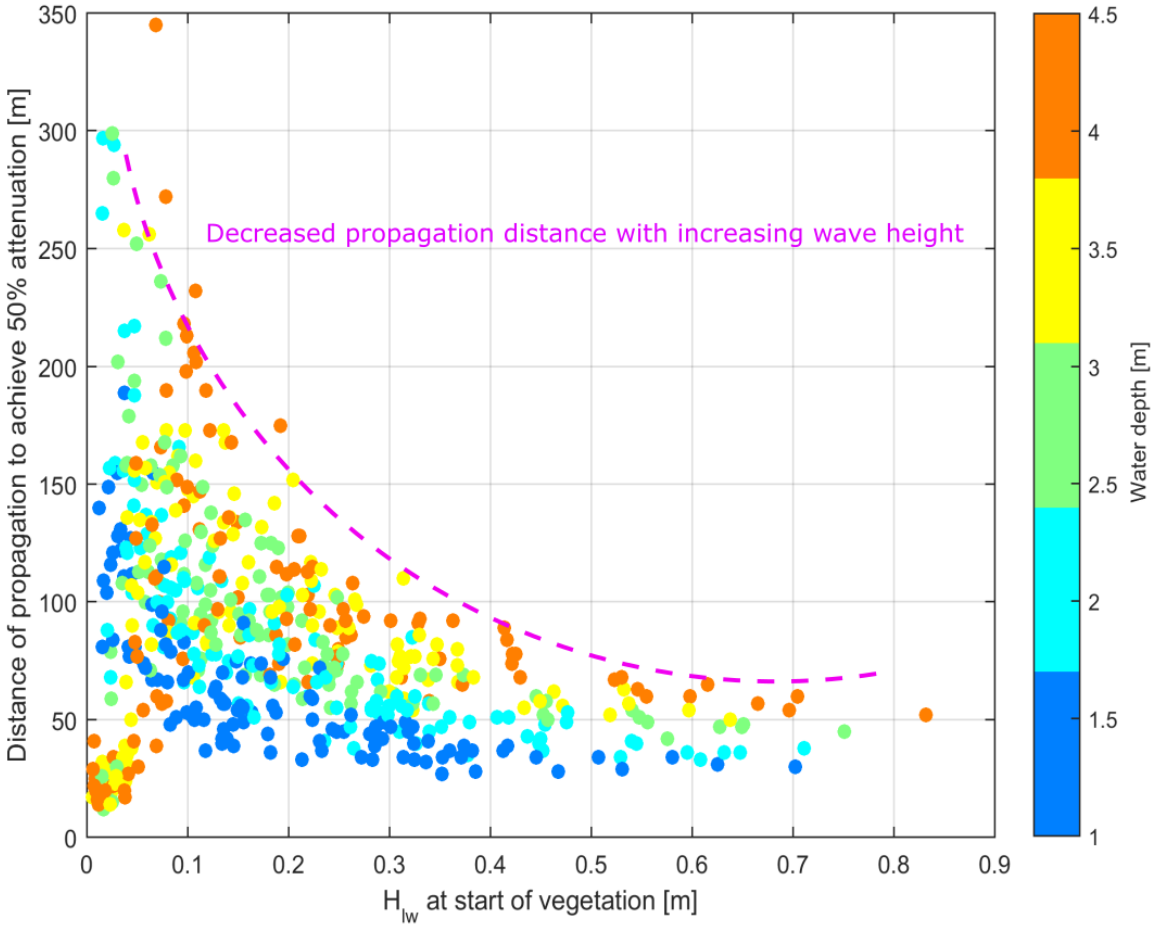

Figure 4.19: Vegetation width required to attenuate incoming long wave energy by 50% (for dense vegetation case). The point colors represent the water depth

4.3 Total wave propagation within vegetation

The total wave height (H_{tot}) of the domain can be found by the total energy of the system (equation 3.3). The variation of the total wave height will include the combined aspects of both short and long waves. Due to the differences in dissipation of energy of the short and long waves, contribution to the total wave height at different locations of the vegetation from the two wave components will be different. Figure 4.20 provides the total wave height variation across the vegetation.

In Figure 4.10 and Figure 4.18 it was observed that for both short and long wave attenuation increased with increasing wave height. In a given wave, the short wave height will be larger than the long wave height. Hence, for a given wave, the attenuation rate of short wave is greater than of the long wave attenuation rate induced by vegetation. Due to the reduced attenuation rate, the long wave starts to dominate after some distance of propagation. In Figure 4.20 the variation in long wave contribution to the H_{tot}at different propagation distances is provided.

Figure 4.20 (bottom plot) provides the long wave contribution with water depth. At shallower water depths, the long wave starts to dominate quickly as the wave propagates within the vegetation. Due to depth induced breaking the short wave height

is limited by water depth. Hence, for shallow water depths the wave height will be small. The long wave height growth predominantly depends on the profile slope, wave period and short wave forcing. Thus, the long wave height can be comparatively high compared to short waves. As the water depth increases short wave height will increase, furthermore deeper water depths will reduce energy dissipation due to vegetation. Hence at deeper water depths the short waves will dominate for longer distances compared to shallower waters.

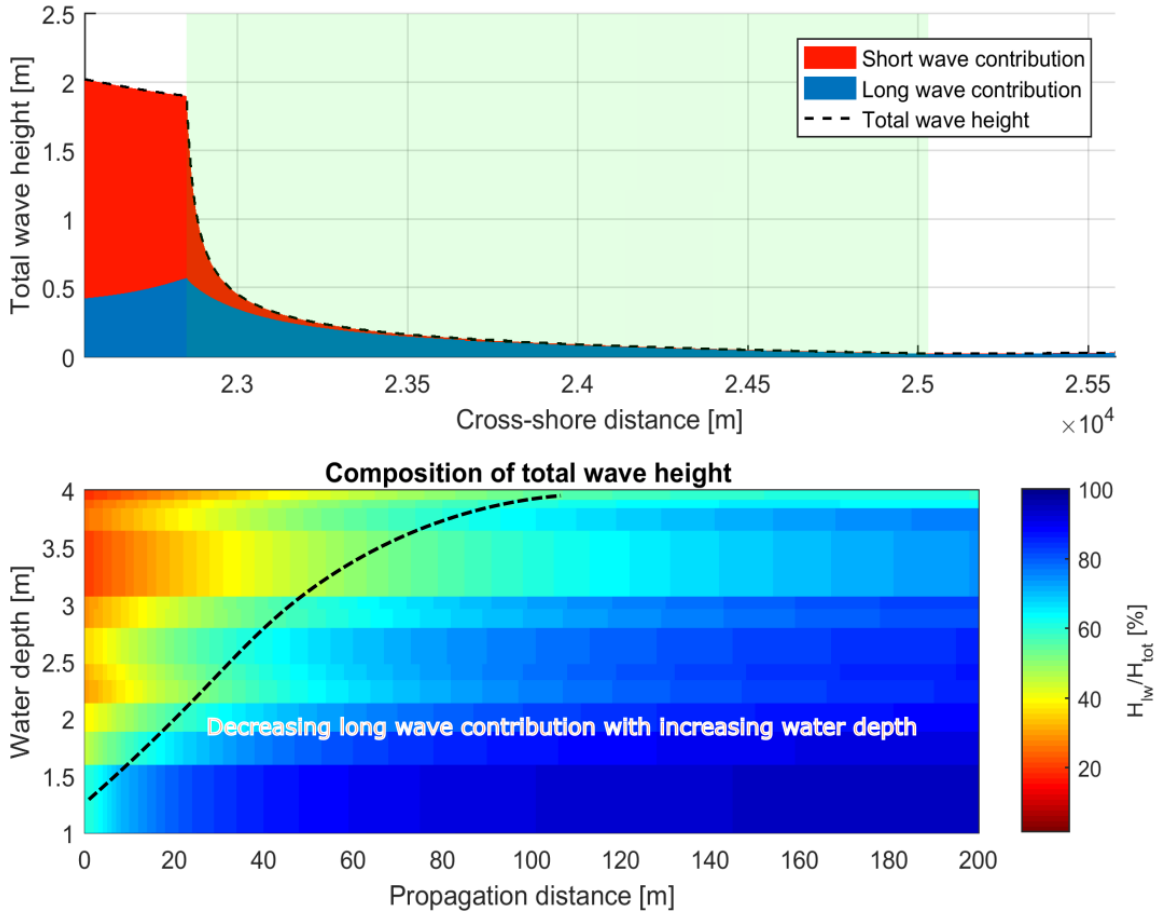

Figure 4.20: Top plot; Example variation in composition of total wave height across dense vegetation. Bottom plot; percentage long wave contribution to total wave height (H_{lw}/H_{tot}) within the vegetation (dense vegetation model runs).

Figure 4.21 provides the total wave height variation across the vegetation for different vegetation densities. The reduction in attenuation with lower densities is apparent. The mean vegetation width required to halve the initial wave height of the waves is approximately 50 m for dense vegetation and 150m, 300m for medium dense and sparse vegetation respectively. Thus, it can be observed that the width required to attenuate waves are vary according to the vegetation density. Less dense vegetation will require a wider mangrove forest to archive the same attenuation levels provided by a much narrower dense mangrove forest.

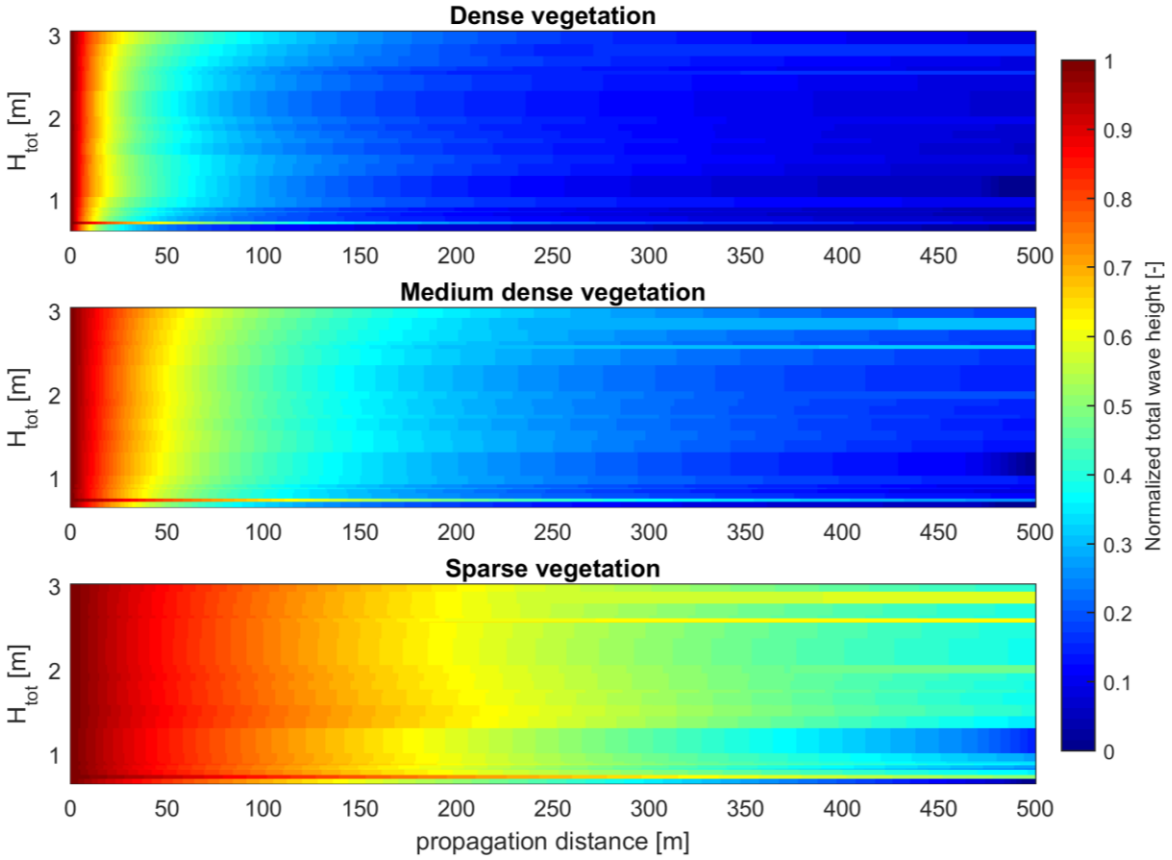

Figure 4.21: Total wave height(H_{tot}) variation across the vegetation for different vegetation densities (all model runs). The color represents the normalized total wave height

4.4 Energy variation through the vegetation

Wave energy propagation of short waves and long waves were provided in section 4.2.1 & 4.2.2. Within this section the energy variation in terms of frequency is discussed. Figure 4.22 provides the wave spectra for the different vegetation densities at start, mid and end of the vegetation for an example model run. As the waves propagate through the vegetation, the reduction in the spectral energy (area of the spectra) can be observed. The reduction is larger at higher frequencies than at lower frequencies. It should be noted that the reduction in the unvegetated case is due to wave breaking.

The difference rate in energy dissipation between short waves and long waves was observed before (section 4.2.1 & 4.2.2). The observation can be more clearly studied by splitting the waves by the frequency. Waves can be classified by their frequency into groups. Table 4.2 provides classification of waves by frequency (Pearson, 2016).

Table 4.2: Classification of waves by frequency

	Wave classification	Frequency [Hz]	T [s]
H_{ss}	Sea/Swell (SS)	0.04-1.0	1-25
H_{IG}	Infragravity (IG)	0.004-0.04	25-250
H_{VLF}	Very Low Frequency (VLF)	0.001-0.004	250-1000

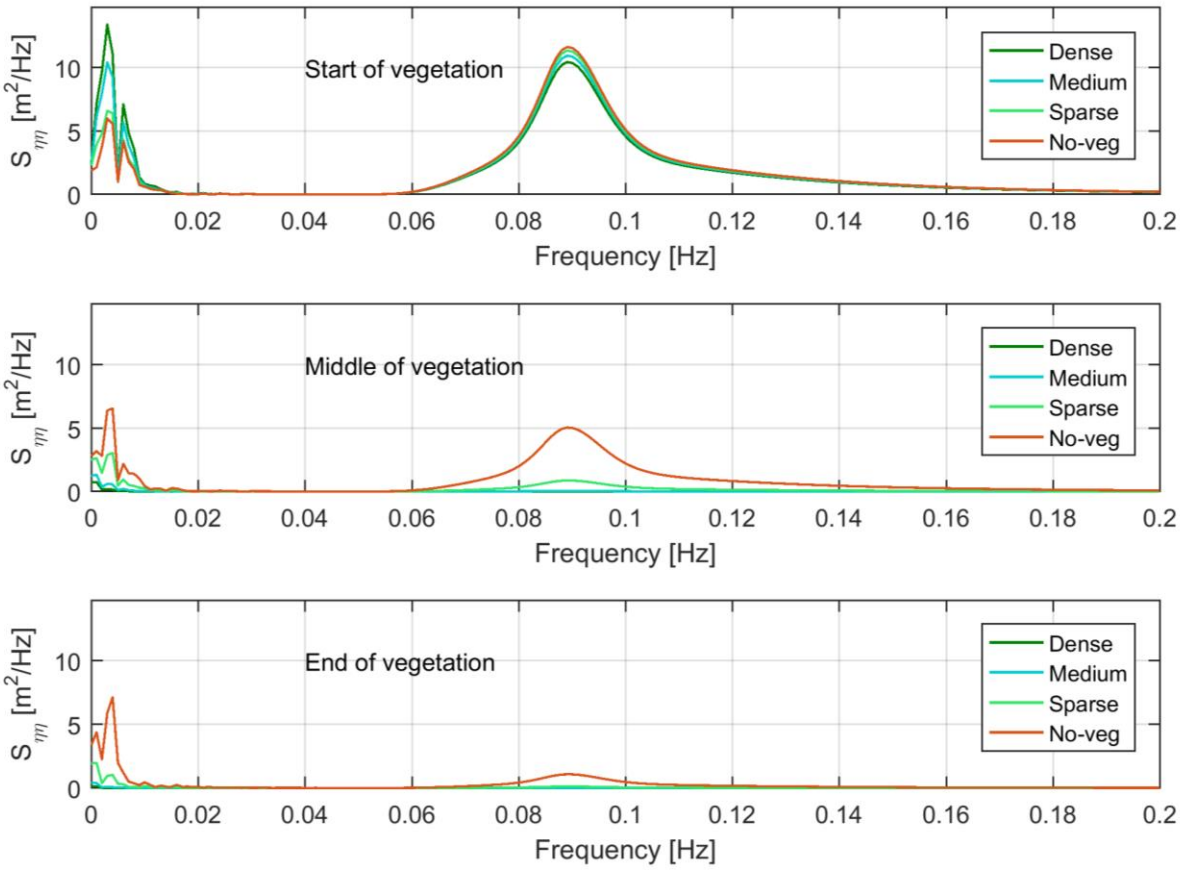

Figure 4.22: Spectral energy variation across vegetation according to the vegetation density for an example model run. Top plot; observation point 2- start of vegetation. Middle plot; observation point 3- middle of vegetation and bottom plot; observation point 4- end of vegetation.

Figure 4.23 provides the composition of the total wave energy according to the wave band frequency at the different observation points within vegetation. The short wave energy component of the total energy reduces at a higher rate than the IG and VLF band energy composition. Hence, an increased contribution from the IG and VLF components to the total wave energy can be observed as the waves propagate through the vegetation.

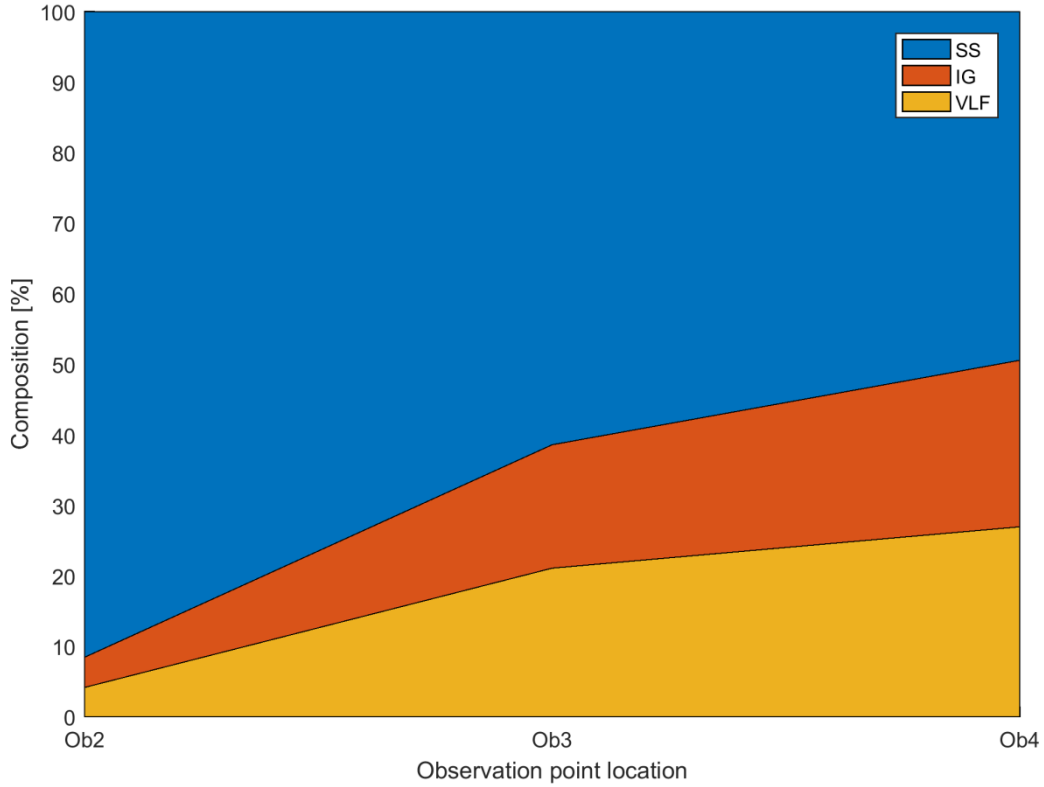

Figure 4.23: Average composition of total wave energy within each band as waves propagate through the vegetation. Results for all medium dense vegetation model cases.

4.5 Wave runup at hinterland of vegetation

The wave runup value for each model was calculated just after the vegetation from the procedure given in section 3.4. The runup was calculated for a uniform slope of 1/10 using wave characteristics obtained after the vegetation. As for the formula, a higher runup is predicted for larger wave heights and longer wave periods. Increased runup in larger wave heights are due to the high energy presence in the system. A longer wave period will suggest the system contain a high percentage of low frequency energy. The long waves (low frequency) was found to increase the run up (van Gent, 2001). Figure 4.24 provides the runup variation with wave height and wave period. The increase in runup with wave height can be observed. For a given wave height the runup also increase with wave period. As the formula is applied after the vegetation, the pattern in the runup change with wave inputs will be similar irrespective of the vegetation density, and only will change in runup magnitude.

In section 4.2.1 and 4.2.2 it was observed that the wave energy was dissipated by the vegetation. A lower wave height would imply a reduced wave runup. Since the wave period also affect the runup strongly, the change in the wave period for wave propagation through the vegetation is important. Figure 4.25 provides the variation in $T_{m-1,0}$ as the waves propagate across the model domain. In general, the wave period increases due to the higher attenuation in short waves compared to the long waves. Very large wave periods will suggest the energy of the system is almost fully dissipated.

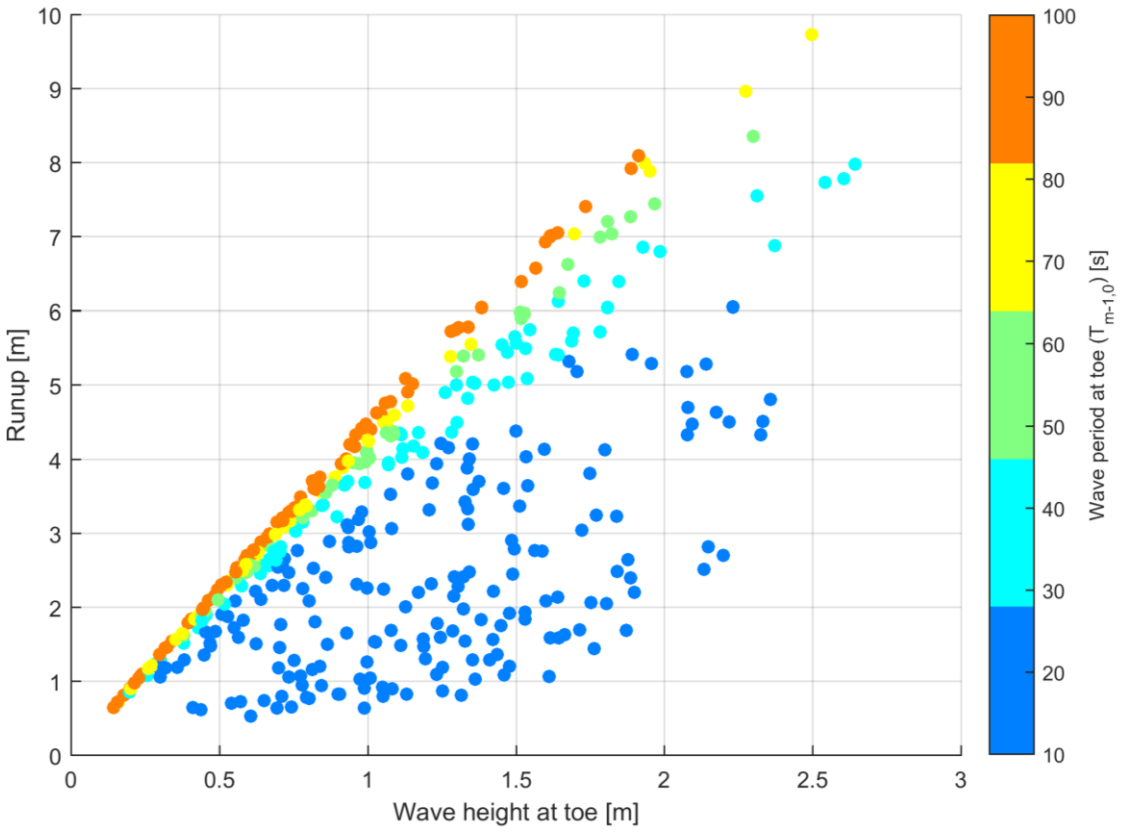

Figure 4.24: Runup variation with the wave height and the wave period ($T_{m-1,0}$) at the toe. Results for the non-vegetated model runs.

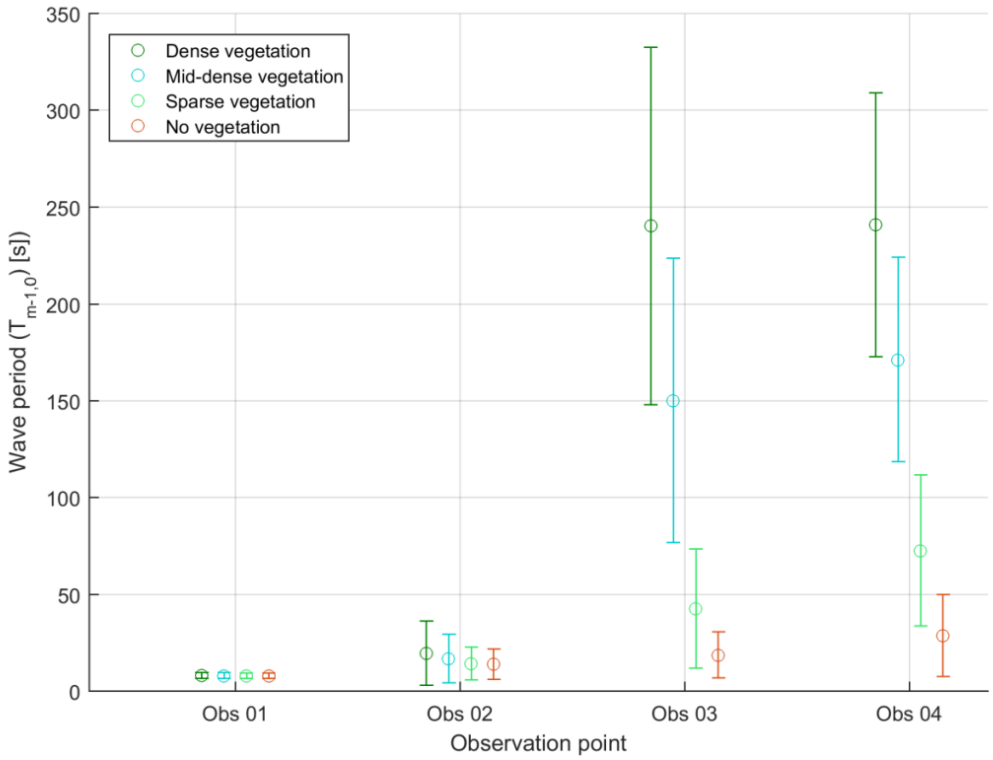

Figure 4.25: Variation in the wave period($T_{m-1,0}$) at observation points for the different vegetation densities (all model runs). The plot provides the median wave period and the interquartile range.

The runup calculations from the empirical equation provide runup levels from the still water level. However, due to the differences in setup generation, the still water level will be different from the initial mean water level. The setup/set down level should also be considered for the total runup level. Hence the setup/set down water heights were added to the runup values calculated from the empirical formula. However, the setup/ set down heights are much smaller compared to the runup heights.

Figure 4.26 provides the runup comparison between the vegetated models and the base case of non-vegetated case. Points below the solid line present cases where the runup is lower than the non-vegetated model cases. As observed in section 4.3 all vegetated models provide an attenuation of wave energy. The degree of wave attenuation has a strong effect on the runup reduction. Higher reduction in the wave height results in a substantial reduction in runup height. Thus, dense vegetation shows the most runup reduction followed by medium dense vegetation.

Mangrove forest width also effects the runup reduction observed in the models. Larger forest widths are capable of increasing the runup attenuation. Figure 4.27 provides the increase in runup attenuation with forest width for medium dense mangrove cases. The runup attenuation rates are calculated relative to the corresponding no-vegetation model cases. Dense and sparse vegetation also provide a similar variation in runup attenuation with mangrove forest width.

The mean relative runup attenuation rates observed for dense vegetation is 87%. The rates for medium dense and sparse vegetation is 76% and 44% respectively.

Even though wave energy is attenuated for all vegetated models, a few model results show an increase runup compared to the non-vegetated models. After propagation of wave across the vegetation, the wave period increased due to higher short wave dissipation relative to the long wave dissipation (Figure 4.25). Even though energy is attenuated, in some instances the runup formula predicts a larger wave runup compared to the non-vegetated models.

The increase in wave period can result in a larger wave runup prediction. Figure 4.28 provides the wave spectra at the end of the vegetation for an example case where the vegetated model provides a higher runup (4.79m) than the unvegetated model (4.52m). From Figure 4.28, it can be observed that the high frequency energy in the vegetated model is considerably lower than the unvegetated model, while the low frequency energy difference is much smaller. Due to the uneven attenuation in the low frequency and high frequency energy the wave period shift will be different. The wave period ($T_{m-1,0}$) for the unvegetated case is 17s while the vegetated model is 24s, prompting a higher runup for the case with higher wave period. Since, an energy transfer from high frequency to low frequency during propagation is not seen in the spectra, the runup should be lower in the vegetated model due to lower energy. The contrary result from the runup formula can thus be due to the runup formula been not valid for such cases of wave height/periods.

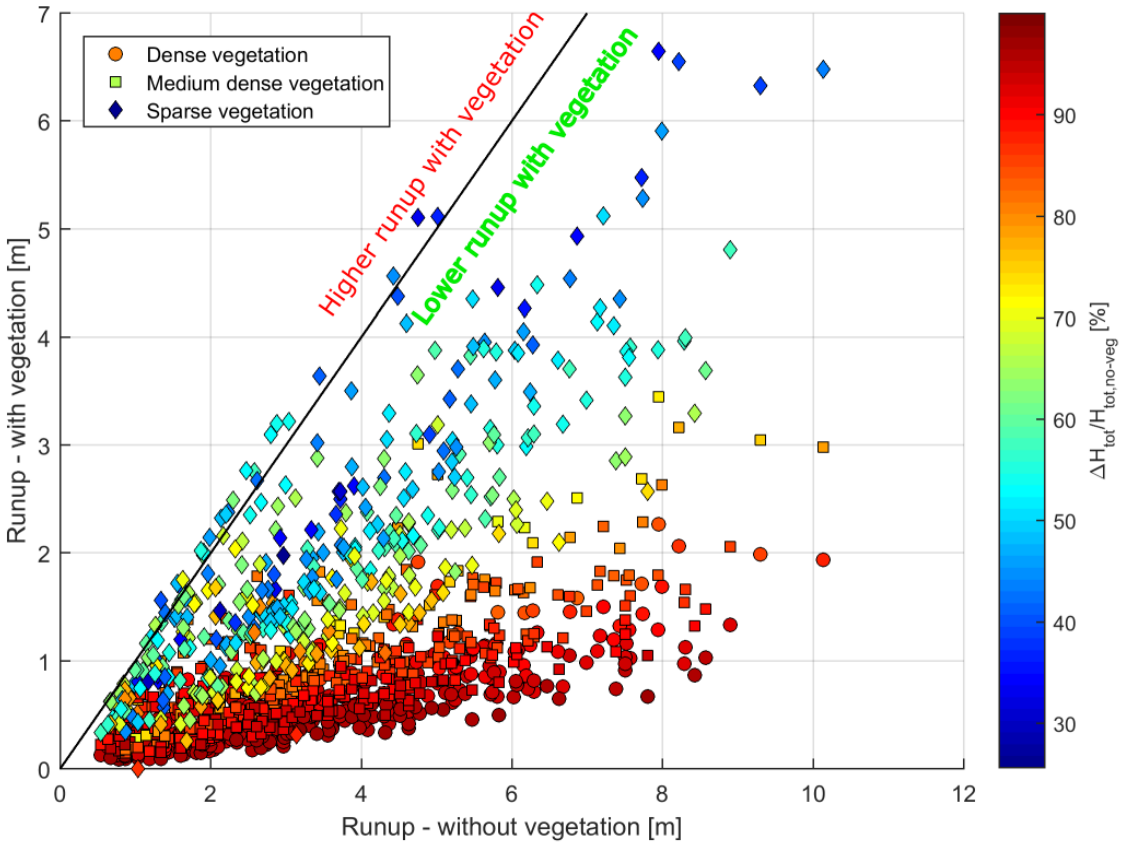

Figure 4.26: Comparison of the runup between vegetated (dense, medium and sparse densities) and non-vegetated models. The point colors provide the wave attenuation at observation point 4. The solid line presents Runup non-vegetated = Runup vegetated.

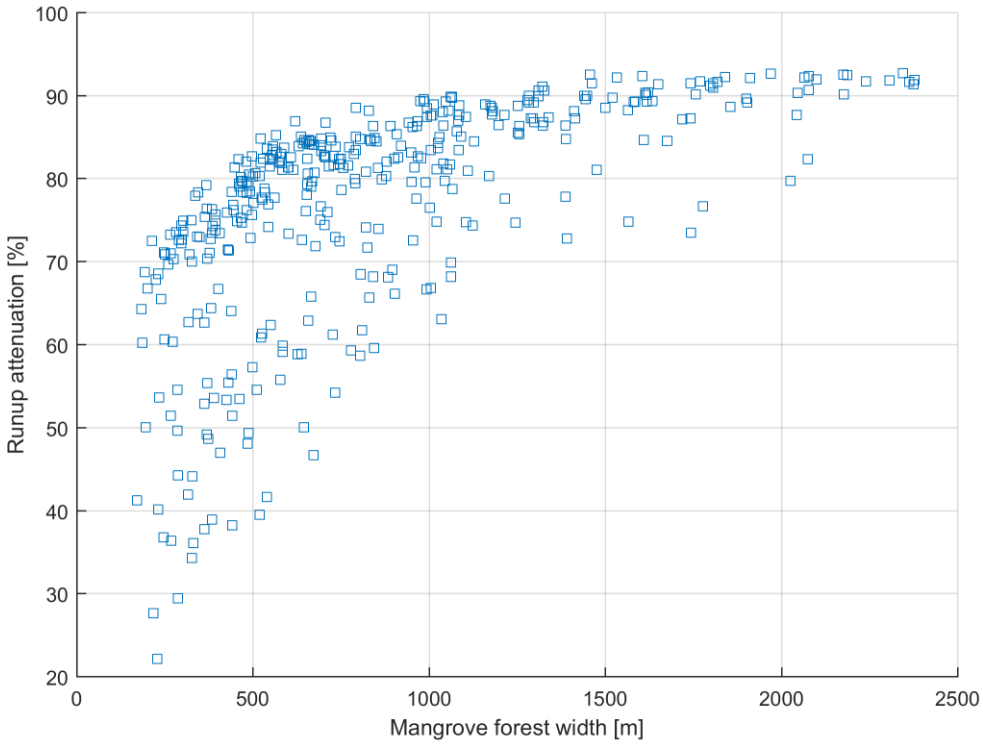

Figure 4.27 Runup attenuation (relative to no-vegetation cases) variation with mangrove forest width for medium dense mangrove model cases

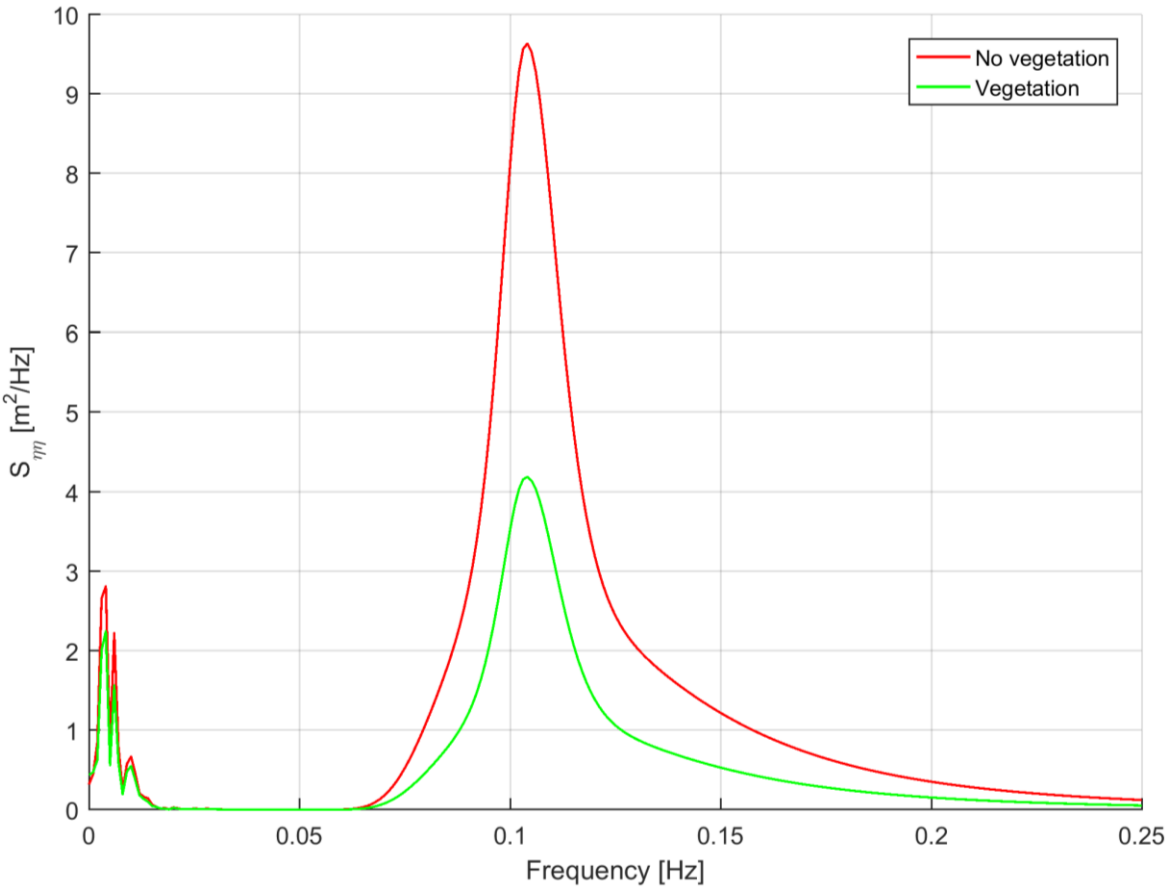

Figure 4.28 Wave spectra for a model case where the vegetated model runup > corresponding unvegetated model runup.

5 Discussion

The model study performed considers a comprehensive parameter space with varying input conditions. By accounting for parameters in a wide range, a broad set of combinations that can be expected in the field is taken into consideration. Hence, the results will portray the trends and the spread expected in real life cases. Due to the substantial number of model runs to be carried out certain simplifications and assumptions had to be made.

A 1D model domain was selected mainly due to the low computational time required, data availability and simplicity in modeling. To use a 1D model certain aspects that may influence the results had to be neglected. These include wave direction and the assumption of uniform longshore bathymetry. The neglected parameters will influence the wave hydrodynamic forcing on the vegetation. However, most of the main parameters that effect the wave-vegetation interactions (wave height, period, water level, vegetation width, vegetation type, density and profile slope) were considered within the study. The profile used in the 1D model was simplified to a uniform sloping bed. Since the study consider parameters over a wide range extracted from a global viewpoint, a uniform sloping bed was taken to represent the general variation in the sea bed of a mangrove coast.

The hydrodynamic conditions were selected from the ERA-I dataset for extreme wave events (return period 100 years). The data gathered were used as the offshore boundary condition of the model. Mangroves are more commonly found in sheltered areas rather than open coasts. Hence, direct propagation of offshore wave climate to the mangrove coast is a limitation of the study. Furthermore, the application of a single-peaked JONSWAP spectrum to represent a storm will also deviate from reality.

Since the tests were run on an idealized 1D model and hydrodynamic conditions, the results may not be directly applicable for design of a mangrove forest/restoration as a mitigation method where the neglected parameters and bathymetric conditions will change the forcing on the vegetation. However, the study can be used to identify the influence of parameters (wave height, water depth, vegetation density and forest width) on wave attenuation. Furthermore, range of wave and runup attenuation observed in study will help in a preliminary stage of a design for a mangrove forest for wave hazard mitigation.

The numerical model used (XBeach-surfbeat) will also introduce some limitations. Since the model propagates short wave as energy, reflection of short waves from the vegetation is not included in the model which can be an important factor.

The energy dissipation induced by vegetation incorporated in the model does not consider a maximum threshold which the trees will be able to resist. In reality, the trees will break or uproot under very high forcing (Janssen, 2016). The monotonic increase of energy dissipation with wave height will be a deviation from the reality and can be identified as a limitation of the model.

The mangrove characteristics were selected from data accumulated from previous studies. The vegetation parameters of interest were diameter of the trees, height, density (number of trees per square meter) and drag coefficient. Three densities of mangroves (dense, medium and sparse) were selected in the study to represent variation in the mangrove vegetation. The use of three distinct densities meant the vegetation characteristics were all increased/decreased proportionally (e.g. Taller mangrove trees with larger stem sizes denser root system, shorter mangrove trees with smaller stem sizes and less dense root system). Even though the general pattern in vegetation is as above, there is a significant spread in the vegetation characteristics (e.g. Tall mangrove tree with a small stem size and vice versa) (Janssen, 2016). Not considering such vegetation can be considered a limitation.

The mangroves show a distinctive variation in parameters over the vertical of the tree. The vertical variation was included in the models by providing vegetation parameters in three layers (roots, stem and canopy). In reality, a variation of vegetation is also seen across the cross section of a mangrove forest which was not included in the numerical model. All modeled mangrove vegetation in the study are emergent. Hence the effect of the height of the vegetation itself cannot be separated which is a limitation of the current study.

Current study results show the trends observed in the findings of previous researchers; The increase in wave attenuation with increasing wave height (section 4.2, (Horstman et al., 2014)), variation of wave attenuation rate across a vegetated forest (section 4.2.1), reduction in wave attenuation with increasing water depth (section 4.2.1). However, the attenuation rates observed in previous filed studies and the current model study show differences. Field studies show lower attenuation rate compared with the results obtained in the current study (section 4.2.1). The variation can be attributed to the lower wave heights and lower densities of the mangroves at the filed observations sites.

A difference in setup variation in the current model and previous studies were also witnessed. The current study shows an increase of setup for denser vegetation and reduction in setup for sparser vegetation which is not observed in previous studies. Numerical modeling preformed with XBeach-Non-hydrostatic also show a difference from the obtained results. Further investigations will be needed to understand the reasons for the deviation.

6 Conclusions

The conclusion section is presented under two main areas.; Conclusion towards research objective and conclusions towards research questions.

6.1 Conclusions towards research objective

Mangrove vegetation is useful in attenuating wave energy. The mitigation capacity of the vegetation depends on many different criteria, chief among which is the density of the vegetation. Dense vegetation was the most efficient in reducing wave energy. Reducing vegetation density results in further propagation of waves. Mangrove forest width also play a major role in wave attenuation. However, the forest width required to achieve a certain level of wave attenuation will depend on the density of the vegetation. E.g. a narrow dense mangrove forest will provide the same attenuation as a wider sparse mangrove forest.

Wave height attenuation for long and short waves was proportional to the wave height. Moreover, water depth plays a major role in energy propagation. Wave energy propagation increased with increasing water depth.

Wave-driven setup attenuation differs on the vegetation density. For example, dense vegetation, the wave setup increased compared to non-vegetated models, specifically for narrow widths. Sparse vegetation with sufficient width was capable of reducing the setup.

Mangroves are capable of reducing the runup levels due to the reduction in wave energy. Dense vegetation reduced runup levels the most due to higher energy dissipation.

Finally, it can be concluded that mangroves are an effective method of mitigating coastal hazards by reducing the wave energy and runup. The level of mitigation will mainly depend on vegetation density, vegetation width, wave height and the water depth.

6.2 Conclusions towards research questions

The objective of the project was achieved by answering three main sub questions (section 1.4). This section provides the conclusions derived for each question.

6.2.1 Setup variation due to mangrove vegetation

Wave force (F_w) and mean vegetation force due to undertow ($F_{v,m}$) assist the setup while wave-induced vegetation forces ($F_{v,w}$) reduce the setup. The bed shear stress (τ_{bx}) was found to be negligible in most model cases. F_w is a direct outcome of the short wave dissipation by vegetation and was confined towards the front of the vegetation. $F_{v,w}$ is much smaller in magnitude compared to other forces and will become dominant

towards the back of the vegetation due to lack of other force components. Water level variation within the vegetation was found to be satisfactorily explained by the use of simplified momentum equation using the above said forces.

The forces induced on the water column varied with hydrodynamic conditions and vegetation. Dense vegetation induced a large F_w force due to the rapid reduction in short wave energy. The large wave force induced, results in a quick increase in the water level. Due to the more gradual reduction in short wave energy in the sparse vegetation, the setup within the vegetation increases gradually.

From comparison with the non-vegetated model cases, it was found that some model runs with vegetation induced a higher setup than the non-vegetated models. The increase in the setup can be associated with F_w and $F_{v,m}$ forces. The increase of setup was mostly found in dense vegetation cases while sparse vegetation models resulted in a lower setup.

The reason for the difference is explained as follows,

In dense vegetation, almost all the wave energy is dissipated in the front section of the vegetation increasing the setup. The forces that can reduce the setup is $F_{v,w}$. However, $F_{v,w}$ is induced by the wave orbital motion. Since there is very little short wave energy present, $F_{v,w}$ will be very small. Hence, it will be unable to reduce the setup. In contrast, for sparse vegetation, the increase in setup due to F_w will be small and as the wave propagates, $F_{v,w}$ will have enough energy to dominate and reduce the wave setup.

Higher dissipation combined with a narrow vegetation width will result in an increased setup. For vegetation to bring down the initial increased setup the vegetation must be sufficiently wide. The increased setup that may occur due to the vegetation is an adverse outcome of using vegetation as a mitigation method.

6.2.2 Short wave propagation through vegetation

Mangrove vegetation was found to attenuate the short wave energy efficiently. The rate of attenuation varied mainly with initial short wave height, depth of water and vegetation density. The wave height reduction was a direct function of the short wave height (H_{sw}). Higher H_{sw} leads to more attenuation. The rate of dissipation reduced as the waves propagate inwards of the vegetation (due to the lower wave height).

The range of short wave height attenuation rates (calculated according to equation 2.1) observed in the mangrove vegetation within the first 100m considering all the model results is provided in Table 6.1.

Table 6.1 Short wave height attenuation rates observed in mangrove vegetation

Vegetation density	Rate of short wave attenuation ($x10^{-3}$) [m^{-1}]
Dense	6-22
Medium	3-16
Sparse	1-7

Due to the variation in dissipation, the vegetation width required to reduce the H_{sw} changes with vegetation density. For the model runs conducted, on average, dense vegetation was able to reduce the H_{sw} energy by 50% within 20m while for medium dense and sparse vegetation the width required was 50m and 125m respectively.

The water depth plays a major role in short wave propagation. Deeper water depth enabled the waves to propagate further inside the vegetation due to lower dissipation. Short wave height at the start of the vegetation is depth limited due to breaking. Deeper water depths will be able to accommodate larger wave heights. Even though the dissipation will be higher for larger wave heights, the increased water depth will override the dissipation by a certain extent, increasing the propagation. In the context of coastal hazard mitigation this will be a disadvantage.

The propagation of the short waves was not found to be a function of the profile slope. Hence no effect of profile slope on attenuation was found on propagation of short waves in vegetation.

6.2.3 Long wave propagation through vegetation

Long wave propagation across the vegetation was found to be more complex than the short wave propagation. An energy attenuation formula by bed friction in the long waves was changed accordingly to understand the long wave height transformation within the vegetation. The equation was calibrated and satisfactorily validated from the output results of the model runs.

Similar to the short waves, energy attenuation by the long waves increased with increasing long wave height (H_{lw}). H_{lw} growth over the profile is dependent on the profile slope and the wave period. Steeper slopes and longer wave periods produce larger long wave heights. Thus, the effect of slope and the wave period in the energy attenuation of long wave is absorbed within H_{lw}.

The attenuation rate of long waves was found to be smaller than of the short waves. The reduced attenuation results in long waves becoming the dominant component of the total wave height after certain distance of propagation. As expected the denser vegetation attenuates long wave energy more effectively compared to less dense vegetation. Deeper water depths increased the propagation similar to short waves.

6.2.4 Runup after the vegetation

Runup levels were calculated for the models just after the vegetation using an empirical formula. In general, almost all models resulted in a lower runup compared to non-vegetated models. The reduction is attributed to the reduction in wave energy. Dense vegetation model provides the highest attenuation in runup. The runup was calculated with the addition of setup/set down induced by vegetation. The ranges of the relative runup attenuations observed increased with mangrove forest width. A breakdown of the empirical formula prediction of runup was observed for few sparse dense models.

7 Recommendations

The research provides analysis of the vegetation-hydrodynamic interactions in order to understand the processes that are important. Building upon the findings of this research a Bayesian network can be constructed to improve the understanding of how several factors interact in mitigation of coastal hazards by mangroves. The Bayesian network can be complemented with more mangrove densities as well.

The current research project had several limitations. The zonation of mangroves in the cross shore was not taken into consideration. Simulating the variation of mangroves in such zones (as seen in the field) will provide more applicability of the results obtained from the numerical modeling.

The Bayesian network will be able to quantify the expected mitigation of flooding by a mangrove forest under certain conditions. Use of a validated Bayesian network to measure the attenuation of actual mangrove forests around the globe will be an interesting recommendation.

For a design of a mangrove forest at a certain location, the outputs of a Bayesian network can be used. To refine the designs, it is recommended to use a numerical model including the bathymetric variations of the specific location and long-shore components that were neglected in the current study.

Finally, field studies to validate the results are important. Studies into mangrove attenuation in hazardous wave climates are scarce. Improved data from field studies looking into wave height variation, water elevation variation and spectral variation wave energy under different vegetation densities will enable to calibrate and validate the numerical model also which will increase the confidence in the model.

8 Bibliography

Albers, T., San, D. C., & Schmitt, K. (2013). Coastal Protection in the Lower Mekong Delta.

Anderson, M., Smith, J., & McKay, S. (2011). Wave dissipation by vegetation, CHETN-I-82. *US Army Corps of Engineers Engineer Research and Development Center: Vicksburg, MS.*, (September), 22 pp. Retrieved from http://repository.tudelft.nl/view/hydro/uuid:17f2915f-bb57-47f9-8e85-67ff0c82510c/

Augustin, L. N., Irish, J. L., & Lynett, P. (2009). Laboratory and numerical studies of wave damping by emergent and near-emergent wetland vegetation. *Coastal Engineering*, *56*(3), 332–340. https://doi.org/10.1016/j.coastaleng.2008.09.004

Bao, T. Q. (2011). Effect of mangrove forest structures on wave attenuation in coastal Vietnam. *Oceanologia*, *53*(3), 807–818.

Battjes, J. A., Bakkenes, H. J., Janssen, T. T., & Van Dongeren, A. R. (2004). Shoaling of subharmonic gravity waves. *Journal of Geophysical Research: Oceans*, *109*(C2).

Borsje, B. W., van Wesenbeeck, B. K., Dekker, F., Paalvast, P., Bouma, T. J., van Katwijk, M. M., & de Vries, M. B. (2011). How ecological engineering can serve in coastal protection. *Ecological Engineering*, *37*(2), 113–122. https://doi.org/10.1016/j.ecoleng.2010.11.027

Brinkman, R. M. (2006). Wave attenuation in mangrove forests: an investigation through field and theoretical studies. James Cook University.

Brown, B. (2007). Resilience thinking applied to the mangroves of Indonesia. *IUCN & Mangrove Action Project*.

Costanza, R. (1999). Costanza, 1999 - The ecological, economic, and social importance of the oceans, *31*, 15. Retrieved from papers://27281f87-3b7a-4de6-820c-ad3b64393d15/Paper/p4050

D'odorico, P., He, Y., Collins, S., De Wekker, S. F. J., Engel, V., & Fuentes, J. D. (2013). Vegetation–microclimate feedbacks in woodland–grassland ecotones. *Global Ecology and Biogeography*, *22*(4), 364–379.

Dalrymple, R. A., Kirby, J. T., & Hwang, P. A. (1984). Wave diffraction due to areas of energy dissipation. *Journal of Waterway, Port, Coastal, and Ocean Engineering*, *110*(1), 67–79.

Das, S., & Vincent, J. R. (2009). Mangroves protected villages and reduced death toll during Indian super cyclone. *Proceedings of the National Academy of Sciences* , *106*(18), 7357–7360. https://doi.org/10.1073/pnas.0810440106

Dean, R. G., & Bender, C. J. (2006). Static wave setup with emphasis on damping effects by vegetation and bottom friction. *Coastal Engineering*, *53*(2–3), 149–156. https://doi.org/10.1016/j.coastaleng.2005.10.005

Dijkstra, J. T., & Uittenbogaard, R. E. (2010). Modeling the interaction between flow and highly flexible aquatic vegetation. *Water Resources Research*, *46*(12), 1–14. https://doi.org/10.1029/2010WR009246

Feagin, R. A., Mukherjee, N., Shanker, K., Baird, A. H., Cinner, J., Kerr, A. M., … Dahdouh-Guebas, F. (2010). Shelter from the storm? Use and misuse of coastal vegetation bioshields for managing natural disasters. *Conservation Letters*, *3*(1), 1–11. https://doi.org/10.1111/j.1755-263X.2009.00087.x

Fonseca, M. S., & Cahalan, J. A. (1992). A preliminary evaluation of wave attenuation by four species of seagrass. *Estuarine, Coastal and Shelf Science*, *35*(6), 565–576. https://doi.org/10.1016/S0272-7714(05)80039-3

Gedan, K. B., Kirwan, M. L., Wolanski, E., Barbier, E. B., & Silliman, B. R. (2011). The present and future role of coastal wetland vegetation in protecting shorelines: Answering recent challenges to the paradigm. *Climatic Change*, *106*(1), 7–29. https://doi.org/10.1007/s10584-010-0003-7

Giri, C., Ochieng, E., Tieszen, L. L., Zhu, Z., Singh, A., Loveland, T., … Duke, N. (2011). Status and distribution of mangrove forests of the world using earth, 154–159. https://doi.org/10.1111/j.1466-8238.2010.00584.x

Guza, R. T., Thornton, E. B., & Holman, R. A. (1985). Swash on steep and shallow beaches. In *Coastal Engineering 1984* (pp. 708–723).

Hanley, M. E., Hoggart, S. P. G., Simmonds, D. J., Bichot, A., Colangelo, M. A., Bozzeda, F., … Thompson, R. C. (2014). Shifting sands? Coastal protection by sand banks, beaches and dunes. *Coastal Engineering*, *87*, 136–146. https://doi.org/10.1016/j.coastaleng.2013.10.020

Henderson, S. M. (2002). Observations of surf beat forcing and dissipation. *Journal of Geophysical Research*, *107*(C11), 3193. https://doi.org/10.1029/2000JC000498

Horstman, E. M., Dohmen-Janssen, C. M., Narra, P. M. F., van den Berg, N. J. F., Siemerink, M., & Hulscher, S. J. M. H. (2014). Wave attenuation in mangroves: A quantitative approach to field observations. *Coastal Engineering*, *94*, 47–62. https://doi.org/10.1016/j.coastaleng.2014.08.005

Jadhav, R. S., Chen, Q., & Smith, J. M. (2013). Spectral distribution of wave energy dissipation by salt marsh vegetation. *Coastal Engineering*, *77*, 99–107. https://doi.org/10.1016/j.coastaleng.2013.02.013

Janssen, M. P. J. M. (2016). Flood hazard reduction by mangroves. *Tudelft Repository*, *June*.

Knutson, P. L., Brochu, R. A., Seelig, W. N., & Inskeep, M. (1982). Wave damping inSpartinaalterniflora marshes. *Wetlands*, *2*(1), 87–104.

Lamberti, A., & Zanuttigh, B. (2005). An integrated approach to beach management in Lido di Dante, Italy. *Estuarine, Coastal and Shelf Science*, *62*(3 SPEC. ISS.), 441–451. https://doi.org/10.1016/j.ecss.2004.09.022

Longuet-Higgins, M. S., & Stewart, R. W. (1964). Radiation stresses in water waves; a physical discussion, with applications. In *Deep Sea Research and Oceanographic Abstracts* (Vol. 11, pp. 529–562). Elsevier.

Lovas, S. M., & Torum, A. (2001). Effect of the kelp Laminaria hyperborea upon sand dune erosion and water particle velocities. *Coastal Engineering*, *44*(1), 37–63. https://doi.org/10.1016/S0378-3839(01)00021-7

Martínez, M. L., Intralawan, A., Vázquez, G., Pérez-Maqueo, O., Sutton, P., & Landgrave, R. (2007). The coasts of our world: Ecological, economic and social importance. *Ecological Economics*, *63*(2–3), 254–272. https://doi.org/10.1016/j.ecolecon.2006.10.022

Mazda, Y., Magi, M., Ikeda, Y., Kurokawa, T., & Asano, T. (2006). Wave reduction in a mangrove forest dominated by Sonneratia sp. *Wetlands Ecology and Management*, *14*(4), 365–378. https://doi.org/10.1007/s11273-005-5388-0

Mazda, Y., Wolanski, E., King, B., Sase, A., Ohtsuka, D., & Magi, M. (1997). Drag force due to vegetation in mangrove swamps. *Mangroves and Salt Marshes*, *1*(3), 193–199.

Mendez, F. J., & Losada, I. J. (2004). An empirical model to estimate the propagation of random breaking and nonbreaking waves over vegetation fields. *Coastal Engineering*, *51*(2), 103–118. https://doi.org/10.1016/j.coastaleng.2003.11.003

Möller, I. (2006). Quantifying saltmarsh vegetation and its effect on wave height dissipation: Results from a UK East coast saltmarsh. *Estuarine, Coastal and Shelf Science*, *69*(3–4), 337–351. https://doi.org/10.1016/j.ecss.2006.05.003

Möller, I., Kudella, M., Rupprecht, F., Spencer, T., Paul, M., van Wesenbeeck, B. K., … Schimmels, S. (2014). Wave attenuation over coastal salt marshes under storm surge conditions. *Nature Geoscience*, *7*(September), 727–731. https://doi.org/10.1038/ngeo2251

Möller, I., & Spencer, T. (2002). Wave dissipation over macro-tidal saltmarshes: Effects of marsh edge typology and vegetation change. *Journal of Coastal Research*, *36*(1), 506–521.

Nielsen, P. (1989). Wave setup and runup: An integrated approach. *Coastal Engineering*, *13*(1), 1–9. https://doi.org/10.1016/0378-3839(89)90029-X

Oosterlo, P. (2015). A method to calculate the probability of dike failure due to wave overtopping, including the infragravity waves and morphological changes. *Repository.Tudelft.nl*, 218.

Pearson, S. G. (2016). Predicting Wave-Induced Flooding on Low-Lying Tropical Islands.

Phan, L. K., Vries, J. S. M. V. T. De, & Stive, M. J. F. (2011). Coastal Mangrove Squeeze in the Mekong Delta. https://doi.org/10.2112/JCOASTRES-D-14-00049.1

Quartel, S., Kroon, A., Augustinus, P. G. E. F., Van Santen, P., & Tri, N. H. (2007). Wave attenuation in coastal mangroves in the Red River Delta, Vietnam. *Journal of Asian Earth Sciences*, *29*(4), 576–584. https://doi.org/10.1016/j.jseaes.2006.05.008

Roelvink, D., van Dongeren, A., McCall, R., Hoonhout, B., van Rooijen, A., van Geer, P., … Quataert, E. (2015). XBeach Technical Reference : Kingsday Release, 1–141. https://doi.org/10.13140/RG.2.1.4025.6244

Ruessink, B. G., Miles, J. R., Feddersen, F., Guza, R. T., & Elgar, S. (2001). Modeling the alongshore current on barred beaches. *Journal of Geophysical Research*, *106*(C10), 22451. https://doi.org/10.1029/2000JC000766

Samaranayake, R. (2006). Pre-and post-tsunami coastal planning and land-use policies and issues in Sri Lanka. *Coast Conservation Department, Sri Lanka*.

Schüttrumpf, H., Van der Meer, J., Kortenhaus, A., Bruce, T., & Franco, L. (2010). Wave run-up and wave overtopping at Armored Rubble Slopes and Mounds. *Handbook of Coastal and Ocean Engineering. Word Scientific Publishing Co. Pte. Ltd., Singapore*, 383–411.

Shepard, C. C., Crain, C. M., & Beck, M. W. (2011). The Protective Role of Coastal Marshes: A Systematic Review and Meta-analysis. *PLOS ONE*, *6*(11), e27374. Retrieved from http://dx.doi.org/10.1371%2Fjournal.pone.0027374

Small, C., & Nicholls, R. J. (2003). A global analysis of human settlement in coastal zones. *Journal of Coastal Research*, *19*(3), 584–599. Retrieved from https://www.scopus.com/inward/record.uri?eid=2-s2.0-0042427253&partnerID=40&md5=54d0b2fecf6a42203312b33402854499

Smit, P. B., Roelvink, J. A., van Thiel de Vries, J. S. M., McCall, R. T., van Dongeren, A. R., & Zwinkels, J. R. (2014). XBeach: Non-hydrostatic model, 69.

Songy, G. (2016). Wave Attenuation by Global Coastal Salt Marsh Habitats. *Tudelft Repository*, (June). Retrieved from uuid:f00e7416-f330-4d99-90fe-bf54367da78b

Sutton-Grier, A. E., Wowk, K., & Bamford, H. (2015). Future of our coasts: The potential for natural and hybrid infrastructure to enhance the resilience of our coastal communities, economies and ecosystems. *Environmental Science and Policy*, *51*, 137–148. https://doi.org/10.1016/j.envsci.2015.04.006

Suzuki, T., Zijlema, M., Burger, B., Meijer, M. C., & Narayan, S. (2011). Wave dissipation by vegetation with layer schematization in SWAN. *Coastal Engineering*, *59*(1), 64–71. https://doi.org/10.1016/j.coastaleng.2011.07.006

Suzuki, T., Zijlema, M., Burger, B., Meijer, M. C., & Narayan, S. (2012). Wave dissipation by vegetation with layer schematization in SWAN. *Coastal Engineering*, *59*(1), 64–71.

Tanaka, N., Sasaki, Y., Mowjood, M. I. M., Jinadasa, K. B. S. N., & Homchuen, S. (2007). Coastal vegetation structures and their functions in tsunami protection: Experience of the recent Indian Ocean tsunami. *Landscape and Ecological Engineering*, *3*(1), 33–45. https://doi.org/10.1007/s11355-006-0013-9

Tang, J., Shen, Y., Causon, D. M., Qian, L., & Mingham, C. G. (2017). Numerical study of periodic long wave run-up on a rigid vegetation sloping beach. *Coastal Engineering*, *121*(December 2016), 158–166. https://doi.org/10.1016/j.coastaleng.2016.12.004

Tschirky, P., Hall, K., & Turcke, D. (2001). Wave attenuation by emergent wetland vegetation. In *Coastal Engineering 2000* (pp. 865–877).

van Dongeren, A., Battjes, J., Janssen, T., van Noorloos, J., Steenhauer, K., Steenbergen, G., & Reniers, A. (2007). Shoaling and shoreline dissipation of low-frequency waves. *Journal of Geophysical Research: Oceans*, *112*(2), 1–15. https://doi.org/10.1029/2006JC003701

van Gent, M. (2001). Wave Runup on Dikes with Shallow Foreshores. *Journal of Waterway, Port, Coastal, and Ocean Engineering*, *127*(October), 254–262. https://doi.org/10.1061/(ASCE)0733-950X(2001)127:5(254)

van Rooijen, A. A., McCall, R. T., van Thiel de Vries, J. S. M., van Dongeren, A. R., Reniers,

A. J. H. M., & Roelvink, J. A. (2016). Modeling the effect of wave-vegetation interaction on wave setup. *Journal of Geophysical Research: Oceans*, *121*(6), 4341–4359. https://doi.org/10.1002/2015JC011392

van Rooijen, A. A., van Thiel de Vries, J. S. M., McCall, R. T., van Dongeren, A. R., Roelvink, J. A., & Reniers, A. J. H. M. (2015). Modeling of wave attenuation by vegetation with XBeach. *E-Proceedings of the 36th IAHR World Congress*, 7.

Vo-Luong, P., & Massel, S. (2008). Energy dissipation in non-uniform mangrove forests of arbitrary depth. *Journal of Marine Systems*, *74*(1–2), 603–622. https://doi.org/10.1016/j.jmarsys.2008.05.004

Wu, W. C., & Cox, D. T. (2015). Effects of wave steepness and relative water depth on wave attenuation by emergent vegetation. *Estuarine, Coastal and Shelf Science*, *164*, 443–450. https://doi.org/10.1016/j.ecss.2015.08.009

Wu, W. C., Ma, G., & Cox, D. T. (2016). Modeling wave attenuation induced by the vertical density variations of vegetation. *Coastal Engineering*, *112*, 17–27. https://doi.org/10.1016/j.coastaleng.2016.02.004

Zhang, S., Yang, H., & Singh, L. (2014). Mangroves as a coastal protection from waves in the Tong King Delta, Vietnam. *CEUR Workshop Proceedings*, *1225*(March 2015), 41–42. https://doi.org/10.1023/A

A. Equation formulation

A.1 Short wave energy dissipation by vegetation

The short wave energy dissipation equation is based on work Mendez & Losada (2004) and the derivations can be presented as follows.

Wave energy is lost during propagation through vegetation due to work carried out by vegetation. Assuming linear wave theory is valid and considering shore normal incident waves, the energy conservation equation is presented as,

$$\frac{\partial EC_g}{\partial x} = -\varepsilon_v \tag{A.1}$$

Where E is the energy density, C_g is the group velocity, ε_v is the time-averaged rate of energy dissipation per unit horizontal area induced by vegetation.

The energy dissipation by a given vegetation can be provided as,

$$\varepsilon_v = \overline{\int_{-h}^{-h+\alpha h} Fudz} \tag{A.2}$$

h is the water depth and αh is the mean vegetation height. $F = (F_x, F_z)$ is the force acting on a unit volume. $u = (u, w)$ is the velocity. The force component from F_z can be neglected. Neglecting swaying motion and inertial forces from the plant-induced force acting on vegetation, F_x can be expressed using a Morison-type equation.

$$F_x = \frac{1}{2}\rho C_D b_v N_v u|u| \tag{A.3}$$

Where u is the horizontal velocity, C_D, b_v, N_v are depth averaged drag force, plant area per unit height and number of plant strands per unit area respectively.

Using liner wave theory substituting for the velocity, the energy dissipation by wave can be provided as,

$$\varepsilon_v = \frac{2}{3\pi}\rho C_D b_v N_v \left(\frac{kg}{2\sigma}\right)^3 \frac{sinh^3 kh_v + 3sinhkh_v}{3\ kcosh^3 kh} H^3 \tag{A.4}$$

The formula is adjusted for random waves as,

$$\varepsilon_v = \left(\frac{kg}{2\sigma}\right)^3 \frac{\rho C_D b_v N_v sinh^3 kh_v + 3sinhkh_v}{6\sqrt{\pi}\ kcosh^3 kh} H_{rms}^3 \tag{A.5}$$

B. Model setup procedure

B.1 Grid geometry and boundary conditions

For the numerical implementation of the bathymetry of mangrove coasts in XBeach following offshore boundary conditions must be fulfilled. i) Significant wave height to the water depth criteria. ii) Wave group velocity to wave celerity ratio. The satisfactory conditions required by XBeach in these requirements are provided in Figure B.1

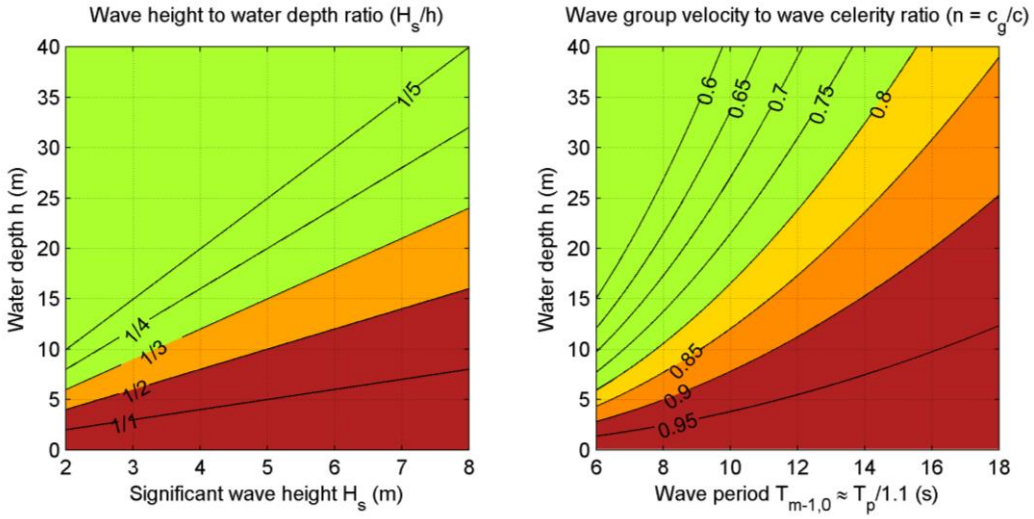

Figure B.1: Satisfactory conditions for the implementation of XBeach (Roelvink et al., 2015). Left plot provides the water wave height-water depth condition. Right plot provides the wave period-water depth condition. Green color depicts satisfactory conditions of application.

As for the selected input parameter space, the maximum significant wave height at boundary is 7m (section 3.2.1) thus a minimum depth of 21m is required at the boundary (wave height/water depth condition). The maximum wave period of the incoming waves is at 14s (section 3.2.1) hence for the implementation of the model a minimum boundary water depth of 30 m is required (group velocity /wave celerity condition).

To satisfy both these conditions an offshore boundary depth of 35m was used. The onshore boundary is located 500 m after the end of vegetation. Both boundaries are set to absorbing -generating (keyword: abs1d) (Roelvink et al., 2015).

Due to the very mild slopes, the computational domain extends for many kilometers (e.g., a bed slope of 1/1000 will result in a grid length of 35 km from the offshore boundary up to the vegetation). Long cross-shore model domains result in a large computational effort. In order to reduce the computational time, the grid can be truncated (cut-off at a certain depth).

The truncation was performed at a certain depth by using a steeper slope. Since the grid resolution criteria is based on CFL condition and points per wave length, deeper sections of the grid results in coarser grid cells thus reducing the number of grid points and the model simulation time. The truncation of the grid, results in a deviation in the

outputs compared to the conventional grid. The depth of truncation and truncated steep slope determines the model run time and the deviation of the outputs.

An "optimal grid" would be a set-up in which the deviations from the original grid are minor, but the model run time is considerably less. In order to find such an optimal grid several grid geometries were considered. Initial model results showed that there was a significant variation in time with different profile break points but only minor time saving with different truncation slopes. Hence, cross-shore profiles with a series of profile breaks (-3 m, -5 m, -8 m, -12.5 m, 15 m, -20 m, -25 m, -30 m) and a truncated slope of 1/300 was used for the analysis. Figure B.2 depicts an example of the cross-shore computational domains chosen.

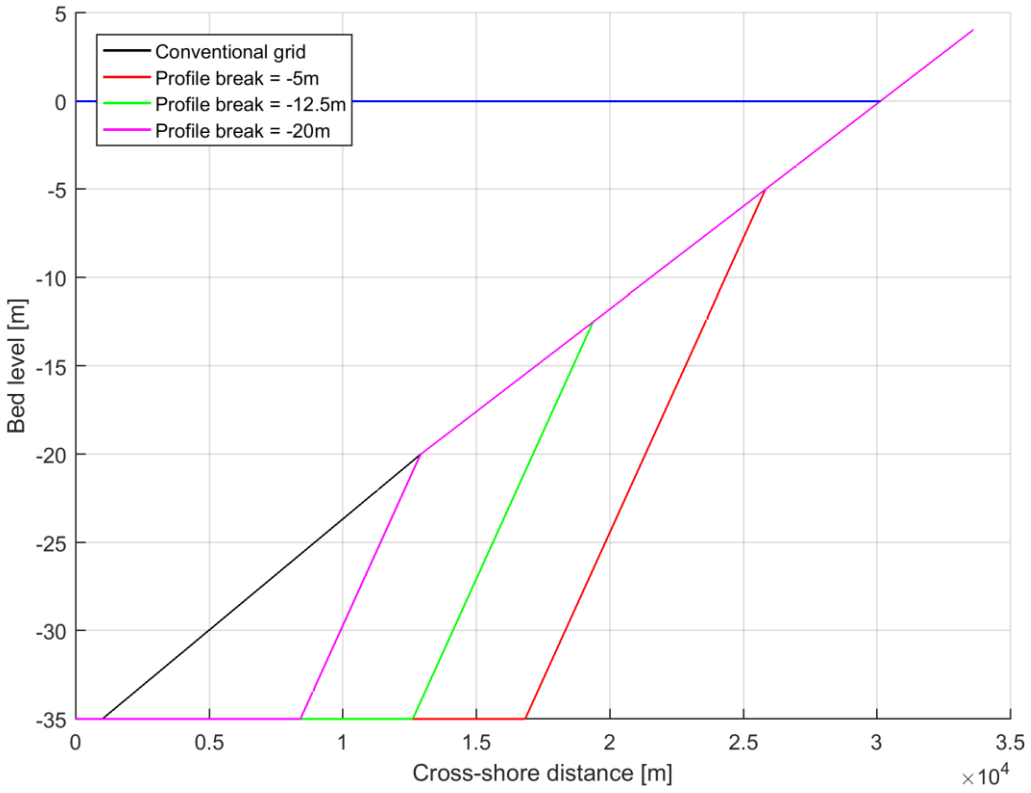

Figure B.2: Example of a conventional grid and truncated grids, truncation at -5m -12.5m and -20m with a slope of 1/300

A set of 32 model runs was used for each model domain. The input parameters were selected such that it covers the entire parameter space (section 3.2) that will be used. The same offshore signal was used for each of counterpart the model runs. Wave setup, mean short wave height and mean long wave height were considered for the comparison between the different grid geometries. The output results of these parameters were compared at the start of the vegetation. A percentage deviation between the truncated grid and the conventional grid was calculated for each of the three parameters according to equation B.1.

$$\% \text{ deviation } = \frac{(\text{Truncated grid result} - \text{Conventional grid result})}{\text{Conventional grid result}} \% \qquad \text{(B.1)}$$

Box plot diagrams are used to show the spread of the error observed for the different profile breaks. Figure B.3 provides the boxplots for the error in short wave height, water level and long wave height. A similar pattern of the deviation can be observed in all three outputs. The deviation in the results reduces as the profile break is situated in deeper water (left to right of the x axis in Figure B.3, the truncation of profile is located at deeper depths.). The deviations in mean setup and mean shortwave height for models are almost negligible with a mean deviation near zero (note the difference in scale of the y axis between Figure B.3 top/middle plot and the bottom plot). A much larger deviation in the results is observed for the long wave heights.

The deviation in long wave height can be associated to the difference in the shoaling of waves under different grid geometries. Deeper profile breaks will have a lesser effect on the waves as they will not feel the bottom variations compared to grid geometries where the profile break is at much shallower depths. From further investigation into the deviations it was observed that the incident wave period was of major importance governing the deviation percentage. For higher wave periods the deviation increased, since the effect of the bottom topography will be larger due to long wave lengths.

Figure B.4 shows the variation in the long wave propagation with the wave period. For the larger wave periods, the variations from the conventional grid are apparent throughout the profile while for the lower wave period the long-wave wave height varies only at shallower water depths. Thus, to minimize the variations from the conventional grid profile, the profile break should be situated at a sufficient depth.

Figure B.5 provides the distribution of the observed deviation in the results for the long wave height over the incidence peak wave period (Tp) and varying profile breaks. The distribution of error across the profile break is as anticipated with the deviation reducing as the profile break is situated in deeper water. The deviation in terms of wave period is more confined to wave periods between 7.5s – 10s. Comparatively a lower deviation is observed for both lower and higher periods over the above range. The low deviations observed for low wave periods were explained previously (Figure B.4) where the bottom variation is not felt by the shoaling wave thus reducing the deviation. The higher wave period waves will shoal more pronouncedly but the infragravity waves start to break before reaching the vegetation. The breaking of the wave results in an equal long (and short) wave height at the observation point lowering the deviation. The mid-range wave period waves will shoal just the right amount to create large deviations in the results.

In the selection of the appropriate grid geometry, the model run time should also be considered. Figure B.6 provides the deviation observed as a function of the model time.

The Model time increases as the deviation reduces. The mean model run time for the conventional grid was 27 minutes on one computational core. The optimal grid geometry is selected for a percentage deviation is less than 5%. Thus, according to Figure B.6, the grid geometry with a profile break at -12.5 m (and a truncated slope of 1/300) is chosen as the model domain.

In the grid geometry selection, all grids were constructed with a minimum grid size of 2m. During the selection of the minimum grid resolution, a 1m grid resolution was chosen for the final grid. Due to the lower minimum grid resolution in the final grid compared to the grid resolution used in the test, the time saving from the truncation will be much larger compared to a conventional grid with a minimum grid resolution of 1m.

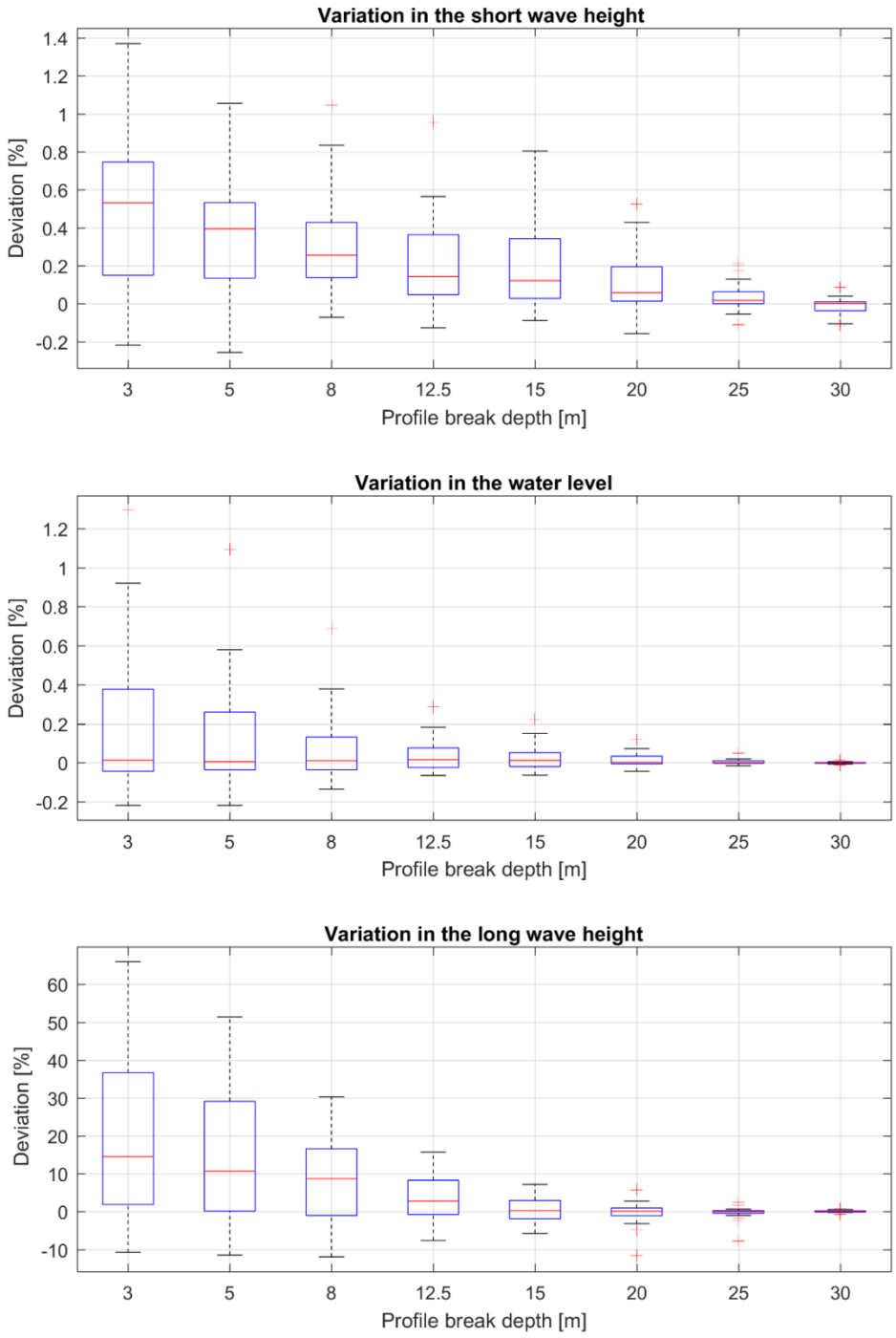

Figure B.3: Percentage deviation between the conventional grid results (shortwave height. Water level and long-wave height) and the truncated grid results for the different truncation depths.

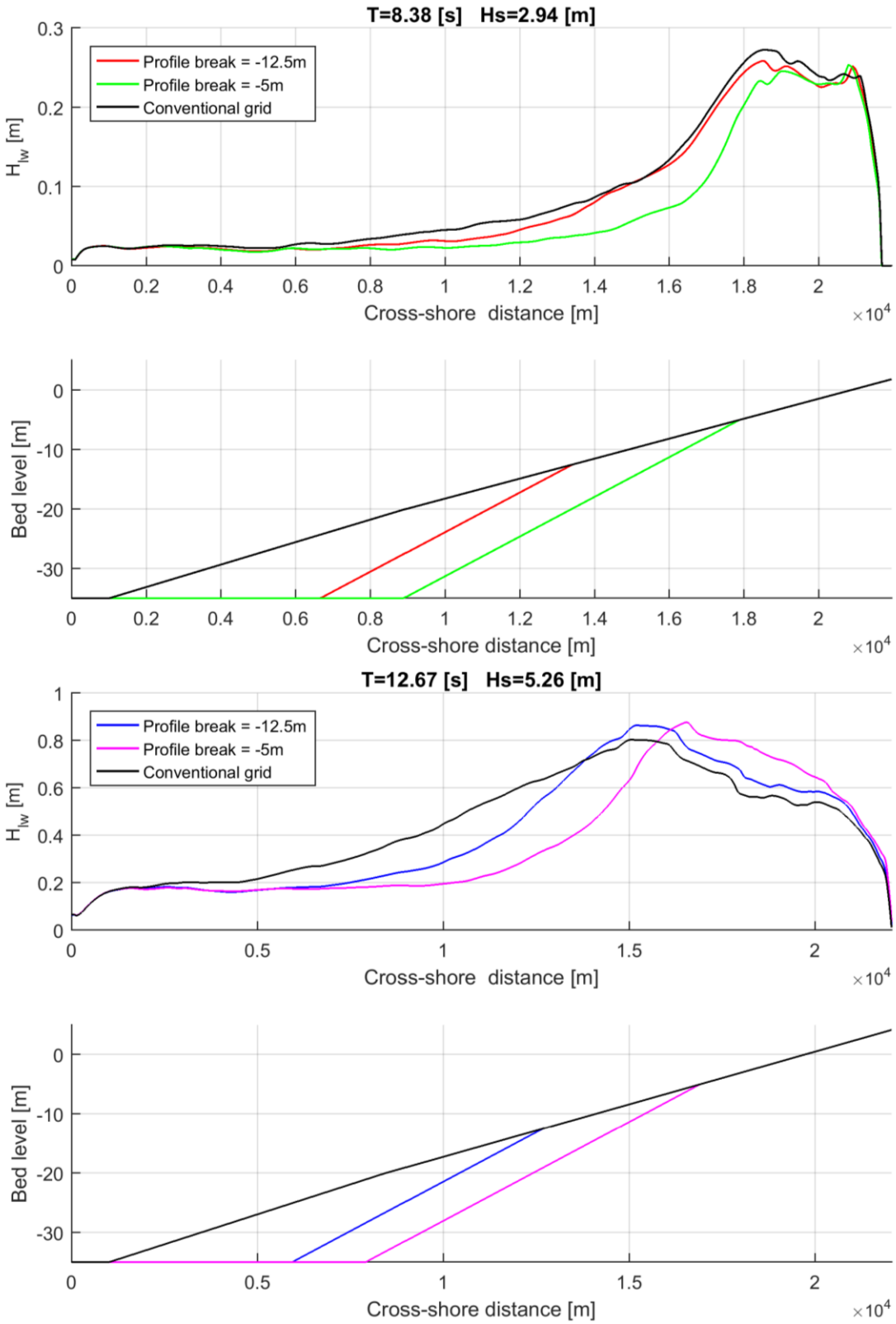

Figure B.4: Variation of long wave height variation with incidence wave period. Model outputs for Tp=8s (top plot) and Tp=12s (bottom plot)

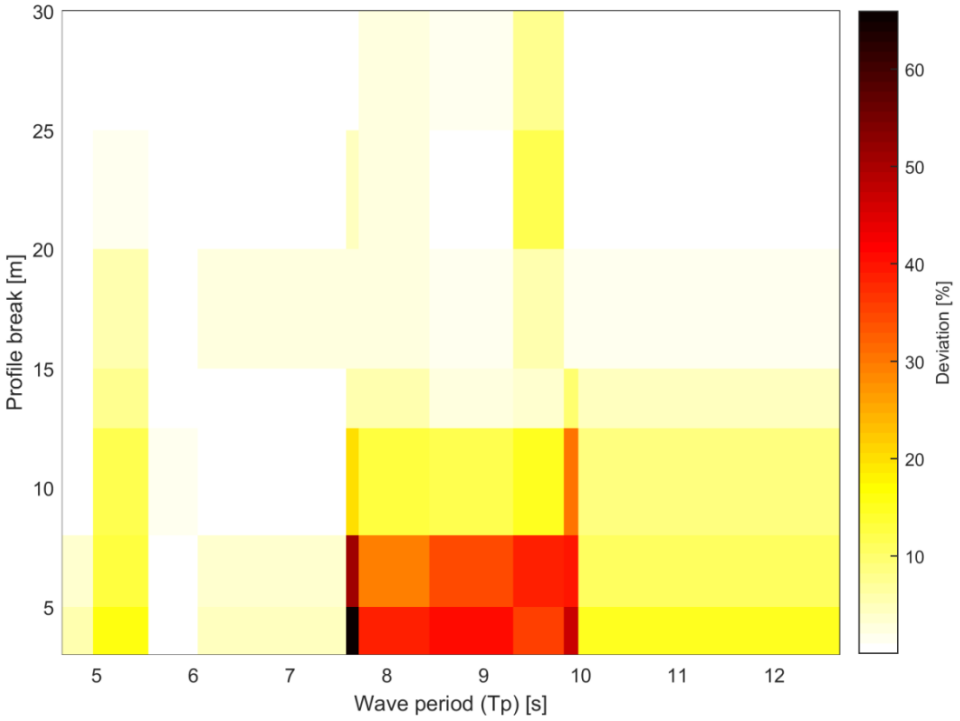

Figure B.5: Distribution of percentage deviation of the long-wave wave height over the different profile breaks and the incidence wave period Tp

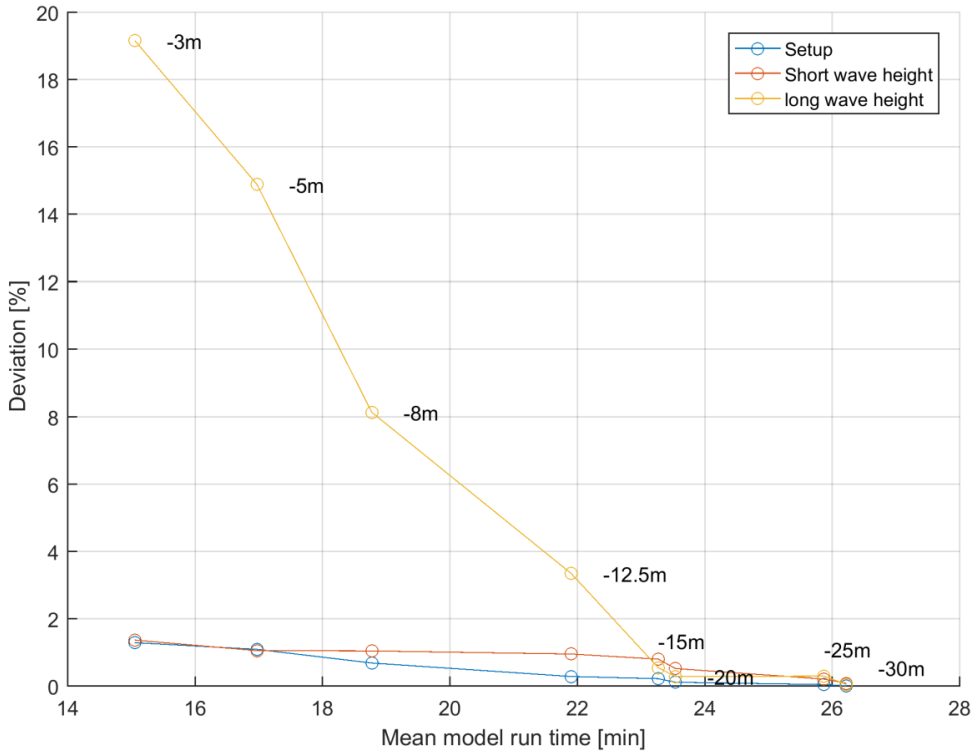

Figure B.6: Mean deviation in long wave height vs. model time, maximum observed deviation in setup and shortwave height at front of vegetation. The annotations on the graph provide the profile break at the corresponding data point.

B.1.1 Equilibrium bound long wave at boundary

During the analysis of results in the grid geometry, a peculiar increase in long wave height close to the offshore model boundary was observed. This boundary issue is visible in the long wave height propagations given Figure B.4.

To identify the reasons for the issue a set of model runs were done using an equidistance grid with a flat profile with a depth of 35m and a length of 30km. Similar to the main model setup. the other input parameters were varied.

The reason to use a flat profile was to exclude any growth that might occur on a sloping profile due to shoaling of the wave. The output results of the test showed that in fact there was an initial increase in the long wave height (H_{lw}).

Figure B.7 provides an example of H_{lw} increase with distance for three different input conditions. The growth in the wave height indicates a mismatch between the prescribed equilibrium long wave at boundary and the actual equilibrium long wave of the model.

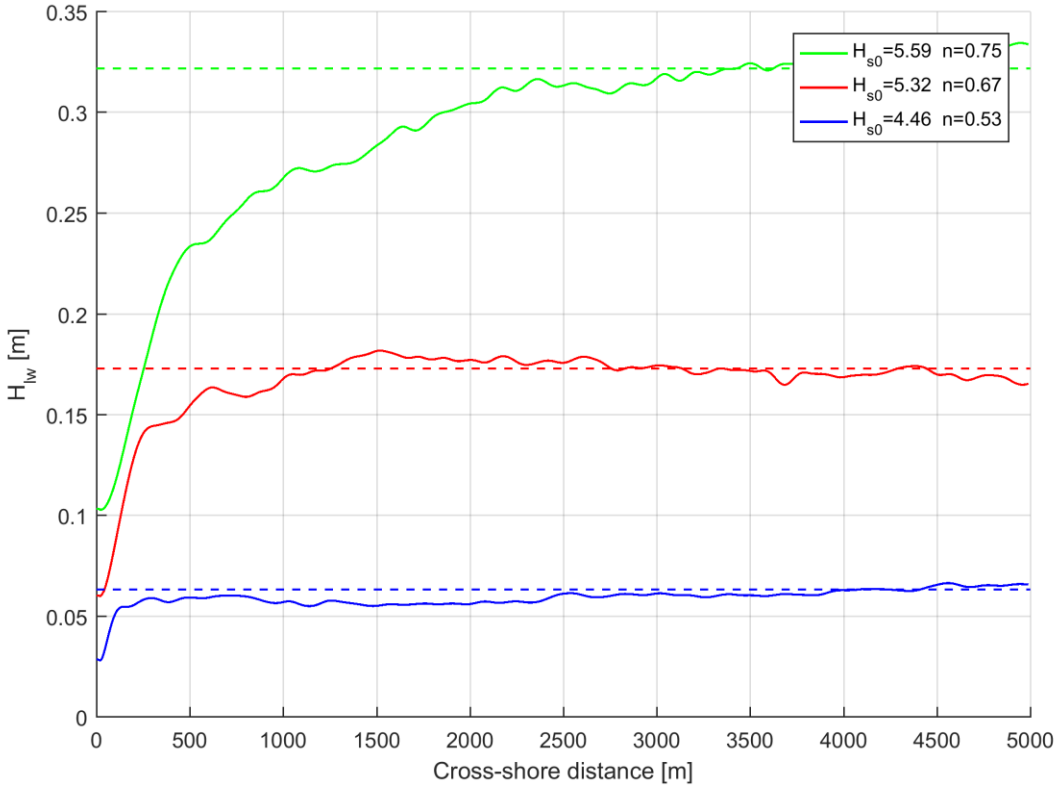

Figure B.7: Increase in H_{lw} at the boundary along a flat profile for three different input conditions. The dashed line represents the mean equilibrium wave height for each model.

One reason for the mismatch was postulated to be the directional spreading parameter (s) in XBeach which has a default value of 10. The bound long wave signal is calculated by considering the wave interaction (wave number and wave frequency). A directional spreading value (s) of 10 would mean there is significant spread of the waves in different directions. Due to the directional spreading considered the interactions between the waves will be lower compared to unidirectional waves. The lower

interactions will result in a lower wave height at the boundary. Since the actual model domain is a 1D model, the actual wave interactions in the model domain will be higher than the calculated boundary signal, resulting in an increase in the wave height.

The same flat profile test was done again for an increased s value (s=10,000). It was then observed that the boundary calculated wave height did indeed increase with the reduced directional spreading. However, the model still showed an increase in long wave height to reach the equilibrium.

The distance of propagation from the boundary to reach the equilibrium wave height is important, because if the appropriate distance to reach equilibrium is not given, and there is a profile variation within the distance needed for equilibrium, the initial variations can be amplified due to shoaling of waves.

In the analysis, it was noted that the distance required by the waves to reach equilibrium height strongly correlate to the wave number n ($n = c_g/c$). Waves with higher n values needed longer distance for equilibrium and vise-versa for smaller n values. Figure B.8 presents the Longwave height (H_{lw}) at a given place as a ratio of the equilibrium long wave height ($H_{lw,eqm}$).

The distance required for the waves to reach equilibrium increase with increasing n. A maximum propagation distance of about 1500 m was needed to reach 90% of the equilibrium long wave height. Hence a minimum distance of about 1500m should be provided at the start of the XBeach profile for the long waves to reach equilibrium.

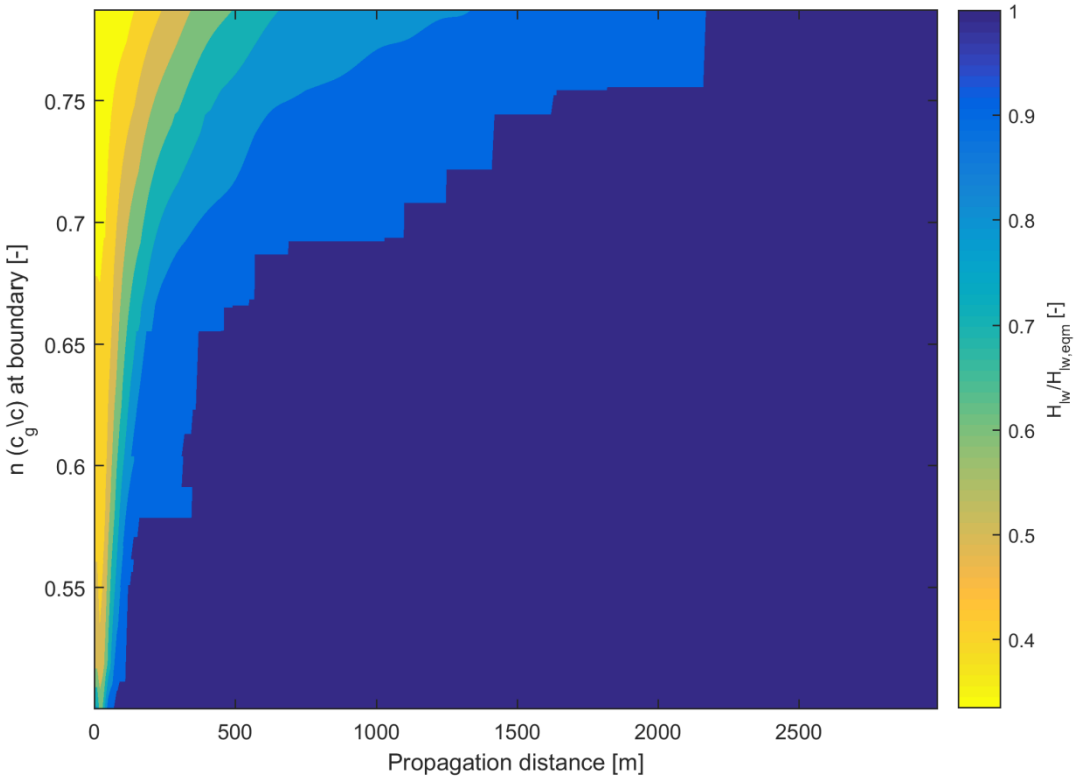

Figure B.8: Distance required for the waves to reach equilibrium wave height. The values represent the deviation from the equilibrium. Value of 1 represent the wave has reached equilibrium wave height.

B.2 Selection of the optimum grid resolution

A spatially varying grid size is applied to satisfy both the satisfactory runtimes and acceptable results in the onshore region. A MATLAB-based function to create non-equidistance grid with the grid resolution varying according to the CFL condition and the grid points per wave length is used. Under these conditions, a non-equidistance grid with an increasing resolution towards shoreward is generated.

The grid resolution varies from a given maximum grid length to a minimum grid length. As the grid resolution approaches shallower water, the grid resolution will opt to the set minimum grid resolution. Finding the optimum minimum grid length will be important as the interaction of vegetation will occur in the shallow water region. Furthermore, the minimum grid length will determine the number of grid cells and therefore will also affect the computational effort of the models. A set of tests were done to identify the minimum grid resolution to satisfy both computational efficiency and accuracy of results.

Figure B.9 provides grid resolution variation across the model domain for one of the model runs where maximum grid resolution is set to infinity and the minimum grid resolution is set to a certain value. According to the CFL condition and points per wave length, the maximum grid resolution will be set automatically.

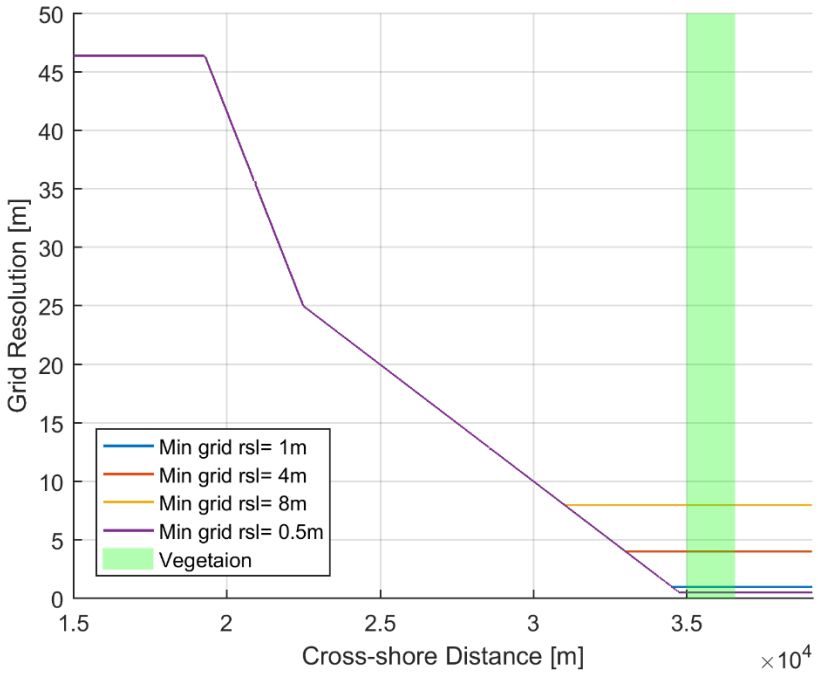

Figure B.9: Variation of grid resolution across the model domain for different minimum grid resolutions prescribed

In order to determine the minimum grid resolution, tests were performed for minimum grid resolutions of 0.5m, 1m, 2m, 4m and 8m. Minimum grid resolution of 0.5m was taken as the benchmark value to compare the other minimum grid resolution grid outputs. The deviations of outputs were calculated in a similar manner.

$$\%\ \text{deviation} = \frac{(\ \text{output for min grid rsl}\ m - \text{output for min grid rsl}\ 0.5m)}{\text{output for min grid rsl}\ 0.5m}\ \% \qquad \text{(B.2)}$$

The output results that compared were short wave height, long wave height and mean setup at the start of the vegetation. The mean wave force over the vegetation widths were also compared. Figure B.10 provides boxplot diagrams of the percentage deviation in the outputs considered. In all outputs, an increase in deviation with increasing grid length is apparent. Deviation in model results is assumed to negligible if the variations compared to a minimum grid resolution of 0.5 meter is less than 5%.

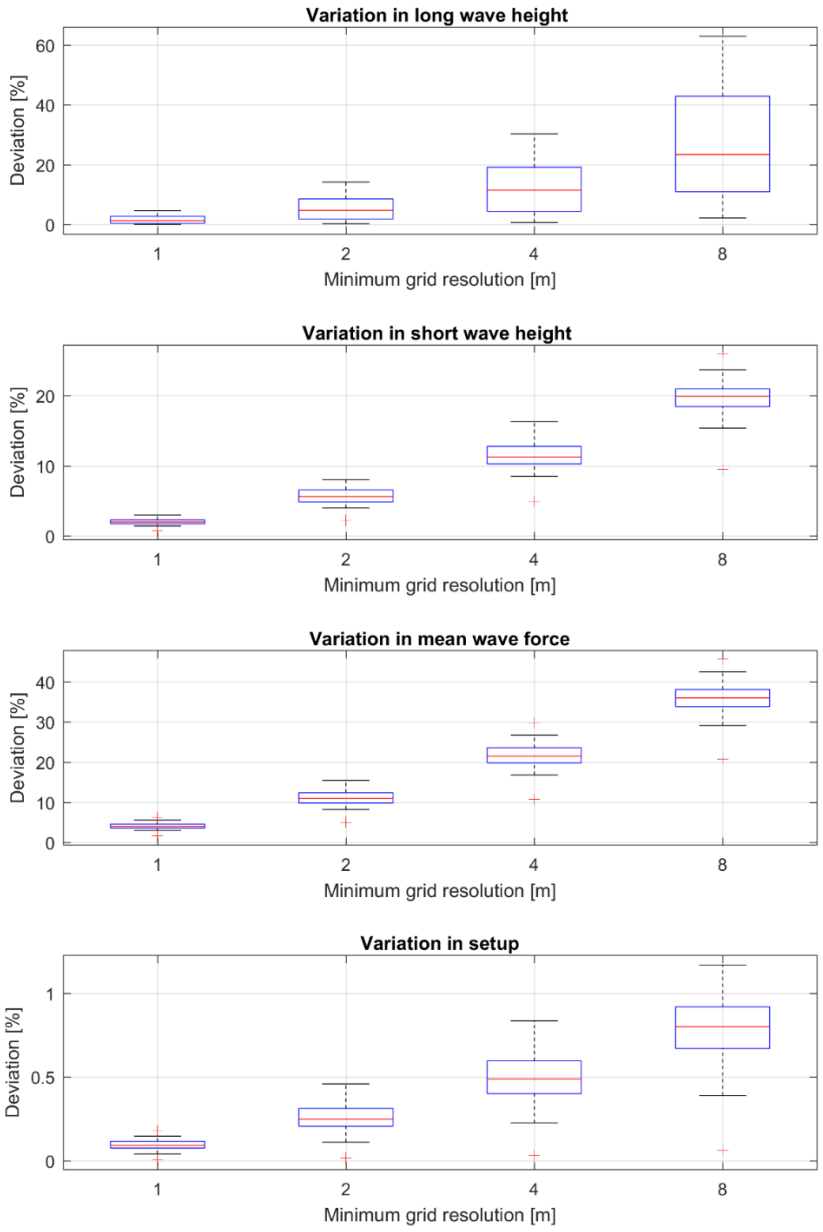

Figure B.10: Percentage deviation of results from minimum the grid resolution 0.5m for shortwave height, long wave height, setup at the start of the vegetation and mean wave force within the vegetation.

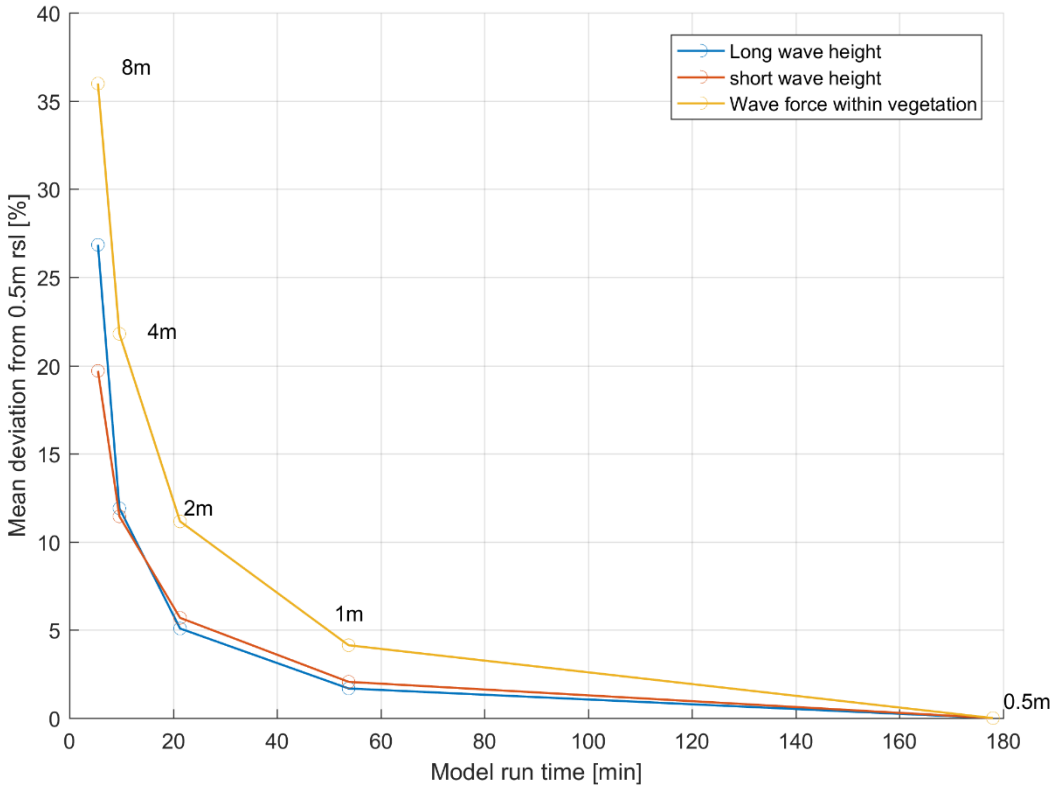

Figure B.11: Mean deviation of long wave height, short wave height and wave force vs. model runtime, observed for different minimum grid resolutions. The annotations on the graph provide the minimum grid resolution at the corresponding data point.

Figure B.11 provides the model time and deviation relationship for the grid resolution. First it can be noticed that the model time is very much influenced by the minimum grid resolution. The computational time required reduces considerably with coarser grid. However, the deviation also increases rapidly. Taking the significant deviation level to be 5% and deviations less than that can be neglected, minimum grid resolution of 1m is chosen for the grid.

B.3 Model spin up and run time

For analysis of model data, it is imperative that the model has a reached stationary condition. A model is considered to have reached the stationary state if the model results (time averaged) for a given location does not change with time. Due to the very long grid domains (O (10 km)) sufficient time should be allowed for the models to reach the stationary state.

The time required to reach this state is checked using the time taken for the short waves to reach the shoreline and the setup buildup.

A series of test models were run for duration of 5 hours. The shortwave heights (H_{sw}) and setup ($\Delta\eta$) at the start of the vegetation was then analyzed.

The outputs were averaged over a several 30-mintue bursts. The burst means was then normalized by the final burst mean value of each model ($\overline{\Delta\eta}$ *and* $\overline{H_{sw}}$). A model was considered to be stationary when the normalized value of setup and shortwave height is larger than 0.95 ($\frac{\Delta\eta}{\overline{\Delta\eta}} \geq 0.95$ *or* $\frac{H_{sw}}{\overline{H_{sw}}} \geq 0.95$). The time required for the model to reach this condition is defined as the spin-up time.

Figure B.12 presents setup at the start of the vegetation for one of the model runs. An initial increase and a leveling off the setup can be observed. The spin-up time required for this specific model will be 120 minutes.

The spin-up time is a function of the model domain, since longer profiles will need more time for the propagation of the waves from the offshore boundary. The domain length is a function of the profile slope. Figure B.13 provides the distribution of the normalized burst mean values for all model runs at different time values for the different model slopes. The increase in time to reach the stationary condition with milder slopes is apparent.

From the analysis, an average spin-up time of 70 minutes based on the setup criteria and 90 minutes according to mean short waves criteria was obtained.

As a conservative measure accounting for the variation in spin-up time observed between models, a constant spin-up time of 120 minutes was used for all the models. However, certain model runs need more spin-up time (Figure B.13). Therefore, in a post-processing step stationary of all model results is double checked and bursts which are not stationary were discarded.

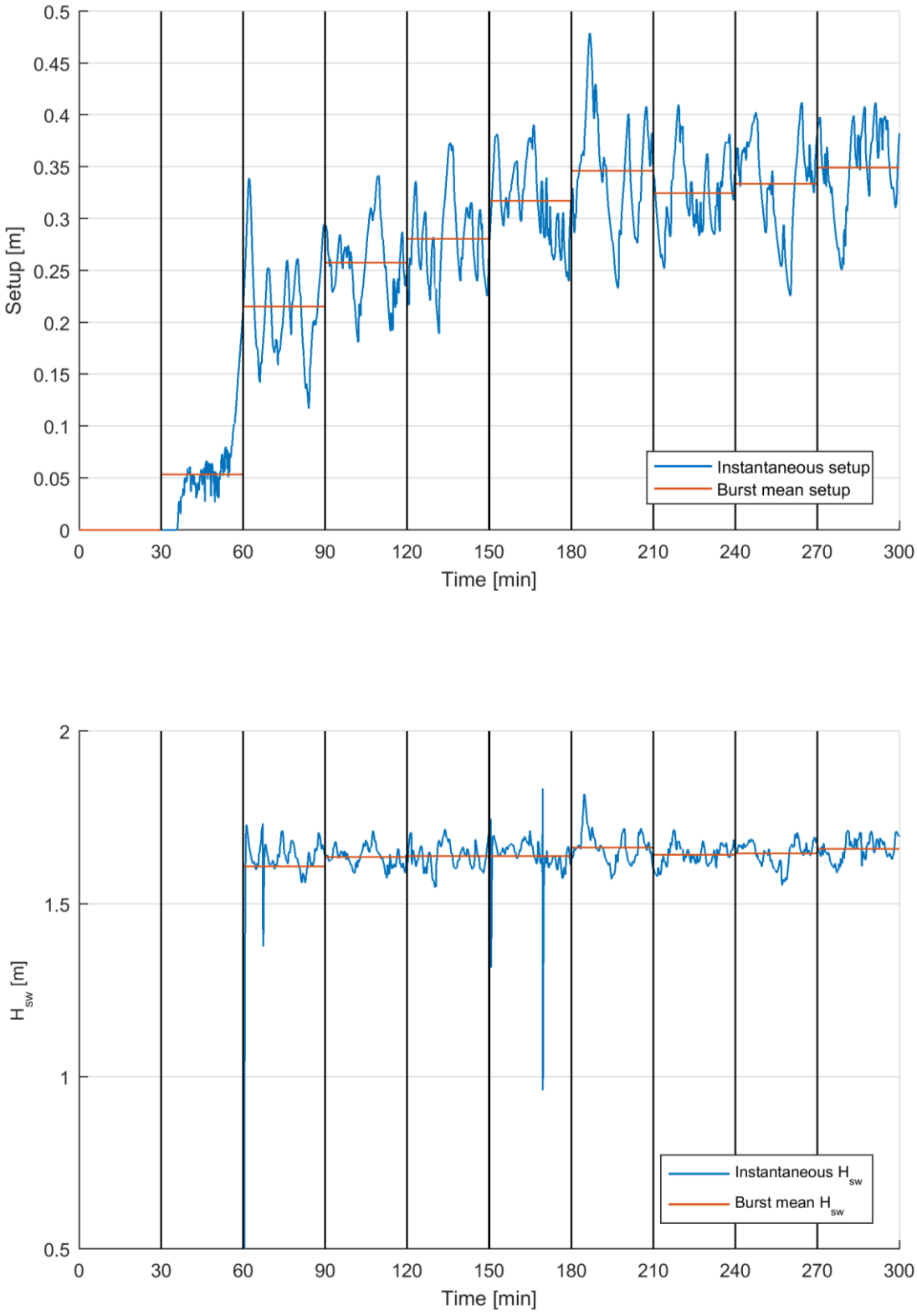

Figure B.12: Output results for spinup calculation. Instantaneous and burst mean variation with time. Top plot: instantaneous setup variation and burst mean setup. Bottom plot: instantaneous short wave height and corresponding burst mean variation

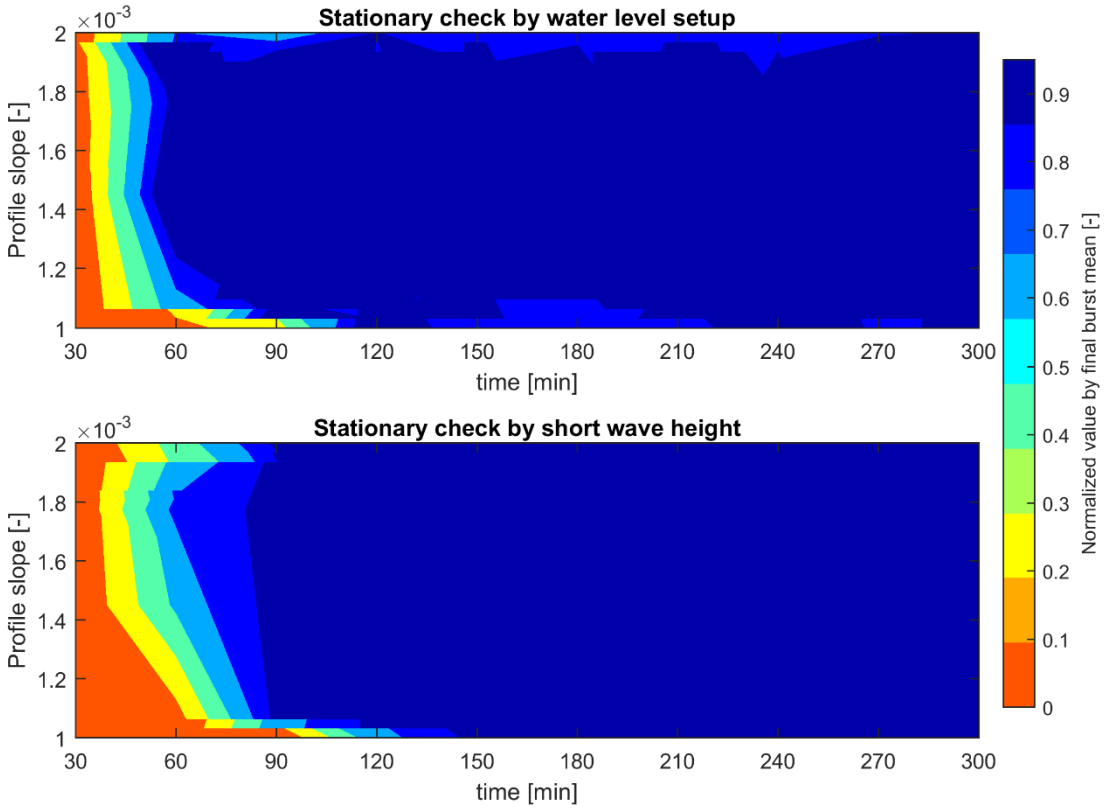

Figure B.13: Variation in burst mean setup and shortwave height at observation point 2 over time. The burst mean setup and wave height values have been normalized by the final burst mean value. The dark blue color represents the normalized values which are larger than 0.95 (stationary condition)

The total model run time is 240 minutes and includes at least 120 minutes of spinup. The 120 minutes of actual model runtime is divided into 4 bursts of 30 minutes to acquire time averaged results from XBeach.